USGS
science for a changing world

History of Surface Displacements at the Yellowstone Caldera, Wyoming, from Leveling Surveys and InSAR Observations, 1923–2008

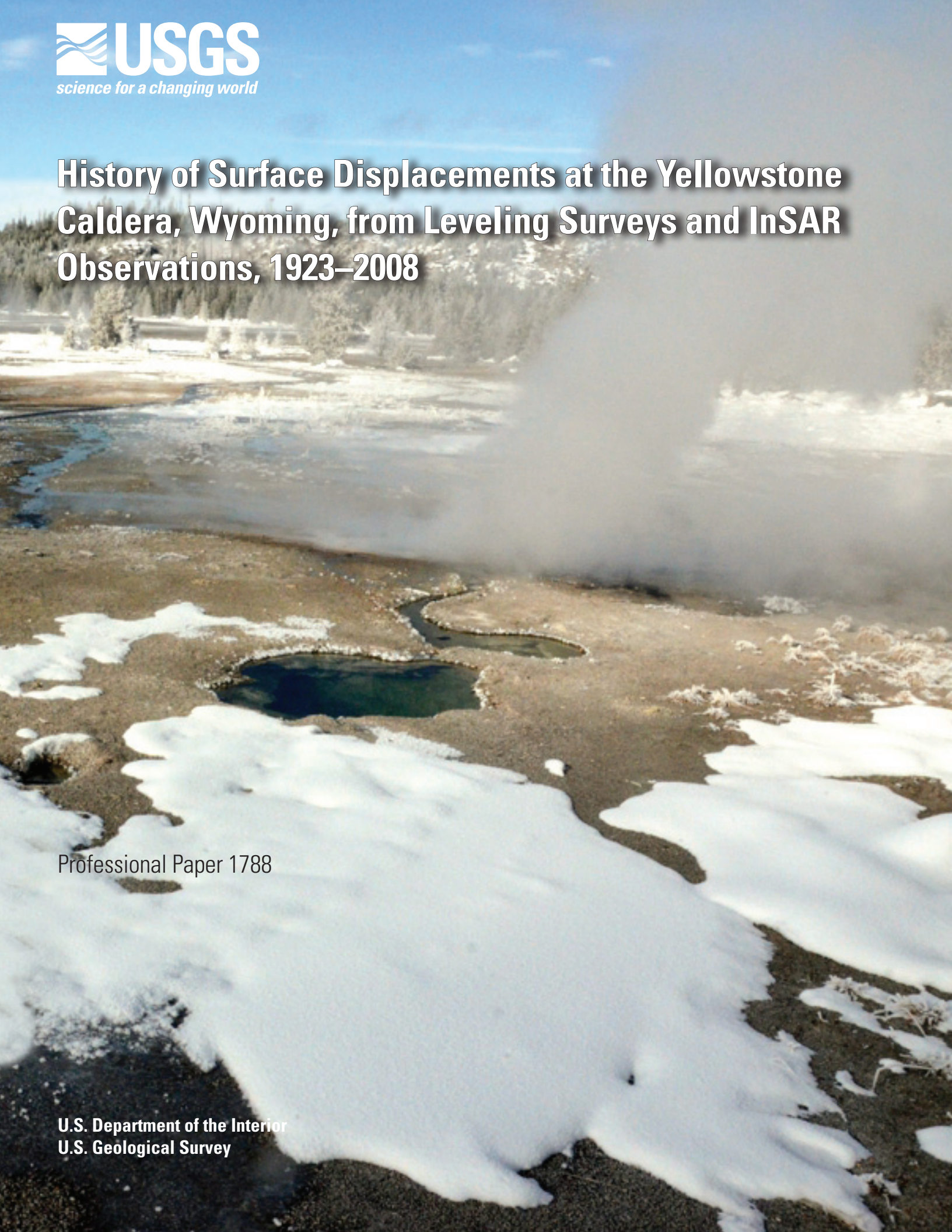

Professional Paper 1788

U.S. Department of the Interior
U.S. Geological Survey

COVER:
Hydrothermal features in the vicinity of Mushroom Geyser in the Back Basin of Norris Geyser Basin, Yellowstone National Park. Norris Geyser Basin is the hottest and most changeable thermal area in Yellowstone. One of three deformation centers discussed in this report is located along the north rim of the Yellowstone caldera near Norris Geyser Basin. Pressure changes within Yellowstone's hydrothermal system likely play a role in causing episodic ground-surface deformation, together with inflation/deflation cycles of the underlying basalt-rhyolite magmatic system. (U.S. Geological Survey photograph by Dan Dzurisin.)

History of Surface Displacements at the Yellowstone Caldera, Wyoming, from Leveling Surveys and InSAR Observations, 1923–2008

By Daniel Dzurisin, Charles W. Wicks, and Michael P. Poland

Professional Paper 1788

U.S. Department of the Interior
U.S. Geological Survey

U.S. Department of the Interior
KEN SALAZAR, Secretary

U.S. Geological Survey
Marcia K. McNutt, Director

U.S. Geological Survey, Reston, Virginia: 2012

This report and any updates to it are available online at:
http://pubs.usgs.gov/pp/1788/

For more information on the USGS—the Federal source for science about the Earth, its natural and living resources, natural hazards, and the environment—visit http://www.usgs.gov or call 1–888–ASK–USGS

For an overview of USGS information products, including maps, imagery, and publications, visit http://www.usgs.gov/pubprod

To order this and other USGS information products, visit http://store.usgs.gov

Suggested citation:
Dzurisin, D., Wicks, C.W, and Poland, M.P., 2012, History of surface displacements at the Yellowstone Caldera, Wyoming, from leveling surveys and InSAR observations, 1923–2008: U.S. Geological Survey Professional Paper 1788, 68p.

TITLE PAGE
Photograph of a U.S. Coast and Geodetic Survey benchmark in Yellowstone National Park.

Contents

Figures

Tables

This page intentionally left blank.

History of Surface Displacements at the Yellowstone Caldera, Wyoming, from Leveling Surveys and InSAR Observations, 1923–2008

By Daniel Dzurisin[1], Charles W. Wicks[2], and Michael P. Poland[3]

Abstract

Modern geodetic studies of the Yellowstone caldera, Wyoming, and its extraordinary tectonic, magmatic, and hydrothermal systems date from an initial leveling survey done throughout Yellowstone National Park in 1923 by the U.S. Coast and Geodetic Survey. A repeat park-wide survey by the U.S. Geological Survey (USGS) and the University of Utah during 1975–77 revealed that the central part of the caldera floor had risen more than 700 mm since 1923, at an average rate of 14±1 mm/yr. From 1983 to 2007, the USGS conducted 15 smaller surveys of a single level line that crosses the northeast part of the caldera, including the area where the greatest uplift had occurred from 1923 to 1975–77. The 1983 and 1984 surveys showed that uplift had continued at an average rate of 22±1 mm/yr since 1975–77, but no additional uplift occurred during 1984–85 (-2±5 mm/yr), and during 1985–95 the area subsided at an average rate of 19±1 mm/yr. The change from uplift to subsidence was accompanied by an earthquake swarm, the largest ever recorded in the Yellowstone area (as of March 2012), starting in October 1985 and located near the northwest rim of the caldera.

Interferometric synthetic aperture radar (InSAR) images showed that the area of greatest subsidence migrated from the northeast part of the caldera (including the Sour Creek resurgent dome) during 1992–93 to the southwest part (including the Mallard Lake resurgent dome) during 1993–95. Thereafter, uplift resumed in the northeast part of the caldera during 1995–96, while subsidence continued in the southwest part. The onset of uplift migrated southwestward, and by mid-1997, uplift was occurring throughout the entire caldera (essentially rim to rim, including both domes). Consistent with these InSAR observations, leveling surveys indicated 24±3 mm of uplift in the northeast part of the caldera during 1995–98. The beginning of uplift was coincident with or followed shortly after an earthquake swarm near the north caldera rim during June–July 1995—the strongest swarm since 1985. Rather than a single deformation source as inferred from leveling surveys, the InSAR images revealed two distinct sources—one beneath each resurgent dome on the caldera floor.

Subsequently, repeated GPS surveys (sometimes referred to as "campaign" surveys to distinguish them from continuous GPS observations) and InSAR images revealed a third deformation source beneath the north caldera rim. The north-rim source started to inflate in or about 1995, resulting in as much as 80 mm of surface uplift by 2000. Meanwhile, motion of the caldera floor changed from uplift to subsidence during 1997–8. The north rim area rose, while the entire caldera floor (including both domes) subsided until 2002, when both motions paused. Uplift in the northeast part of the caldera resumed in mid-2004 at a historically unprecedented rate of as much as 70 mm/yr, while the north rim area subsided at a lesser rate. Resurveys of the level line across the northeast part of the caldera in 2005 and 2007 indicated the greatest average uplift rate since the initial survey in 1923—53±3 mm/yr. Data from a nearby continuous GPS (CGPS) station showed that the uplift rate slowed to 40–50 mm/yr during 2007–8 and to near zero by September 2009. Following an intense earthquake swarm during January–February 2010, this one near the northwest caldera rim and the strongest since the 1985 swarm in the same general area, CGPS stations recorded the onset of subsidence throughout the entire caldera.

Any viable model for the cause(s) of ground deformation at Yellowstone should account for (1) three distinct deformation sources and their association with both resurgent domes and the north caldera rim; (2) interplay among these sources, as suggested by the timing of major changes in deformation mode; (3) migration of the area of greatest subsidence or uplift from the northeast part of the caldera to the southwest part during 1992–95 and 1995–97, respectively; (4) repeated cycles of uplift and subsidence and sudden changes from uplift to

[1]U.S. Geological Survey, David A. Johnston Cascades Volcano Observatory, 1300 S.E. Cardinal Court, Building 10, Suite 100, Vancouver, WA 98683-9589.

[2]U.S. Geological Survey, 345 Middlefield Road, MS 977, Menlo Park, CA 94025.

[3]U.S. Geological Survey, Hawaiian Volcano Observatory, 1 Crater Rim Drive, Hawaii National Park, HI 96718.

subsidence or vice versa; (5) spatial and temporal relationships between changes in deformation mode and strong earthquake swarms; and (6) lateral dimensions of all three deforming areas that indicate source depths in the range of 5 to 15 km.

We prefer a conceptual model in which surface displacements at Yellowstone are caused primarily by variations in the flux of basaltic magma into the crust beneath the caldera. Specifically, we envision a magmatic conduit system beneath the northeast part of the caldera that supplies basalt from a mantle source to an accumulation zone at 5–10 km depth, perhaps at a rheological boundary within a crystallizing rhyolite body remnant from past eruptions. Increases in the magma flux favor uplift of the caldera and decreases favor subsidence. A delicate equilibrium exists among the mass and heat flux from basaltic intrusions, heat and volatile loss from the crystallizing rhyolite body, and the overlying hydrothermal system. In the absence of basalt input, steady subsidence occurs mainly as a result of fluid loss from crystallizing rhyolite. At times when a self-sealing zone in the deep hydrothermal system prevents the escape of magmatic fluid, the resulting pressure increase contributes to surface uplift within the caldera; such episodes end when the seal ruptures during an earthquake swarm. To account for the north rim deformation source, we propose that magma or fluid exsolved from magma episodically escapes the caldera system at the three-way structural intersection of (1) the northern caldera boundary, (2) an active seismic belt to the north-northwest that is associated with the Hebgen Lake fault zone, and (3) the Norris–Mammoth corridor—a zone of faults, volcanic vents, and thermal activity that strikes north from the north rim of the caldera near Norris Geyser Basin to Mammoth Hot Springs near the northern boundary of Yellowstone National Park. Increased fluid flux out of the caldera by way of this intersection favors subsidence of the north rim area, and decreased flux favors uplift. This model does not account for poroelastic and thermoelastic effects, nonelastic rheology, or heat and mass transport in the hot and wet subcaldera crust. Such effects almost surely play a role in caldera deformation and are an important topic of ongoing research.

Introduction

Even the largest and deadliest volcanic eruption on Earth during historical time, the 1815 eruption of Mount Tambora on the island of Sumbawa, Indonesia, pales in comparison to the greatest eruptions in our planet's geologic history. The Tambora eruption (1) ejected 30–33 km^3 (magma volume) of trachyandesite magma (Self and others, 2004); (2) formed a caldera 6 km in diameter; (3) killed ~10,000 people directly by bomb impacts, tephra fall, pyroclastic flows, and tsunamis; and (4) produced the "year without a summer" in 1816, which resulted in an additional ~100,000 deaths by starvation, disease, and hunger (Stothers, 1984; Rampino and others, 1988). For comparison, the Yellowstone eruption that produced the Lava Creek Tuff at 0.64 Ma (millions of years before the present) ejected more than 1,000 km^3 of rhyolitic magma and formed a caldera 45 by 85 km across. Yellowstone's 2.1 Ma Huckleberry Ridge Tuff eruption was even larger, with more than 2,450 km^3 of magma ejected and collapse of a caldera measuring perhaps 100 by 60 km across (Christiansen, 2001). There is ample evidence that the Yellowstone magmatic system is still active and likely to erupt again, although the timing, nature, and size of the next eruption cannot be anticipated. Therefore, understanding the current state of the Yellowstone system—including the implications of its dynamic hydrothermal activity, pervasive seismicity, rapid ground motion, high heat flow, and copious gas emissions—is important for both scientific and hazard-assessment reasons.

With reference to ground motion, we have learned in recent decades that restless silicic caldera systems, such as Yellowstone (Wyoming), Long Valley (California), Rabaul (Papua New Guinea), and the Phlegraean Fields (Italy) can be remarkably dynamic—with or without an ensuing eruption (Newhall and Dzurisin, 1988). At Yellowstone, much of this new knowledge has been garnered through repeated leveling surveys, GPS observations, and interferometric synthetic aperture radar (InSAR) deformation imagery. The historical record at Yellowstone is not nearly as long as at the Phlegraean Fields, nor has the amount of surface displacement at Yellowstone been as great as at the Phlegraean Fields or at Rabaul. Although Yellowstone has not erupted during historical time, as have the Phlegraean Fields (1537) and Rabaul (1937, 1994, and other smaller events), we are fortunate to have a relatively complete record from surficial geology of surface deformation throughout postglacial time, a relatively long historical record from leveling, and very detailed information in recent years from both InSAR and a large network of continuous GPS (CGPS) stations. As a result, we have learned that (1) parts of this largest of all restless calderas can move up or down at rates of tens of millimeters per year; (2) the transition from uplift to subsidence or vice versa can occur in a matter of weeks or months; (3) such changes in deformation mode generally are associated with strong earthquake swarms; and (4) there are three distinct deformation sources beneath the caldera that interact in ways that are poorly understood. For these reasons and many others, Yellowstone is a special place that deserves careful scientific study. Here, we compile and discuss results of an ongoing study of Yellowstone's remarkable ground motions, using one technique that is more than a century old (leveling) and another at the forefront of modern geodesy (InSAR).

Introduction to Yellowstone Geography and Place Names

Today the 85-by-45 km Yellowstone caldera is nearly invisible to the untrained eye—largely buried beneath post-caldera rhyolite flows with a veneer of glacial deposits that support verdant subalpine forest and meadows, punctuated by thermal

basins and home to Yellowstone's renowned wildlife. With its winding roads and locally dense forest, Yellowstone National Park can be difficult to navigate for the first-time visitor. Likewise, grasping the geography of the park and the relationships among place names, structural features, and overlapping time scales for leveling and InSAR observations could be a daunting task for the reader. To make the job easier for those unfamiliar with the area, we offer the following primer on relevant Yellowstone geography and place names. Readers who know their way around Yellowstone might want to skip to the next section, where we describe a large body of previous scientific work as context for the leveling and InSAR results.

Established by the U.S. Congress and signed into law by President Ulysses S. Grant on March 1, 1872, Yellowstone National Park—the world's first national park—was included in the World Network of Biosphere Reserves by the United Nations Educational, Scientific, and Cultural Organization (UNESCO) in 1976 and was designated a UNESCO World Heritage Site in 1978. The park spans an area of 8,980 km^2 at the northeast end of the Snake River Plain in the states of Wyoming, Montana, and Idaho. It is accessible by road from five entrances: (1) the North Entrance near Mammoth, Wyoming; (2) the Northeast Entrance near Silver Gate and Cooke City, Montana; (3) the East Entrance west of Cody, Wyoming; (4) the South Entrance north of Jackson, Wyoming; and (5) the West Entrance near West Yellowstone, Montana (fig. 1). The entrance roads connect to the 230-km-long Grand Loop Road, a figure-eight pattern of roads that provide access to the park's front-country attractions by way of Mammoth Hot Springs Junction, Tower-Roosevelt Junction, Canyon Junction, Fishing Bridge Junction, West Thumb Junction, Madison Junction, and Norris Junction. The Old Faithful area is located between West Thumb Junction and Madison Junction. The area named Lake is about 3 km southwest of Fishing Bridge Junction along the north shore of Yellowstone Lake; Grant Village is about 5 km southeast of West Thumb Junction. Most of the park is designated wilderness and accessible only by trails or, in areas of critical wildlife habitat, is off-limits to human visitation.

The Yellowstone caldera occupies approximately one-third of the area of Yellowstone National Park and is accessed by the southern half of the Grand Loop Road (fig. 1). Two resurgent domes are located within the caldera—the Mallard Lake dome in the southwest part and the Sour Creek dome in the northeast part. Madison Junction, Norris Junction, and Canyon Junction are located near the north topographic rim of the caldera. Fishing Bridge Junction and West Thumb Junction are located in the central part of the caldera near the north and west shore of Yellowstone Lake, respectively. With an area of 352 km^2 and maximum depth of 118 m, Yellowstone Lake is the largest body of water in Yellowstone National Park. Other large lakes in the park include Shoshone Lake, Lewis Lake, and Heart Lake. Hebgen Lake is located just outside the park's western boundary; the Hebgen Lake fault zone strikes northwest–southeast and extends to the northwest caldera rim near Madison Junction. The Yellowstone River at Fishing Bridge is the outlet for Yellowstone Lake; an important part of the Yellowstone leveling network follows the road that parallels the course of the Yellowstone River across the northeast part of the caldera between Fishing Bridge Junction and Canyon Junction. Another part crosses the southwest part from Lewis Falls near the south shore of Lewis Lake to Madison Junction, by way of West Thumb Junction and the Old Faithful area.

The Yellowstone leveling network generally follows the public road system throughout the park, including the entire Grand Loop Road and spurs to each of the park's five entrances (fig. 1). In addition, a backcountry line crosses the southern half of the Grand Loop figure-8 along the Mary Mountain trail (figs. 5 and 6). The part of the network that has been surveyed most often is the cross-caldera line between Lake Butte, located on the topographic rim of the caldera along the East Entrance road, and Mount Washburn on the opposite rim. The line follows the East Entrance Road along the northeast shore of Yellowstone Lake from Lake Butte to Fishing Bridge Junction. There, it joins the Grand Loop Road and swings northwestward along the Yellowstone River by way of Le Hardys Rapids, the Mud Volcano area, Hayden Valley, and Canyon Junction. Le Hardys Rapids is an important location because the greatest amount of uplift or subsidence along the Lake Butte–Mount Washburn line typically occurs within a few kilometers of the rapids.

To simplify the discussion, we use generalized locations and a small set of specific place names to describe the observations and modeling results whenever possible. For example, we refer to the southwest, central, and northeast parts of the caldera, to the Norris area along the north caldera rim, and to the Mallard Lake and Sour Creek resurgent domes. Of particular interest are two roughly parallel level lines that skirt the resurgent domes—(1) across the northeast part of the caldera between Lake Butte and Mount Washburn by way of the Sour Creek resurgent dome at Le Hardys Rapids and (2) across the southwest part of the caldera from Lewis Falls to Madison Junction by way of the Mallard Lake resurgent dome at Isa Lake and the Old Faithful area. Roughly perpendicular to those two level lines and coincident with the long axis of the elliptical caldera is an axis of maximum surface uplift and subsidence (fig. 6). Le Hardys Rapids and Isa Lake are located near that axis, so we speak of uplift in the northeast part of the caldera centered near Le Hardys Rapids or subsidence of the southwest part centered near Isa Lake, or (equivalently) we refer to uplift of the Sour Creek dome or subsidence of the Mallard Lake dome.

An additional level of specificity is required to report leveling results at individual benchmarks—for example, the amount of uplift or subsidence for a particular time period at mark DA3 1934 near Le Hardys Rapids or 51 MDC 1976 near Isa Lake (for example, figs. 7–10, 16). Throughout the text, a four-digit number at the end of a benchmark name indicates the year in which the mark was installed. The year is part of the benchmark name, and in a few cases the full name is necessary to distinguish between mark names that otherwise

would be ambiguous (for example, 11 MDC 1976 and 11 MDC 1977, both in Yellowstone National Park).

Previous Work

Yellowstone is one of the most intensively studied large silicic magma systems on Earth. Its structure and eruptive history are known from detailed geologic mapping and petrologic studies (Christiansen, 2001), and the configuration of its magmatic system has been inferred from seismic and other geophysical investigations (Smith and others, 1982; Smith and Siegel, 2000). Conditions within its hydrothermal system have been deduced from observational, experimental, and theoretical studies (Fournier, 1989, 1999, 2007; Fournier and Thompson, 1993) and by scientific drilling (Allen and Day, 1935; Fenner, 1936; White and others, 1971, 1975). This section includes brief summaries and key references for each of these major lines of investigation to provide necessary context for the main subject of this report—the remarkable record of surface displacements at Yellowstone. The report deals mainly with leveling and InSAR results for 1983–2008, because the authors have first-hand experience with those datasets. For completeness, we also discuss (1) results from earlier leveling surveys, including those pertinent to coseismic and postseismic motions associated with two large historical

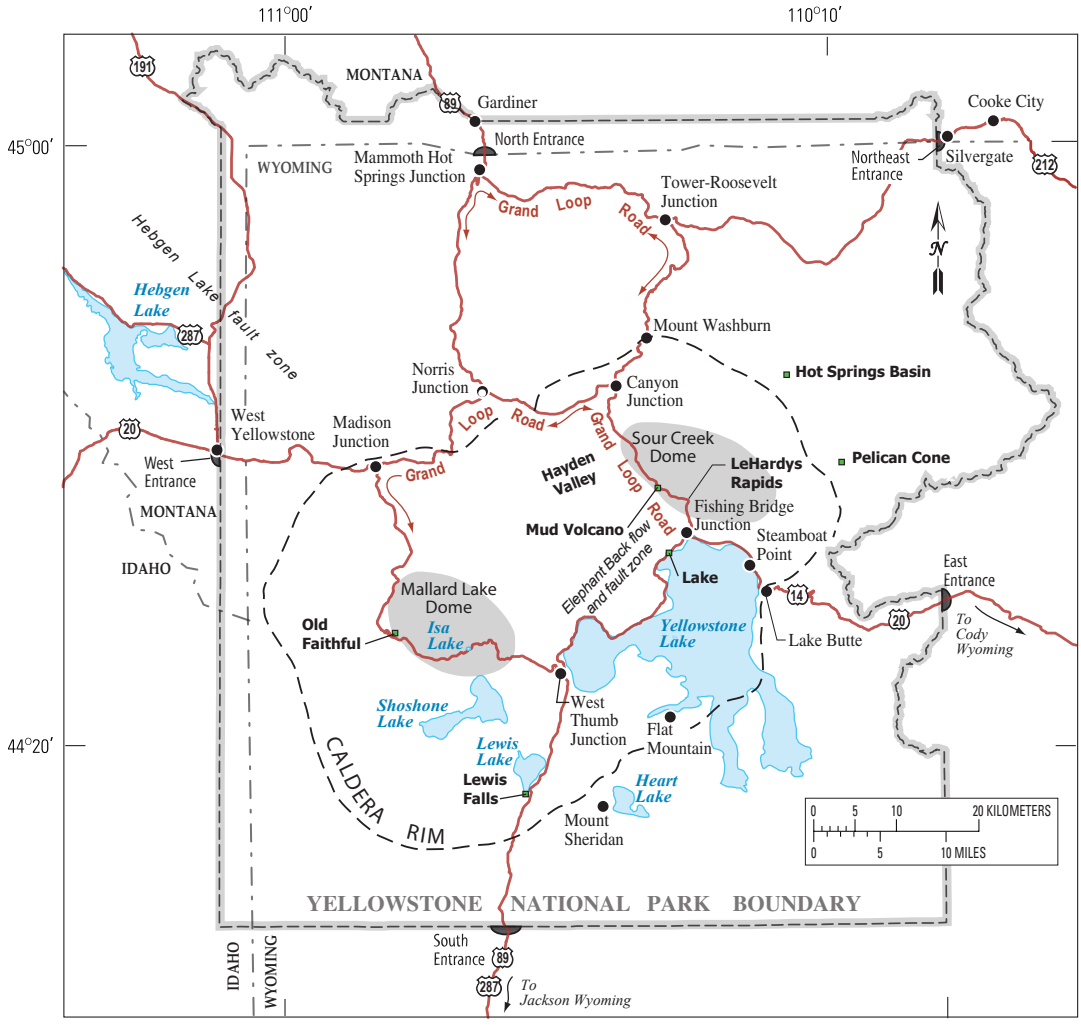

Figure 1. Map of Yellowstone National Park showing the Yellowstone caldera and its two resurgent domes, the park's five entrances and public road system with major junctions, large lakes, and other place names used in the text. See figure 4 for the relation between the Yellowstone caldera shown here and two older calderas on the Yellowstone Plateau. Figures 5 and 6 show the network of level lines in and around Yellowstone National Park, which mostly follows the public road system shown here. The Yellowstone River flows northwestward from the outlet of Yellowstone Lake near Fishing Bridge Junction by way of Le Hardys Rapids to near Canyon Junction and beyond. The Grand Loop Road parallels the river in this area, and one of the main level lines discussed in the text follows the road.

earthquakes in the Yellowstone region; (2) surficial-geology studies that extend the deformation record back in time for several thousand years; and (3) CGPS observations that bring the record up to date since the most recent leveling and InSAR observations in 2007–8. Readers who are familiar with the scientific literature dealing with Yellowstone's eruptive history, magmatic system, and hydrothermal system might prefer to skip this section. Others might find it helpful as context for what follows. Additional information is available in numerous publications cited in the text.

Christiansen (2001) provides an excellent summary of the development of scientific knowledge about Yellowstone, beginning with F.V. Hayden's Geological and Geographical Survey of the Territories (Hayden, 1872; 1873; Bradley, 1873; Peale, 1873). According to Christiansen (2001, p. G3), "Hayden's perceptive first description of the Yellowstone Plateau, viewed from the summit of Mount Washburn, even anticipates the concept of the Yellowstone caldera." Christiansen quotes Hayden (1872, p. 81):

> From the summit of Mount Washburn, a bird's-eye view of the entire basin may be obtained, with the mountains surrounding it on every side without any apparent break in the rim * * *. It is probable that during the Pliocene period the entire country drained by the sources of the Yellowstone and the Columbia was the scene of as great volcanic activity as that of any portion of the globe. It might be called one vast crater, made up of thousands of smaller volcanic vents and fissures out of which the fluid interior of the earth, fragments of rock, and volcanic dust were poured in unlimited quantities * * *.

The view across the Yellowstone caldera from the summit of Mount Washburn, and the opposing view from the summit of Lake Butte toward Mount Washburn, are mostly unchanged since Hayden's time (figs. 2 and 3).[4] What has changed dramatically is our understanding of Yellowstone's tumultuous volcanic history, due in large part to four decades of meticulous study by Christiansen and others. This monumental body of work, documented in Christiansen (2001) and several other seminal papers on the subject (for example, Christiansen, 1984; Christiansen and others, 2002, and references therein; Morgan and others, 2009), defines the current state of knowledge concerning the Yellowstone caldera, the eruptive history of the Yellowstone Plateau volcanic field, and the evolution of the Yellowstone magmatic system.

We know from Christiansen's (2001) work that the Yellowstone caldera is the youngest of three collapse calderas in the Yellowstone Plateau volcanic field of Wyoming, Idaho, and Montana (fig. 4). The first caldera formed 2.1 Ma during eruption of the Huckleberry Ridge Tuff, a rhyolitic ash-flow sheet of more than 2,450 km^3 that was emplaced over an area of 15,500 km^2 (Christiansen, 2001, p. G53–G63). The more than 280-km^3 Mesa Falls Tuff was emplaced 1.3 Ma over nearly 2,700 km^2, resulting in formation of the approximately 16-km-diameter second-cycle caldera (Christiansen, 2001, p. G64–G66). The third Yellowstone Plateau volcanic cycle, which began about 1.2 Ma, culminated at 0.64 Ma with eruption of the >1,000-km^3 Lava Creek Tuff over more than 7,500 km^2 and collapse of the 85-by-45 km Yellowstone caldera.[5] The Sour Creek structural dome in the northeast part of the caldera became resurgent soon after caldera collapse, and the present Mallard Lake dome in the southwestern part formed about 160 ka (thousands of years before the present) in response to renewed influx of magma beneath the caldera.[6] In a series of eruptive episodes at 164 ka, 152 ka, 114 ka, 102 ka, and 72 ka, intracaldera rhyolitic lava flows with an aggregate volume of more than 500 km^3 partly filled the caldera and in places overtopped its rim (Christiansen, 2001. p. G16–G48). As recently as 59.15 ± 1.97 ka ($^{40}Ar/^{39}Ar$ age), the Obsidian Creek rhyolite flows erupted just north of the Yellowstone caldera near the south end of the Norris–Mammoth corridor (Wooton and Spell, 2007).[7] Since Yellowstone's most recent magmatic eruption, an extensive hydrothermal system has developed within the caldera (Fournier, 1989). At least 18 large hydrothermal explosions have formed craters more than 100 m wide since the Yellowstone Plateau was last glaciated about 16 ka, and at least 26 smaller hydrothermal explosions have been documented since the park was established in 1872; others undoubtedly escaped observation (Muffler and others, 1971; Christiansen and others, 2007). Considering the prospects for future volcanism at Yellowstone, Christiansen (2001, p. G131) concluded:

[4]On March 1, 1872, President Ulysses S. Grant signed a declaration by the United States Congress that established Yellowstone National Park "* * * as a public park or pleasuring ground for the benefit and enjoyment of the people." The newly formed National Park Service was given jurisdiction over the country's first national park and charged with preserving its natural wonders for future generations. National Park Service stewardship of Yellowstone has endured numerous challenges over the years, none more daunting than those faced by park managers today. For a fascinating personal account of the pressures involved in preserving the United States' premier national park from the perspective of a former Chief Ranger at Yellowstone, see Sholly and Newman (1991).

[5]Christiansen (2001) refers to the three calderas of the Yellowstone Plateau volcanic field as the first-cycle caldera (2.1 Ma), the second-cycle caldera (1.3 Ma), and the Yellowstone caldera (0.64 Ma). The associated ash-flow sheets he designates are the Huckleberry Ridge Tuff, Mesa Falls Tuff, and Lava Creek Tuff, respectively. Other authors have used the names Huckleberry Ridge caldera, Island Park caldera, and Lava Creek caldera.

[6]Christiansen (2001, p. G39) states: "The present [Mallard Lake] dome, on which only the Mallard Lake flow is exposed, must be about 160,000 years old * * *. Nevertheless, some evidence suggests that there may also have been early resurgent doming of the Mallard Lake block * * *."

[7] The Norris–Mammoth corridor is a zone of faults, volcanic vents, and thermal activity that strikes north from the north rim of the Yellowstone caldera near Norris Geyser Basin to Mammoth Hot Springs near the northern boundary of Yellowstone National Park. It contains most of the young rhyolitic domes and basaltic lava vents of the past few hundred thousand years that are located outside the caldera margin (White and others, 1988, p. 3–4, 73–77).

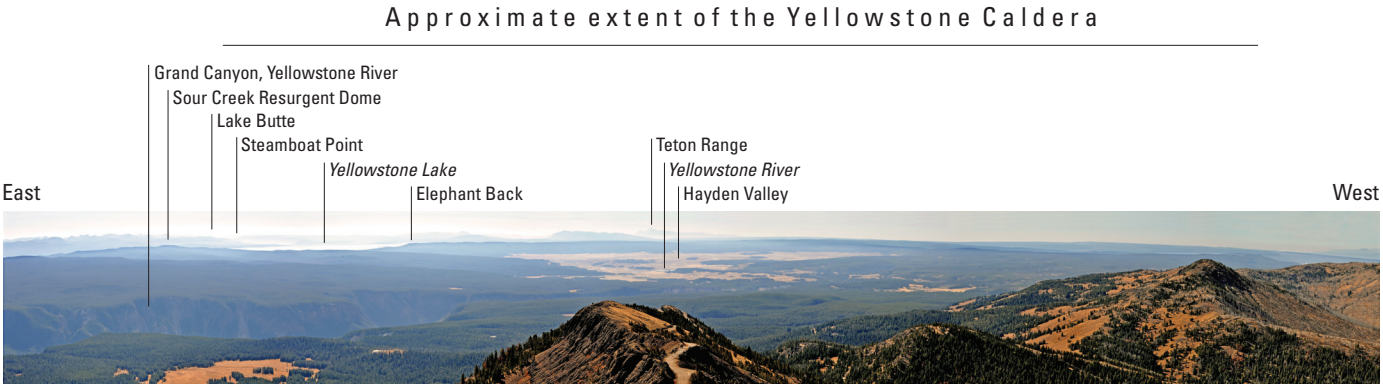

Figure 2. Panoramic photograph looking south across the Yellowstone caldera, Yellowstone National Park, from Mount Washburn, a Tertiary volcanic assemblage that forms part of the northeast caldera rim. The Grand Canyon of the Yellowstone River is visible in the middle ground in the left part of the image. Lake Butte, the vantage point for figure 3, is visible in the distance along the east (left) shore of Yellowstone Lake. Features visible in both figure 2 and figure 3 include the Sour Creek resurgent dome, Steamboat Point, Elephant Back lava flow, and Teton Range. Visible in the left center of this image is the route taken by a level line that was measured in 1923 and repeatedly measured from 1976 to 2007. The line extends from the south flank of Mount Washburn to Canyon Village Junction, through Hayden Valley, past Le Hardys Rapids and the nose of the Elephant Back lava flow and through Fishing Bridge Junction southeastward, past Steamboat Point, to the vicinity of Lake Butte—a road distance of 50 km. The route was chosen because it included Le Hardys Rapids, the site of maximum uplift measured by leveling surveys in 1923 and 1975–77, and because it is the shortest road route across the 85-by-45-km caldera. (USGS composite photograph by D. Dzurisin.)

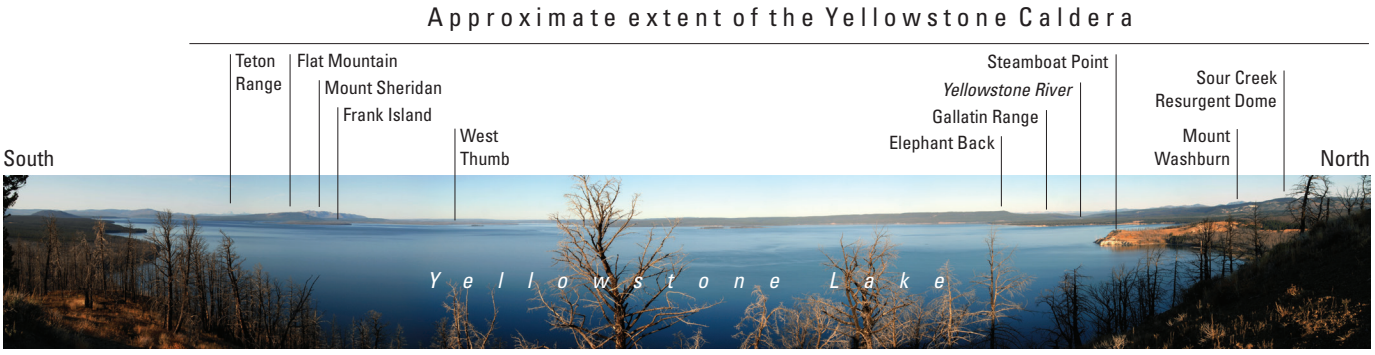

Figure 3. Panoramic photograph looking west across the Yellowstone caldera, Yellowstone National Park, from Lake Butte, an intrusive mass of Tertiary age that forms part of the east caldera rim. The topographic basin occupied by the caldera is approximately 85 km southwest-northeast by 45 km northwest-southeast. The northern part of Yellowstone Lake, in the foreground, occupies about 10 percent of the basin, which is largely buried by rhyolite lava flows that erupted from vents within the caldera between 151.4 ka and 71.2 ka (Christiansen, 2001). The Elephant Back lava flow, visible on the skyline in the right third of the image, is among the oldest of the intracaldera flows. Flat Mountain, 20 km distant and in the left third of the image, forms part of the south caldera rim. Mount Washburn, the vantage point for figure 2, is 34 km distant and near the right edge; it forms part of the northeast rim. The Teton Range, 100 km distant and near the left edge, is one of several ranges trending north-south to northwest-southeast that predate the caldera and remain seismically active. Other examples are the Madison Range and Gallatin Range to the north; the latter is visible in the right third of the image. A 50-km-long level line across the caldera floor from Lake Butte to Mount Washburn by way of Steamboat Point, Le Hardys Rapids (Yellowstone River near nose of Elephant Back flow), and Hayden Valley was measured in 1923 and repeatedly measured from 1976 to 2007 to study uplift and subsidence of the caldera floor. (USGS composite photograph by D. Dzurisin.)

> No rhyolitic eruptions have occurred for about 70,000 years within the third-cycle source area of the volcanic field, and rhyolitic volcanism related to this cycle may have waned. The very high heat flow represented by the Yellowstone hydrothermal system, however, as well as individually inconclusive geologic, gravity, aeromagnetic, geodetic, and seismic evidence, together suggest that rhyolitic magma is still crystallizing and perhaps still rising below the plateau region.

The seismic and other geophysical evidence for magma beneath Yellowstone to which Christiansen (2001) refers was summarized by Eaton and others (1975), who wrote (p. 795–6):

> Doming 150,000 years ago, followed by voluminous rhyolitic extrusions as recently as 70,000 years ago, and high convective heat flow at present indicate that the latest phase of volcanism may represent a new magmatic insurgence. These observations, coupled with (i) localized postglacial arcuate faulting beyond the northeast margin of the Yellowstone caldera, (ii) a major gravity low with steep bounding gradients and an amplitude regionally atypical for the elevation of the plateau, (iii) an aeromagnetic low reflecting extensive hydrothermal alteration and possibly indicating the presence of shallow material above its Curie temperature, (iv) only minor shallow seismicity within the caldera (in contrast to a high level of activity in some areas immediately outside), (v) attenuation and change of character of seismic waves crossing the caldera area, and (vi) a strong azimuthal pattern of teleseismic P-wave delays, strongly suggest that a body of magma underlies the region of the rhyolite plateau, including the Tertiary volcanics immediately to its northeast.

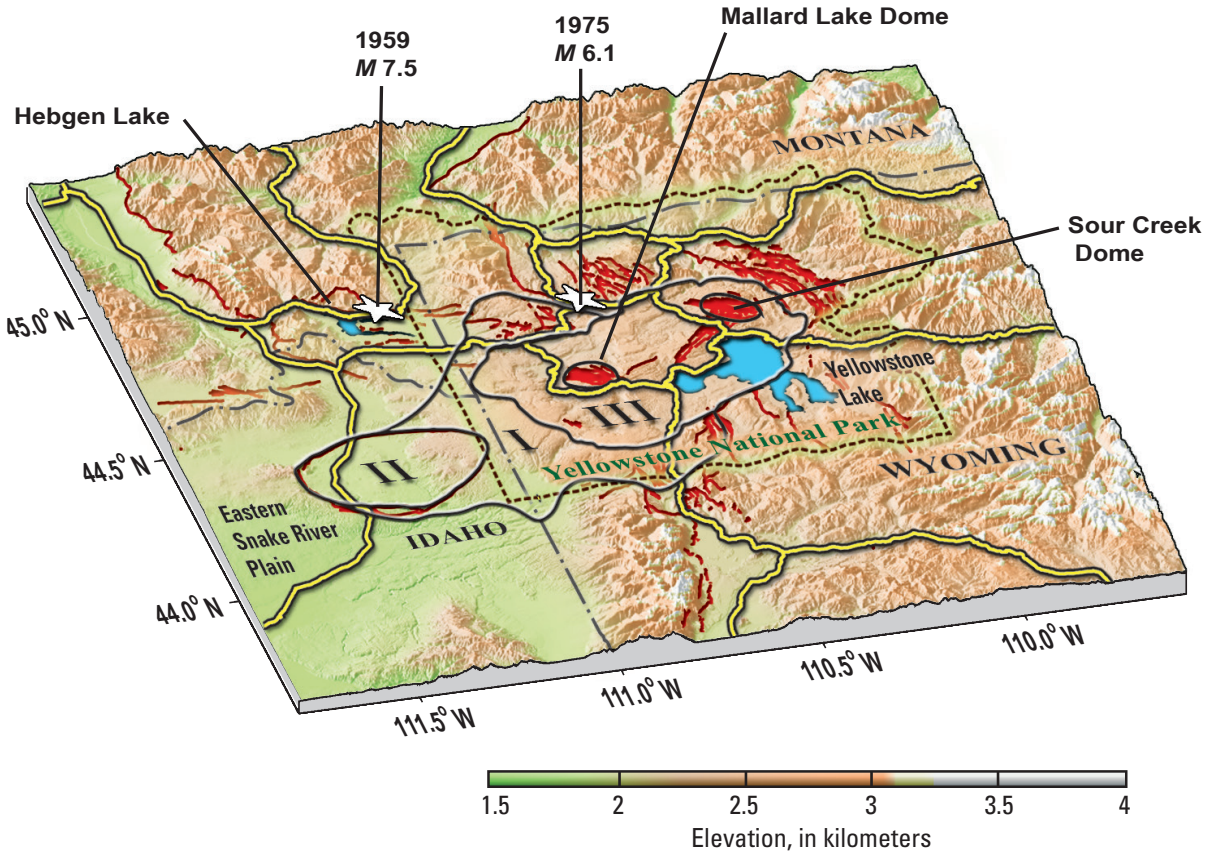

Figure 4. Oblique map diagram of eastern Snake River Plain and Yellowstone Plateau with outlines of three youngest calderas: (I) 2.1 Ma stage 1; (II) 1.3 Ma stage 2; and (III) 0.64 Ma Yellowstone caldera (Christiansen, 2001). The stage-1 caldera is largest; the stage-2 caldera and the Yellowstone caldera lie entirely within the stage-1 caldera. Also shown, outlines of Mallard Lake and Sour Creek resurgent domes. White stars indicate epicenters of 1959 M_s (surface-wave magnitude) 7.5 Hebgen Lake earthquake and 1975 *M* 6.1 Yellowstone Park earthquake.

Eaton and others' (1975) conclusion that magma exists today in the crust beneath Yellowstone has been corroborated by more than three decades of subsequent geophysical investigations, which are documented or summarized in numerous publications (for example, Smith and Braile, 1984, 1994; Smith and Siegel, 2000; Waite and Smith, 2002; Husen and others 2004; Waite and others, 2005, 2006; Lowenstern and others, 2006; Lowenstern and Hurwitz, 2008). The fact that post-caldera basaltic volcanism has occurred around the periphery of, but not inside, the Yellowstone caldera leads to the same conclusion—the presence of a body of partly molten silicic magma in the crust beneath the caldera that prevents denser, basaltic magmas from rising to the surface (Hildreth, 1981; Hildreth and others, 1991; Christiansen, 2001).

There is general agreement that Yellowstone is underlain by a persistent source of mantle-derived, basaltic magma—the Yellowstone hotspot—that produced a linear track of silicic, caldera-forming volcanism stretching from the vicinity of the Oregon-Nevada-Idaho border at 16 Ma to the Yellowstone Plateau today.[8] Whether the Yellowstone hotspot (1) fits the deep-mantle plume model with convection originating at the core-mantle boundary (for example, Morgan, 1971, 1972a,b; Pierce and Morgan, 1992; Smith and Braile, 1994), (2) fits an upper-mantle model with convective plumes rising from a phase-change discontinuity at 410 or 660 km depth (for example, Waite and others, 2006), or (3) instead reflects feedback between upper-mantle convection and regional lithospheric tectonics (Christiansen and others, 2002), remains unresolved. However, we suspect that Waite and others (2006, p. B04303) are correct in their assessment that all three models are relevant at Yellowstone:

> Upper mantle convection models are not contradicted by a [deep] plume model. Rather, convection, lithosphere convection, and upwelling from below likely work together at Yellowstone. Small-scale convection helps explain the strong low-velocity anomaly beneath Yellowstone and the Snake River Plain to ~200 km depth. The high topography on both sides of the ESRP [Eastern Snake River Plain] may be supported by melt residuum that has been pushed away from the upwelling zone under the ESRP. The possible eastward migration of the basin-range extensional regime is partly a consequence of the active system moving in the direction opposite plate motion. Without all three mechanisms, Yellowstone volcanism may not have persisted for ~16 million years.

Germane to our discussion of ground deformation at Yellowstone, all three models for the origin of the Yellowstone hotspot include high intrusion rates of basaltic magma, comparable to the Hawaiian hotspot and as much as 100 times greater than the long-term eruption rate of rhyolite in Yellowstone (0.003 km^3/yr; Christiansen, 2001).

Lowenstern and Hurwitz (2008) make a compelling case for a high intrusion rate of basalt into the lower to mid-crust beneath Yellowstone, although they do not exclude an alternative scenario involving convection of a large volume of low viscosity basalt in the lower crust with episodic release of gases. The Yellowstone system emits at least 45,000±16,000 metric tons per day of CO_2, which is about 5 percent of the global volcanogenic CO_2 flux (Werner and Brantley, 2003). Werner and Brantley (2003) estimate that only 30–50 percent of that total is derived from pre-Tertiary basement rocks; the remainder must have exsolved from magma. Lowenstern and Hurwitz (2008) argue that the only plausible source for that much CO_2 is approximately 0.3 km^3/yr of basalt degassing beneath the caldera. The volume of silicic magma that is estimated to exist beneath the caldera (~1.5×10^4 km^3; Lowenstern and others, 2006) is an insufficient source, because Yellowstone silicic magmas contain less than 500 parts per million dissolved CO_2. At the observed CO_2 degassing rate, the silicic reservoir would be entirely purged of dissolved CO_2 in about 1,000 years. Lowenstern and Hurwitz (2008, p. 37) point out: "Assigning the annual CO_2 flux to a plausible amount of annually degassed and crystallized rhyolitic magma (0.1 km^3; Fournier 1989) requires 5.5 wt percent CO_2, about 20 times that which can be dissolved at 400 MPa (~16 km depth) in rhyolitic liquid (Lowenstern, 2001)." Simply stated, the remarkably high CO_2 flux at Yellowstone can be explained only if the caldera system is underlain by a large reservoir of basaltic magma that is persistently replenished—by intrusion, convection, or both—at a rate comparable to that attributed to the Hawaiian hotspot.

The same conclusion is supported by the relative proportions of magmatic gases emitted at Yellowstone. Lowenstern and Hurwitz (2008, p. 37) note that "* * * orders of magnitude more CO_2 is emitted through the Yellowstone hydrothermal system than Cl, F, or S * * *." Silicate melt inclusions in Yellowstone rhyolitic lavas contain abundant dissolved Cl and F, but scarce CO_2 and S. Basaltic magmas, in contrast, generally contain lower concentrations of dissolved Cl and F, and 10–30 times more dissolved CO_2 than mid-crustal rhyolites. This is due in part to the fact that basalt becomes supersaturated with CO_2 at lower crustal depths. Lowenstern and Hurwitz (2008, p. 37) conclude: "* * * basaltic intrusions could contain 50 to 100 times more available CO_2 than the silicic magmas themselves. The basaltic input means that magma continues to accumulate and sustains the overlying silicic magma reservoir * * *."

Heat from magmatic intrusions in the crust, both fresh influxes of basalt and older, cooling bodies of rhyolite, powers Yellowstone's extensive hydrothermal system. Thermal output

[8]Several authors, including Pierce and Morgan (1992) and Smith and Braile (1994), have noted the following age progression in silicic volcanic fields and associated calderas: McDermitt (Nevada, 16.1 Ma), Owyhee (Idaho, 13.8 Ma), Bruneau–Jarbridge, Twin Falls, and Picabo (Idaho, 11.3–10.3 Ma, respectively), Heise (Idaho, 6.5–4.3 Ma), and Yellowstone (Wyoming, 2.1–0.6 Ma). The pattern is attributed to southwest motion of the crust relative to a mantle hotspot at an average rate of 4.5 cm/yr—a combination of North American Plate motion (~2.5 cm/yr) and crustal extension (1–2 cm/yr). At the present time, the Yellowstone hotspot is beneath the northeast part of the Yellowstone Plateau, about 700 km northeast of the McDermitt volcanic field.

of the Yellowstone system is calculated to be in the range 4.5–6.0 gigawatts (Fournier 1989; Friedman and Norton, 2007), which corresponds to 1,550–2,100 milliwatts per square meter over the 2,900-km^2 Yellowstone caldera. This heat flux density is 30–40 times that of the neighboring Rocky Mountains. Lowenstern and Hurwitz (2008, p. 36) point out:

> If this high surface heat flux were transferred by conduction alone, it would imply a temperature gradient of 700 to 1000°C per kilometer (Fournier 1989), suggesting the presence of very shallow magma; however, research drilling in the 1960s (White et al. 1971) revealed temperature–depth relations inconsistent with temperatures exceeding ~310°C at 1000 m. Clearly, the enormous hydrothermal system is able to act as a wick, transferring heat advectively from a deep but very large magma source.

Various interactions among basaltic intrusions, a large rhyolitic body containing an unknown proportion of partial melt[9], and the overlying hydrothermal system are key to understanding the possible causes of ground deformation at Yellowstone (see, for example, Dzurisin and others, 1990). This subject is explored below in the Discussion section, following a description of leveling, InSAR, and other ground deformation observations.

Nature of This Report

This report (1) summarizes knowledge about Yellowstone's eruptive history, magmatic system, and hydrothermal system, particularly as those topics pertain to the interpretation of ground deformation measurements; (2) describes the history of leveling and InSAR observations at Yellowstone, as well as other evidence for paleo and contemporary ground deformation; (3) discusses the evolution of thought concerning the mechanisms of ground deformation at Yellowstone; and (4) provides an archive of information concerning more than 500 geodetic benchmarks in Yellowstone National Park (see data files that accompany this report; in the printed version, these files are provided on a CD–ROM). We begin with an overview of leveling and InSAR results for 1983–2008 as an introduction to the dynamic nature of the Yellowstone system.

Historical Context

In 1980, the attention of many volcanologists was focused on Mount St. Helens in the aftermath of its historic landslide and eruption on May 18 (Lipman and Mullineaux, 1981). Starting one week after that monumental event, the tiny town of Mammoth Lakes, California, was rattled by an intense swarm of earthquakes, including four magnitude (*M*) 6 shocks on May 25–27, 1980. Mammoth Lakes is nestled in the south moat of the Long Valley caldera, between Mammoth Mountain and the caldera's resurgent dome, along the eastern front of the tectonically active Sierra Nevada range. In September 1980, first-order releveling of a line along U.S. Highway 395 across the western parts of the caldera floor and resurgent dome revealed about 250 mm of surface uplift centered on the dome since the previous survey in 1975.[10] Resurveys showed that the dome rose an additional 100 mm during 1980–82 and 70 mm during 1982–83, accompanied by more earthquake swarms. The latter period encompassed a particularly strong swarm in January 1983, this one with characteristics indicative of dike intrusion to within a few kilometers of the surface (Savage and Cockerham, 1984; Hill, 1984; Hill and others, 1985a,b). The unusual seismicity and ground deformation underscored the possibility of renewed volcanic activity in the area, and in May 1982 the United States Geological Survey (USGS) issued a Notice of Potential Volcanic Hazard (Miller and others, 1982; Miller, 1985; 1989).

In autumn 1983, concern over the developing situation at Long Valley by managers of the USGS Volcano Hazards Program led them to initiate a project, headquartered at the USGS Cascades Volcano Observatory (CVO) in Vancouver, Washington, to study processes of unrest at large silicic calderas. A primary objective of the Physical Processes in Large Silicic Magma Systems project was to establish a context for interpretation of the activity at Long Valley through comparisons with other restless calderas around the world (Newhall and Dzurisin, 1988). Two notable examples were the Phlegraean Fields caldera near Naples, Italy, and the Rabaul caldera in Papua New Guinea, where sporadic earthquake swarms and rapid ground uplift were generating concerns similar to those expressed for Long Valley. It was known from seismic monitoring, repeated leveling surveys, and water-level records from Yellowstone Lake that the Yellowstone caldera also had been restless, having risen at an average rate of 14 mm/yr between leveling surveys in 1923 and 1975–77 (Pelton and Smith, 1979; 1982; Hamilton, 1987). To determine whether the uplift at Yellowstone was continuing and, if so, to study it together with the uplift at Long Valley, CVO staff assigned to the Physical Processes in Large Silicic Magma Systems project decided to relevel a line across the Yellowstone caldera where the greatest uplift had been measured from 1923 to 1975–77.

[9]A recent modeling study by Chu and others (2010) of first teleseismic P-wave arrivals recorded by broadband seismic stations in Yellowstone National Park led those authors to identify a magma body at 5–15 km depth beneath the Yellowstone caldera with a volume greater than 4,300 km^3 and a porosity of about 32 percent—the latter filled with at least 90 percent rhyolite melt and 8 percent water-CO_2 by volume. That proportion of partial melt is considerably higher than indicated by earlier seismic tomography studies (for example, Miller and Smith, 1999; Husen and others, 2004), which place the number at a few to perhaps 10 percent. The discrepancy is sure to receive considerable attention from volcano seismologists following an upgrade of the Yellowstone broadband network in 2010–11.

[10]See section Results of Leveling Surveys and InSAR Observations, 1923–2008, for description of first-order and second-order leveling surveys.

Thus it was that Ken Yamashita, a recent transplant to CVO from the USGS Hawaiian Volcano Observatory (HVO), found himself in Yellowstone leveling through wind-driven snow in October 1983. He managed to complete 17 km of double-run, first-order leveling in three weeks before winter storms forced an end to the survey (see next section for discussion of differences between first-order and second-order leveling surveys). The plan had been to survey a 44-km traverse across the caldera floor where the greatest uplift had been measured by surveys in 1923 and 1975–77. Failure to finish the survey as planned caused some initial disappointment, but the reason soon became clear. Back at CVO, Yamashita discovered that the allowable discrepancy between two height differences measured at each setup of the leveling instrument had been incorrectly set at 0.03 mm, instead of the 0.30 mm value specified by the Federal Geodetic Control Committee (1984) for first-order leveling surveys. He had double-run 17 km of level line with a tolerance comparable to the diameter of a human hair and an order of magnitude more stringent than that specified for the most precise surveys conducted by the National Geodetic Survey (NGS)!

The mistake was corrected before the next Yellowstone leveling survey in September 1984, when the line was extended from Lake Butte on the southeast rim of the caldera by way of Fishing Bridge, Le Hardys Rapids, and Hayden Valley to Canyon Junction near the northeast rim—a distance along the line (stadia distance) of 44 km (figs. 1 and 6). The line was extended 5 km farther north to Mount Washburn in 1987 and, from 1983 to 2007, CVO staff members and dozens of volunteers measured part or all of the line 15 times (figs. 1, 6, 8, and 16). Results of the 1983 and 1984 surveys indicated that uplift of Le Hardys Rapids had continued since the 1975–77 survey, but thereafter the pattern changed. No additional uplift was detected by the 1985 survey and, starting in 1986 and continuing through 1995, Le Hardys Rapids and the adjacent Sour Creek resurgent dome subsided at rates comparable to or greater than the uplift rates measured previously. The discovery triggered renewed interest in the cause(s) of surface deformation at Yellowstone and other large silicic calderas, including Long Valley (Dzurisin and Yamashita, 1987; Dzurisin and others, 1990; 1994; 1999; Hill and others, 1985a,b). Soon, with the introduction of InSAR (then a new remote-sensing technique for measuring deformation), the puzzle became even more complicated.

The first useful InSAR image of the Yellowstone region showed subsidence in the vicinity of the Sour Creek dome during August 1992–June 1993, which was consistent with leveling results for the same period (Wicks and others, 1998).[11] No leveling was done along the Lake Butte–Mount Washburn line in 1994, but surveys in 1993 and 1995 indicated continued subsidence centered near Le Hardys Rapids. An interferogram for June 1993–August 1995 also showed subsidence of the Sour Creek dome, but even more subsidence of the Mallard Lake dome in the southwest part of the caldera. Uplift of the Sour Creek dome resumed during August 1995–September 1996, while subsidence of the Mallard Lake dome continued. By July 1995–June 1997, InSAR observations indicated that both domes were rising—a result that was corroborated by leveling along the Lake Butte–Mount Washburn line in September 1998 (Wicks and others, 1998; Dzurisin and others, 1999).

A third deformation source, this one beneath the north caldera rim near Norris Geyser Basin, was identified from InSAR images that collectively span 1996–2002 (Wicks and others, 2006). Localized uplift in that area was first detected by GPS surveys made in 1995 and 2000 (Puskas and others, 2007). As the north rim source inflated from 1995 to 1997, motion of the central part of the caldera, including both resurgent domes, changed from uplift to subsidence between late 1997 and early 1998. The north rim source continued to inflate, while the caldera floor subsided until 2002, when both motions paused (Wicks and others, 2006). Then, starting in mid-2004, CGPS observations and interferograms showed strong uplift of the entire caldera floor, at rates as high as 70 mm/yr, and lesser subsidence along the north caldera rim. Leveling surveys along the Lake Butte–Mount Washburn line in 2005 and 2007 likewise indicated historically high rates of uplift near Le Hardys Rapids. Uplift of the caldera floor slowed during 2007–8, and by September 2009, it had slowed to the point that it may have stopped (Yellowstone Volcano Observatory (YVO) Monthly Update issued January 4, 2010; http://volcanoes.usgs.gov/yvo/activity/archive/2009.php). An undertaking that started 25 years earlier, using a century-old surveying technique to monitor a pattern of ground motion that was thought to be simple in space and time, had evolved into a multifaceted investigation of a complex and unexpectedly dynamic system.

Results of Leveling Surveys and InSAR Observations, 1923–2008

Initial Leveling Surveys, 1923 and 1934

The history of geodetic measurements in the Yellowstone region begins in 1923, when the U.S. Coast and Geodetic Survey (USC&GS) conducted initial leveling surveys along first-order lines from Livingston, Montana, to Mammoth, Wyoming; from West Yellowstone, Montana, to Marysville, Idaho; and along second-order lines in Yellowstone National Park. Within the park the leveling network follows major roads, including the figure-eight-shaped Grand Loop Road and spurs to each of five park entrances (figs. 1, 5, and 6).[12] In 1934, the USC&GS did additional second-order surveys on lines from

[11]From 1984 to 2007, all of the CVO leveling surveys along the line from Lake Butte to Canyon Junction by way of Le Hardys Rapids were conducted in the month of September. The 1983 survey was conducted in October.

Bozeman, Sappington, and Monida, Montana, each of which terminate at the town of West Yellowstone, Montana (Holdahl and Dzurisin, 1991). West Yellowstone is along the western boundary of Yellowstone National Park, adjacent to the park's West Entrance (fig. 1). All of these lines are part of a nationwide vertical control network with a main purpose of establishing benchmark elevations, but they also provide a means to measure vertical surface displacements by repeated surveys. The primary purpose of the early USC&GS surveys was to upgrade the vertical control network in the Yellowstone region, not to serve as a baseline for future caldera deformation studies. In 1923, Yellowstone National Park had been in existence for more than 50 years, and it was time to tie its road system into the nation's vertical control network. At the time, no one could have imagined that some of the benchmark elevations established by the 1923 survey would change by several decimeters by the time they were resurveyed during 1975–77.

Procedures and Accuracy for Leveling Surveys

A report by the Federal Geodetic Control Committee (1984) establishes standards and specifications for geodetic control networks in the United States, including leveling networks and surveys. The FGCC report divides leveling surveys into five types based on the procedures and equipment used and on the expected accuracy. The most stringent specifications apply to first-order, class I networks and surveys, which provide the greatest precision. Next in order of decreasing precision are first-order, class II; second-order, class I and II; and third-order leveling surveys. The report specifies, for each order and class of leveling, the requirements for network geometry, instrumentation, calibration procedures, field procedures, and office procedures. All of the Yellowstone leveling surveys conducted by CVO between 1983 and 2007 conformed to first-order, class II standards or better. First-order, class I surveys are double-run; first-order, class II surveys can be single run (Dzurisin, 2007, p. 53–61).

The equipment and procedures used for leveling surveys at Yellowstone were described by Dzurisin and Yamashita (1987) and by Dzurisin and others (1990, 1994, and 1999). Uncertainties associated with leveling and InSAR observations are addressed in appendix A. Throughout this report, uncertainties in vertical displacement measurements from leveling surveys are expressed as one standard deviation from the combination of random leveling error and long-term benchmark instability. The one-sigma uncertainty in range changes (that is, line-of-sight surface displacements) from InSAR observations is difficult to specify, so we adopt what we believe to be a conservative estimate of ±1 cm (see appendix A).

[12]The public road system within Yellowstone National Park has changed since the 1923 leveling survey such that several segments of the leveling network now lie along closed service roads or trails. A notable example is a line along an abandoned road—now the Mary Mountain trail—across the central part of the Yellowstone caldera by way of Mary Lake (figs. 1 and 6).

1959 M_s 7.5 Hebgen Lake Earthquake, Coseismic and Postseismic Displacements

On August 18, 1959, the largest earthquake ever recorded in the Yellowstone region, the M_s (surface-wave magnitude) 7.5 Hebgen Lake earthquake, occurred about 20 km northwest of the northwest rim of the Yellowstone caldera and about 15 km north of West Yellowstone.[13] Within 24 hours, six aftershocks of M 5.5–6.3 had occurred in an east-west-trending zone nearly 100 km long, centered on the main shock. The Hebgen Lake earthquake caused 28 fatalities and extensive damage to highways and timber, produced a 26-km-long zone of surface faulting with scarps as high as 6 m, and triggered a catastrophic rockslide that dammed the Madison River and created Quake Lake (Smith and Arabasz, 1991). To measure coseismic and postseismic vertical surface displacements associated with the earthquake and its aftershocks, the USC&GS conducted first-order relevelings in 1959, 1960, 1964, and 1967 along lines in Idaho and Montana that converge at West Yellowstone (fig. 5). All lines in Yellowstone National Park, plus the line from Sappington, Montana, to West Yellowstone, Montana, were releveled to first-order standards in 1987. Holdahl and Dzurisin (1991) summarized results of those surveys, including 6 m of coseismic subsidence along the Sappington to West Yellowstone profile, based on surveys in 1934 and 1959, and 32 cm of postseismic uplift that occurred between surveys in 1959 and 1987.[14]

Reilinger (1986) fit an exponential curve to the changing height relationship between two benchmarks 1.2 km apart on the Norris to West Yellowstone profile, deduced a 10-year decay period for postseismic uplift, and attributed postseismic motion to viscoelastic response of the asthenosphere. Holdahl and Dzurisin (1991) fit the changing height relationships among more marks along the same profile and deduced a 2-year decay period for the motion, which according to their preferred model essentially had stopped by 1970. They noted that the lack of any additional uplift at West Yellowstone, relative to Norris, after 1975 (based on surveys in 1983 and 1987), precludes a decay period longer than 4 years. The discovery by Wicks and others (2006) of a deformation source beneath the north caldera rim near Norris complicates the interpretation of postseismic motion associated with the 1959 Hebgen Lake earthquake, because the north rim source could have caused undocumented height changes at Norris, relative to West

[13]M_s refers to surface-wave magnitude, which is based on the amplitude of Rayleigh surface waves measured at a period near 20 s. Depending on how they were determined, earthquake magnitudes are expressed as local magnitude (M_L), body wave magnitude (M_b, based on the amplitude of P body-waves), or moment magnitude (M_w, based on the seismic moment of the earthquake). Unless specified otherwise, earthquake magnitude M refers to local magnitude.

[14]The 1934–59 result includes any preseismic displacements that might have occurred but were not documented.

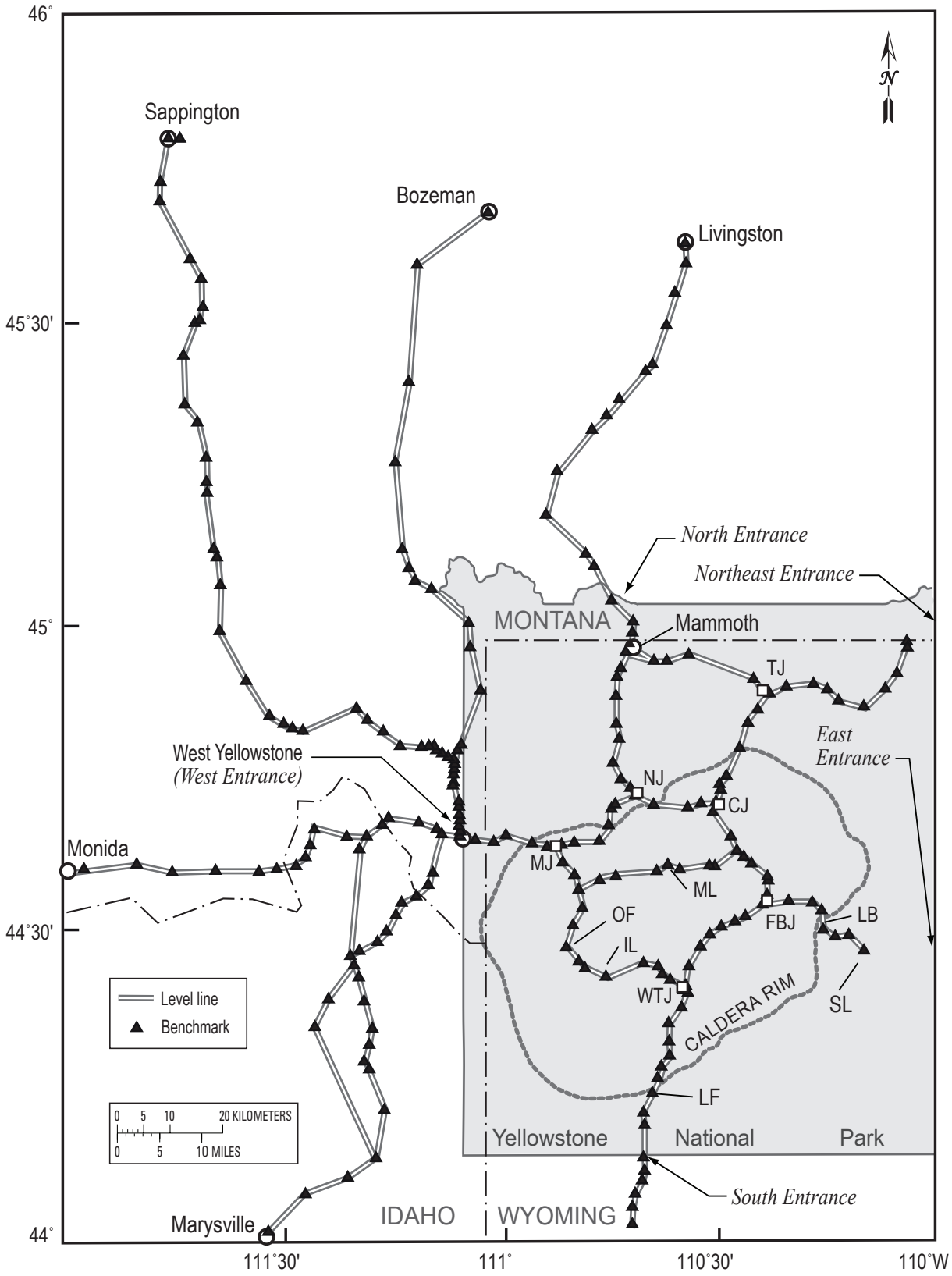

Figure 5. Map of level lines in the Yellowstone-Hebgen Lake region, after Holdahl and Dzurisin (1991). See text for dates of leveling surveys along various lines. TJ, Tower-Roosevelt Junction; CJ, Canyon Junction; NJ, Norris Junction; MJ, Madison Junction; ML, Mary Lake; OF, Old Faithful; IL, Isa Lake; WTJ, West Thumb Junction; FBJ, Fishing Bridge Junction; LB, Lake Butte; SL Sylvan Lake; LF, Lewis Falls.

Yellowstone, during the period of postseismic deformation. The line between West Yellowstone and Norris was measured in 1923, 1975–77, 1983, 1987, and 2004—not frequently enough to distinguish among relative height changes associated with the 1959 Hebgen Lake earthquake, the 1975 Yellowstone Park earthquake (see below), or the north rim source. This ambiguity cannot be resolved in hindsight, so we are left with the less than satisfying necessity of neglecting tectonic stress changes as a primary cause of surface displacements, except perhaps indirectly by enhancing or restricting fluid flow out of the caldera (Wicks and others, 2006). Our concern over this shortcoming is lessened for two reasons. First, Pelton and Smith (1982) rejected tectonic stress as a likely cause of uplift that occurred in the caldera between leveling surveys in 1923 and 1975–77. They cited the predominance of normal Quaternary faults and earthquake fault-plane solutions indicating near vertical *P* axes (inferred axes of maximum compressive stress) as evidence that the dominant horizontal stress in the Yellowstone region is tensional, which is inconsistent with surface uplift. In addition, InSAR observations (Wicks and others, 1998, 2006; Chang and others, 2007, 2010) require a forcing function other than stress changes associated with major earthquakes to explain the complexity and rapidity of changing deformation patterns at the Yellowstone caldera.

1975 *M* 6.1 Yellowstone Park Earthquake

Another major earthquake, the *M* 6.1 Yellowstone Park event, occurred on June 30, 1975, beneath the north rim of the caldera near the Norris Geyser Basin (Pitt and others, 1979) (fig. 4). In August 1975, the USGS performed a first-order resurvey of the line from Madison Junction to Mammoth Hot Springs Junction by way of Norris Junction (figs. 1 and 6). Comparison of the 1923, 1960, and 1975 surveys indicated large relative height changes between Madison and Norris—more than 200 mm during 1923–60 and about 120 mm during and 1960–75—with Norris down with respect to Madison in both cases. Pitt and others (1979) urged that the results be interpreted with caution, because they could not separate effects of the 1959 and 1975 earthquakes. In an attempt to resolve that ambiguity, the USGS and University of Utah releveled the rest of the 1923 network of lines within the park, except for the line across Mary Mountain by way of Mary Lake (figs. 1, 5, and 6), to first-order standards during the summer of 1976. The 1976 survey produced a major surprise—parts of the caldera floor had risen more than 700 mm since the 1923 survey—and more uncertainty. In this case, lack of data from the Mary Lake line, between the Mallard Lake and Sour Creek resurgent domes, left open the possibility that an even greater amount of uplift might have occurred there. That question was addressed by releveling the line along the Mary Mountain trail during the summer of 1977, which completed the 1975–77 resurvey of the entire 1923 network. Those results are discussed in the following section.

It is noteworthy that Hamilton (1987) saw no evidence in data from USGS water-level gages along the shore of Yellowstone Lake for any significant change in the long-term trend of ground tilt at the time of the 1959 M_s 7.5 Hebgen Lake earthquake; that is, 0.4 microradians per year (μradian/yr) up to the northeast. That trend is consistent with uplift of the Sour Creek dome relative to the south caldera rim, as shown by the 1923 and 1975–77 leveling surveys. On the other hand, Hamilton (1987) noted apparent subsidence of the Sour Creek dome and concurrent uplift of the Mallard Lake dome at the time of the 1975 *M* 6.1 Yellowstone Park earthquake. In hindsight this may have been the earliest indication of simultaneous uplift and subsidence at different locations within the caldera, as demonstrated clearly by InSAR images for the period August 1995–September 1996 (see section on Variable Subsidence and Resumption of Uplift from InSAR Observations, 1992–1997).

Discovery of Caldera Floor Uplift, 1923 to 1975–1977

Pelton and Smith (1979, 1982) compared the 1923 and 1975–77 leveling results, which indicated that the central part of the caldera floor had risen substantially during the interval between surveys. Maximum uplift of 726±22 mm, which corresponds to an average rate of 14±1 mm/yr, was measured at benchmark B11 1923 near Le Hardys Rapids.[15] Differential vertical motions along the level line across Mary Mountain were small, indicating that the zone of maximum uplift was elongate and coincided with the long axis of the caldera (figs. 1 and 6; table 1). The deformation field mimicked the shape of the elliptical caldera, except on the north and west sides, where measurable amounts of surface displacement extended well outside the caldera rim. Those areas had risen 200–300 mm with respect to K12 1923, the designated reference benchmark near the southeast caldera rim (fig. 6). The Norris area had subsided a similar amount with respect to its immediate surroundings, such that its net displacement relative to K12 1923 was near zero.

Pelton and Smith (1982) noted the possibility of coseismic and postseismic displacements associated with the 1959 M_s 7.5 Hebgen Lake earthquake and 1975 *M* 6.1 Yellowstone Park earthquake, as had been suggested by Myers and Hamilton (1964) and Reilinger and others (1977). Referring to the newly discovered uplift inside the caldera, Pelton and Smith (1979, p. 1179) wrote: "The most likely cause of this rapid and unusually large surface deformation is a recent influx of partially molten material to a location within the crust beneath

[15]Pelton and Smith (1979, 1982) calculated vertical displacements with respect to K12 1923, a reference benchmark about 8 km outside the southeast caldera rim (fig. 6). Their choice makes sense, because the leveling results show that any differential vertical ground motions outside the caldera were small compared to those in the central part of the caldera, and because K12 1923 is far removed from any effects of the 1959 M_s 7.5 Hebgen Lake earthquake or 1975 *M* 6.1 Yellowstone Park earthquake.

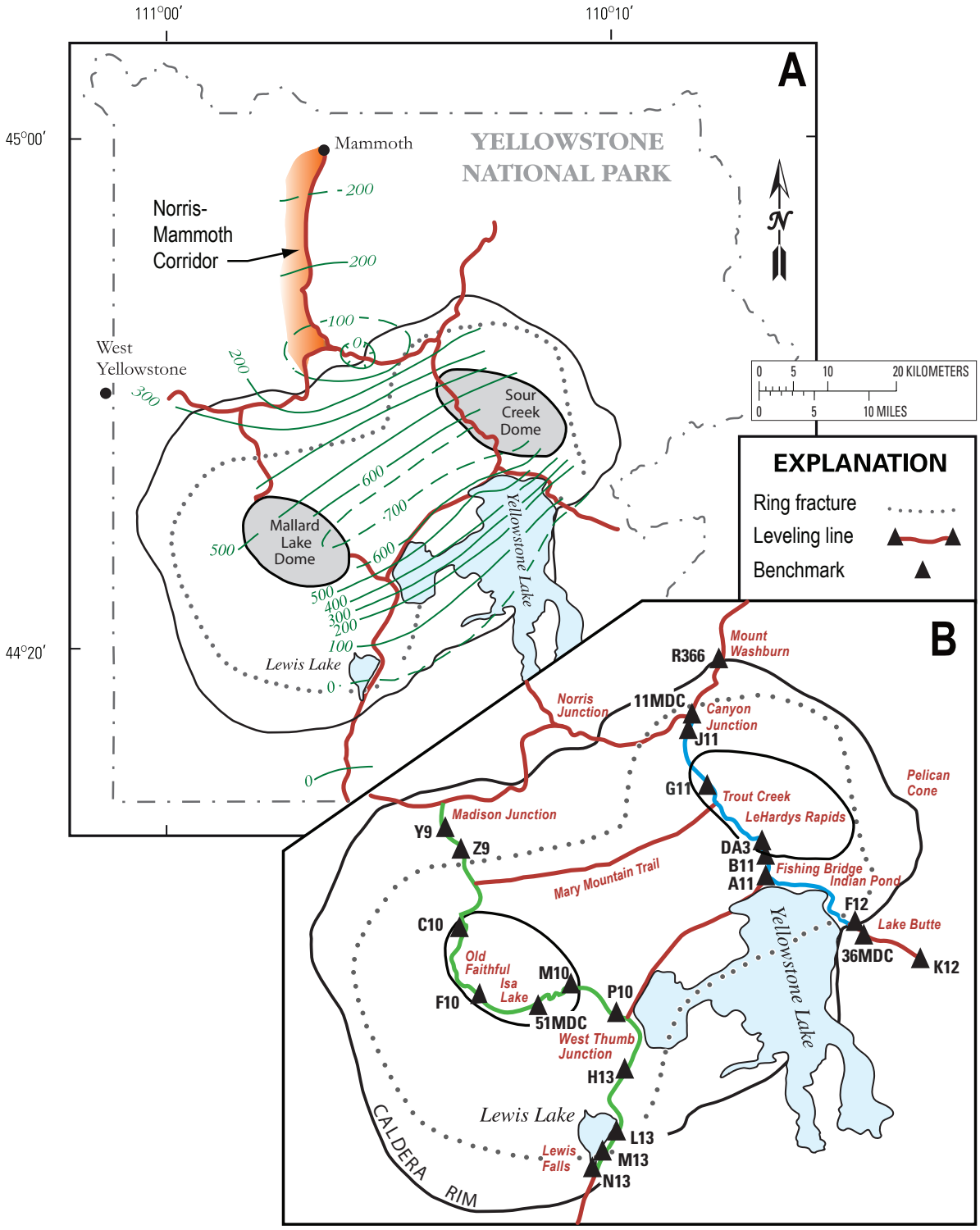

Figure 6. *A,* Map of Yellowstone National Park leveling network and vertical surface displacements measured by comparison of leveling surveys in 1923 and 1975–77. Uplift contours in millimeters are from Pelton and Smith (1982). Salmon-colored highlighting indicates Norris–Mammoth corridor. *B,* Enlargement of Yellowstone caldera area shown in *A*. Blue line shows level line between Lake Butte and Mount Washburn, which was measured in 1923, 1975–77, in whole or part each year from 1983 to 1993, and in 1995, 1998, 2005, and 2007. The line crosses the maximum-uplift axis, which is located within the 700-mm contour line in *A*, near DA3 and Le Hardys Rapids. Green line shows the level line between Lewis Falls and Madison Junction, which was measured in 1923, 1975–77, 1986, and 1987. It crosses the maximum-uplift axis near 51 MDC and Isa Lake. A level line that follows the Mary Mountain trail was measured in 1923, 1977, and 1987.

Yellowstone National Park." That conclusion has withstood the test of time—but not without considerable ongoing debate and elaboration (see Discussion section).

One of the authors of this report (Dzurisin) started working in Yellowstone National Park in 1983, about 4 years after Pelton and Smith (1979) published their discovery of rapid crustal uplift in the prestigious journal Science. Personal experience during 15 leveling surveys across the caldera from 1983 to 2007 provides some insight into what must have been a puzzling and exciting experience for the surveyors and scientists involved in that discovery. During summer 1975, the line between Madison Junction and Mammoth Hot Springs Junction by way of Norris Junction was surveyed in response to the June 30, 1975, *M* 6.1 Yellowstone Park earthquake near Norris (figs. 1 and 6). Results showed that there had been substantial changes since the previous survey in 1923, which prompted leveling of two additional lines during summer 1976—(1) between Norris Junction and reference mark K12 1923 by way of Canyon Junction and Fishing Bridge Junction and (2) between Madison Junction and West Thumb Junction by way of the Old Faithful area. The first line includes benchmark B11 1923 near Le Hardys Rapids, where the 1976 results indicated more than 700 mm of uplift relative to K12 1923 since the 1923 survey. Mark B11 1923 is about 30 km along the level line from K12 1923, so 700 mm of uplift corresponds to an average gradient of more than 20 mm/km—a number that might have seemed implausibly large at the time. One can imagine excitement mounting among members of the survey party as the discrepancy between their results and the 1923 survey continued to accumulate—100 mm, 300 mm, and 700 mm—and increasing away from the epicenter of the 1975 earthquake! Could those huge differences possibly be real? After all, the level lines surveyed in 1975 and 1976 did not form a closed loop, so leveling error could not be eliminated as a possible explanation of the differences. The definitive answer was not found until summer 1977, when three additional lines were surveyed—(1) between Canyon Junction and the Northeast Entrance by way of Tower-Roosevelt Junction, (2) between Fishing Bridge Junction and the South Entrance by way of West Thumb Junction, and (3) across Mary Mountain. Together, the 1975, 1976, and 1977 surveys form a closure loop around the southern part of the Grand Loop Road; that is, from Madison Junction to Norris Junction (surveyed in 1975), Norris Junction

Table 1. Average vertical displacement rates near Le Hardys Rapids, Yellowstone National Park, from leveling surveys.

[The 1923–1976 result is for benchmark B11 1923 relative to K12 1923. The 1998–2005 and 2005–2007 results are for DA3 1934 relative to CVO 84-24. All other results are for DA3 1934 relative to 36 MDC 1976. Benchmarks B11 1923 and DA3 1934 are 2 km apart and near Le Hardys Rapids. Reference benchmarks K12 1923, CVO 84-24, and 36 MDC 1976 are within 11 km of one another and near Lake Butte on the southeast rim of the Yellowstone caldera. Uplift and subsidence profiles in the northeast part of the caldera (fig. 10) show that maximum displacements consistently occur near Le Hardys Rapids and that relative displacements among marks near Lake Butte are small. Therefore, these values are a reasonably consistent measure of the displacement rate at Le Hardys Rapids relative to Lake Butte. See text and references cited in the table for details]

Time period	Average uplift (+) or subsidence (-) rate	Source
1923–1976	+14±1 mm/yr	Pelton and Smith (1979, 1982)
1976–1983	+23±1 mm/yr (see caption)	Dzurisin and Yamashita (1987)
1983–1984	+16±5 mm/yr (see caption)	Dzurisin and Yamashita (1987)
1976–1984	+22±1 mm/yr	Dzurisin and Yamashita (1987) Dzurisin and others (1990)
1984–1985	−2±5 mm/yr	Dzurisin and others (1990)
1985–1986	−25±5 mm/yr	Dzurisin and Yamashita (1987) Dzurisin and others (1990) Dzurisin and others (1994)
1986–1987	−35±5 mm/yr	Dzurisin and others (1994)
1987–1988	−9±5 mm/yr	Dzurisin and others (1994)
1988–1989	−11±5 mm/yr	Dzurisin and others (1994)
1989–1990	−13±5 mm/yr	Dzurisin and others (1994)
1990–1991	−11±5 mm/yr	Dzurisin and others (1994)
1991–1992	−32±5 mm/yr	Dzurisin and others (1994)
1992–1993	−13±5 mm/yr	Dzurisin and others (1994)
1993–1995	−20±3 mm/yr	Dzurisin and others (1999)
1995–1998	−8±3 mm/yr	Dzurisin and others (1999)
1998–2005	+4±1 mm/yr	This paper
2005–2007	+53±3 mm/yr	This paper

to Fishing Bridge Junction by way of Canyon Junction (1976), Canyon Junction to West Thumb Junction (1977), and back to Madison Junction by way of the Old Faithful area (1976). Even though the surveys spanned three successive summers, closure around the loop was within the acceptable limit for first-order surveys. This meant two things: (1) any movement that might have occurred during the course of the surveys was small, so the results could be combined and analyzed as a single large survey, and (2) more importantly, it was clear that something remarkable had happened since the 1923 survey—parts of the caldera floor had risen more than 700 mm at an average rate of 14 mm/yr.

Pelton and Smith (1982) published a thorough analysis of the Yellowstone leveling results in 1982, not long after two other remarkable happenings in the world of volcanology—the May 18, 1980, eruption of Mount St. Helens and a strong earthquake swarm that same month at the Long Valley caldera, California. Until that time, the discovery of crustal uplift in Yellowstone was regarded by many volcanologists as important but not pressing. The 1980 eruption at Mount St. Helens, followed a week later by the intense earthquake swarm at Long Valley, caused some volcanologists to connect the dots and wonder about the possibility of an eruption at Long Valley in our lifetimes—an idea that would have seemed far-fetched just a few months earlier. The Long Valley caldera is similar in many respects to its somewhat larger and younger cousin, the Yellowstone caldera. Pelton and Smith's (1982) paper appeared in the Journal of Geophysical Research amidst a buzz in the volcanological community over the ongoing eruption at Mount St. Helens, where a dacite lava dome was growing episodically on the floor of the 1980 crater, and persistent unrest at Long Valley that led to the USGS Notice of Potential Volcanic Hazard in May 1982. The stage was set for a quarter century of intensive study at Yellowstone—the exciting period of discovery initiated by Pelton and Smith (1979, 1982) and discussed in this report.

Continuing Caldera Floor Uplift, 1976–1984

As mentioned earlier, the 1983 leveling survey across the northeast part of the caldera was not completed owing to the onset of winter weather. Even so, the partial survey showed that uplift had continued since the 1976 survey. That conclusion is based on the shape of the relative displacement profile for 1976–83, which shows that the central part of the level line near Le Hardys Rapids rose 78±4 mm (benchmark DA3 1934) with respect to the south end (32 MDC 1976) and 46±4 mm with respect to the north end (F11 A) (fig. 7). Although the total uplift at Le Hardys Rapids relative to K12 1923, the reference mark for the 1976 survey, was not measured by the 1983 survey, we are confident that an appreciable amount of uplift did occur in the central part of the caldera between 1976 and 1983 (see below).

That confidence is reinforced by results of the 1984 survey, which indicate that DA3 1934 near Le Hardys Rapids rose 177±6 mm with respect to 36 MDC 1976 near Lake Butte during 1976–84—at an average rate of 22±1 mm/yr (fig. 7 and table 1) (Dzurisin and Yamashita, 1987).[16] DA3 1934 is only about 2 km north of B11 1923 and 36 MDC 1976 is only about 6 km northwest of K12 1923, the reference mark for the 1923 and 1975–77 surveys. So the average uplift rate at DA3 1934 during 1976–84 (22±1 mm/yr with respect to 36 MDC 1976) can be compared in a general way to the average uplift rate at B11 1923 during 1923–76 (14±1 mm/yr with respect to K12 1923). Even with the ambiguity introduced by using different reference marks, it seems clear that the average uplift rate was greater during 1976–84 than during 1923–76. On the basis of results of subsequent leveling surveys and InSAR observations (see below), we suspect that this is due in part to one or more unrecorded episodes of subsidence during 1923–76.

The shapes of the 1976–83 and 1976–84 displacement profiles are very similar where they overlap for 17 km in the central part of the caldera. Both profiles are reminiscent of the uplift pattern for the caldera as a whole that Pelton and Smith (1979, 1982) deduced from the 1923 and 1975–77 surveys. This observation led Dzurisin and Yamashita (1987) to extrapolate the 1976–83 vertical displacement profile to 36 MDC 1976, using the 1976–84 profile as a guide. The resulting maximum uplift value, 161±6 mm at DA3 1934 with respect to 36 MDC 1976 from 1976 to 1983, corresponds to an average uplift rate of 23±1 mm/yr during 1976–83 and 16±5 mm/yr during 1983–4. Owing to uncertainty inherent in the extrapolation, we are not confident that the apparent difference in average uplift rates near Le Hardys Rapids for 1976–83 and 1983–84 is real. On the other hand, the average uplift rate for 1976–84 (22±1 mm/yr) is more than 50 percent greater than for 1923–76 (14±1 mm/yr), and that difference is almost surely real. The difference might indicate that (1) uplift began sometime after 1923 and proceeded at a relatively constant rate, (2) the uplift rate increased over time, or (3) some more complicated history, which could have included pauses or periods of subsidence. The latter possibility was underlined by results of the 1985 survey.

A Pause in Vertical Surface Motion, 1984–1985

The 1985 leveling survey between Lake Butte and Canyon Junction produced a surprise—that is, the vertical displacement measured near Le Hardys Rapids (DA3 1934) with respect to the south caldera rim (36 MDC 1976) from September 1984 to September 1985 was essentially zero (−2±5 mm)

[16]Benchmark 36 MDC 1976 is along the East Entrance Road, 3 km southeast of the summit of Lake Butte and 6 km northwest of K12 1923. Lake Butte is an intrusive mass of Tertiary age along the southeast rim of the Yellowstone caldera. Mark 36 MDC 1976 was used as a reference mark for leveling surveys from 1984 to 1998. It was not recovered for the 2005 survey and is presumed destroyed by roadwork. Nearby mark CVO 84-24 was used as reference for the 2005 and 2007 surveys. Results of the 1923 and 1975–77 surveys (fig. 5) indicate that any relative motions among K12 1923, 36 MDC 1976, and CVO 84-24 were probably small relative to motions in the central part of the caldera.

(fig. 8 and table 1). None of the marks along the line moved by an amount that is statistically significant at two standard deviations. This was the first documented occurrence of a pause in caldera-floor uplift since the initial leveling survey in 1923, although such occurrences could have gone unnoticed as a result of the sporadic nature of the surveys. Another surprise came just one year later.

Caldera-Floor Subsidence, 1986–1995

In 1986, leveling surveys were conducted along two lines that cross the long axis of the Yellowstone caldera—(1) the 44-km line from Lake Butte to Canyon Junction in the northeast part of the caldera and (2) the 76-km line from Lewis Falls to Madison Junction, by way of West Thumb Junction and the Old Faithful area, in the southwest part (fig. 6). The lines skirt the southwest margins of the Sour Creek and Mallard Lake resurgent domes, respectively, and cross the axis of maximum uplift deduced by Pelton and Smith (1979, 1982). We were surprised to discover that since the 1985 survey mark DA3 1934 near Le Hardys Rapids had moved down by 25±5 mm with respect to reference mark 36 MDC 1976 near the south caldera rim—the first documented occurrence of caldera-floor subsidence (fig. 8) (Dzurisin and Yamashita, 1987; Dzurisin and others, 1990). In the southwest part of the caldera, mark 51 MDC 1976 near Isa Lake moved up 107±7 mm with respect to reference mark N13 1923 near Lewis Falls, along the southwest caldera rim, between the surveys in 1976 and 1986 (fig. 9).[17] The average uplift rate for 1976–86 at 51 MDC 1976, 11±1 mm/yr, was less than the rate at DA3 1934 near Le Hardys Rapids for the same period. However, the rate was comparable to the maximum value of 14±1 mm/yr

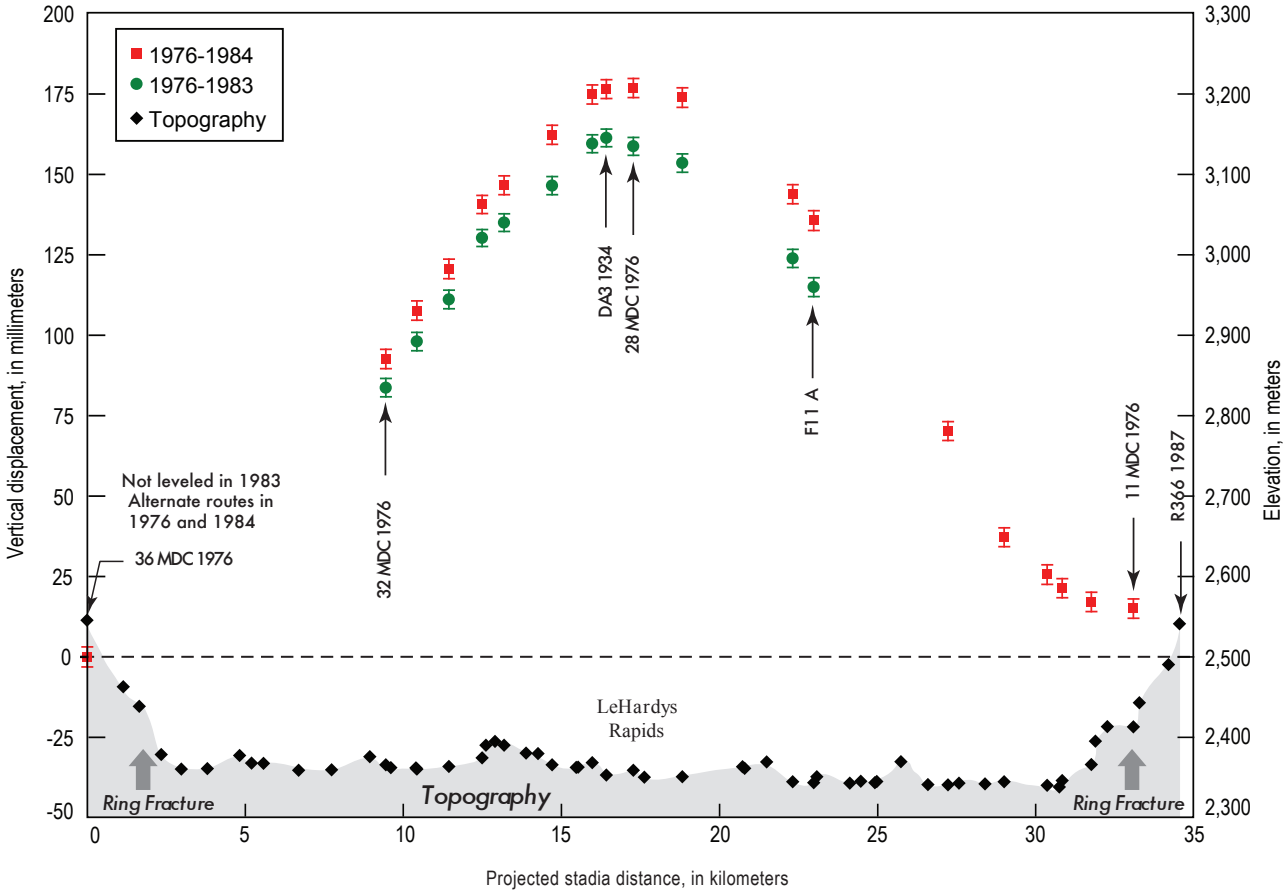

Figure 7. Diagram showing profiles of topography (black diamonds, bottom) and vertical displacements during 1976–83 (green circles) and 1976–84 (red squares) along the level line between Lake Butte and Canyon Junction by way of Le Hardys Rapids in Yellowstone National Park (Dzurisin and Yamashita, 1987). Error bars are one standard deviation from the combination of random leveling error and random-walk benchmark instability, as discussed in the text. Results of the smaller 1983 survey were extrapolated from 32 MDC 1976 to 36 MDC 1976, assuming that 36 MDC 1976 did not move up or down and using the shape of the 1923–76 uplift profile as a guide. Descriptions and photographs of benchmarks, which are indicated by arrows with labels, are included in appendix B in the interactive data files that accompany this report. The benchmark information is available online at http://pubs.usgs.gov/pp/1788/pp1788_benchmarks/.

at B11 1923 (also near Le Hardys Rapids) for 1923–76 from Pelton and Smith (1979, 1982). Whether or not any subsidence occurred in the southwest part of the caldera during 1985–6, as it had in the northeast part, could not be determined until the next survey in 1987.

The discovery of subsidence in the northeast part of the caldera during 1985–86 led the USGS to contract to the National Geodetic Survey (NGS) for a complete resurvey of the Yellowstone network during summer 1987. Results for the level line between Lewis Falls and Madison Junction indicated that the area near Isa Lake in the west-central part of the caldera subsided 13±6 mm (51 MDC 1976) with respect to the south caldera rim (N13 1923) from 1986 to 1987. Marks several kilometers farther east (that is, closer to the Mallard Lake resurgent dome), which were not surveyed in 1976, subsided as much as 25±6 mm during the same period (fig. 9). Along the other level line, Le Hardys Rapids moved down 35±5 mm (DA3 1934) with respect to the south rim (36 MDC 1976) during 1986–7. Within the uncertainty in the measurements, and allowing for the possibility of relative motion between 36 MDC 1976 and N13 1923, the maximum subsidence rates measured in the northeast and southwest parts of the caldera were essentially the same. In 1996, a partial survey across the southwest part of the caldera indicated that mark MEERTENS2 near Old Faithful subsided 149±8 mm with respect to B144 near West Yellowstone during 1987–96, at an average rate of 17±1 mm/yr. For the same period, the subsidence rate at MEERTENS2 with respect to USBPR 6802 at Madison Junction was 15±1 mm/yr (fig. 9).

Taken together, the leveling results for 1986–96 indicate that the uplift pattern reported by Pelton and Smith

[17]Level lines between 36 MDC 1976 and N13 1923 were not measured in 1986, so each of those marks is a local reference only for a line across the caldera floor (Lake Butte to Mount Washburn and Lewis Falls to Madison Junction, respectively). A tie between the cross-caldera lines was made next during a complete survey of the Yellowstone leveling network in 1987.

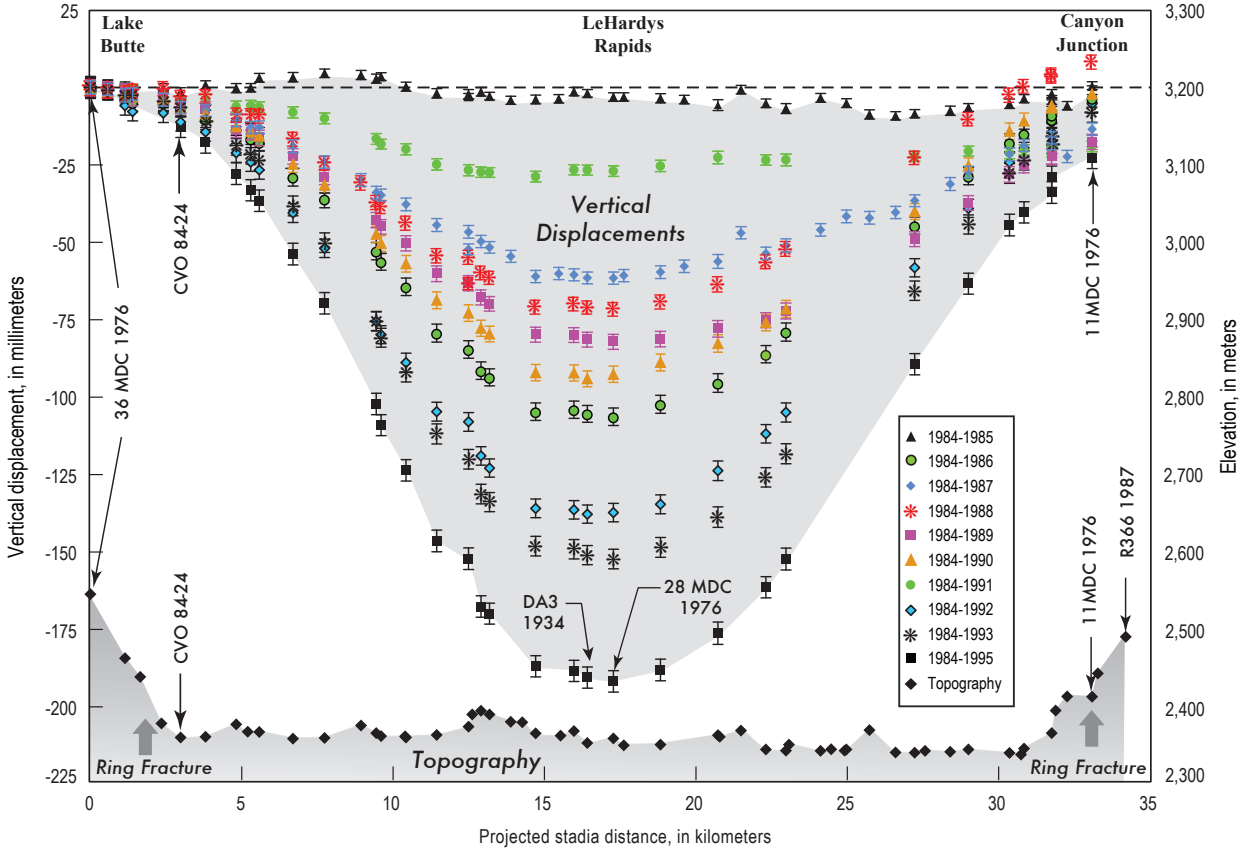

Figure 8. Diagram showing profiles of topography (black diamonds, bottom) and cumulative vertical displacements from 1984 to 1995 along the level line between Lake Butte and Canyon Junction by way of Le Hardys Rapids in Yellowstone National Park. Data are from leveling surveys conducted in September of each year, except 1994. Error bars are one standard deviation from the combination of random leveling error and random-walk benchmark instability, as discussed in the text. Descriptions and photographs of benchmarks, which are indicated by arrows with labels, are included in appendix B in the interactive data files that accompany this report. The benchmark information is available online at http://pubs.usgs.gov/pp/1788/pp1788_benchmarks/.

(1979, 1982) for 1923–76 reversed to one of subsidence, with approximately the same shape and average rate, sometime during 1984–86. During that interval, beginning in October 1985 and continuing for more than 3 months, the largest earthquake swarm ever recorded in the Yellowstone region (excluding mainshock-aftershock sequences) occurred near Madison Junction just outside the northwest caldera rim (Waite and Smith, 2002). In the Discussion section of this report, we infer a causal relationship between that swarm and the onset of caldera-floor subsidence during 1984–86.

Leveling surveys between Lake Butte and Mount Washburn carried out each September from 1988 to 1995, except 1994, showed progressive subsidence near Le Hardys Rapids at rates that ranged from 11±5 mm/yr to 32±5 mm/yr (fig. 8 and table 1). At DA3 1934, the average uplift rate during 1976–84 was 22±1 mm/yr, and the average subsidence rate during 1985–93 was 19±1 mm/yr—nearly identical displacement rates, but in opposite directions, during successive 8-year periods. The shapes of the uplift and subsidence profiles are nearly mirror images of each other (fig. 10), suggesting a common source—a topic to be addressed in the Discussion section.

Variable Subsidence and Resumption of Uplift from InSAR Observations, 1992–1997

No leveling surveys were conducted in Yellowstone National Park in 1996 or 1997, but InSAR observations that collectively span 1992–97 provided two additional surprises. Wicks and others (1998) presented interferograms produced from ERS-1 and ERS-2 C-band radar images that show a subsidence bowl in the northeast part of the caldera from August 1992 to June 1993, an occurrence that is consistent with the results of leveling surveys across that part of the caldera in September 1992 and September 1993 (fig. 11). An interferogram for the period from June 1993 to August 1995 showed additional subsidence in the same area, as corroborated by a leveling survey in September 1995. However, the 1993–95

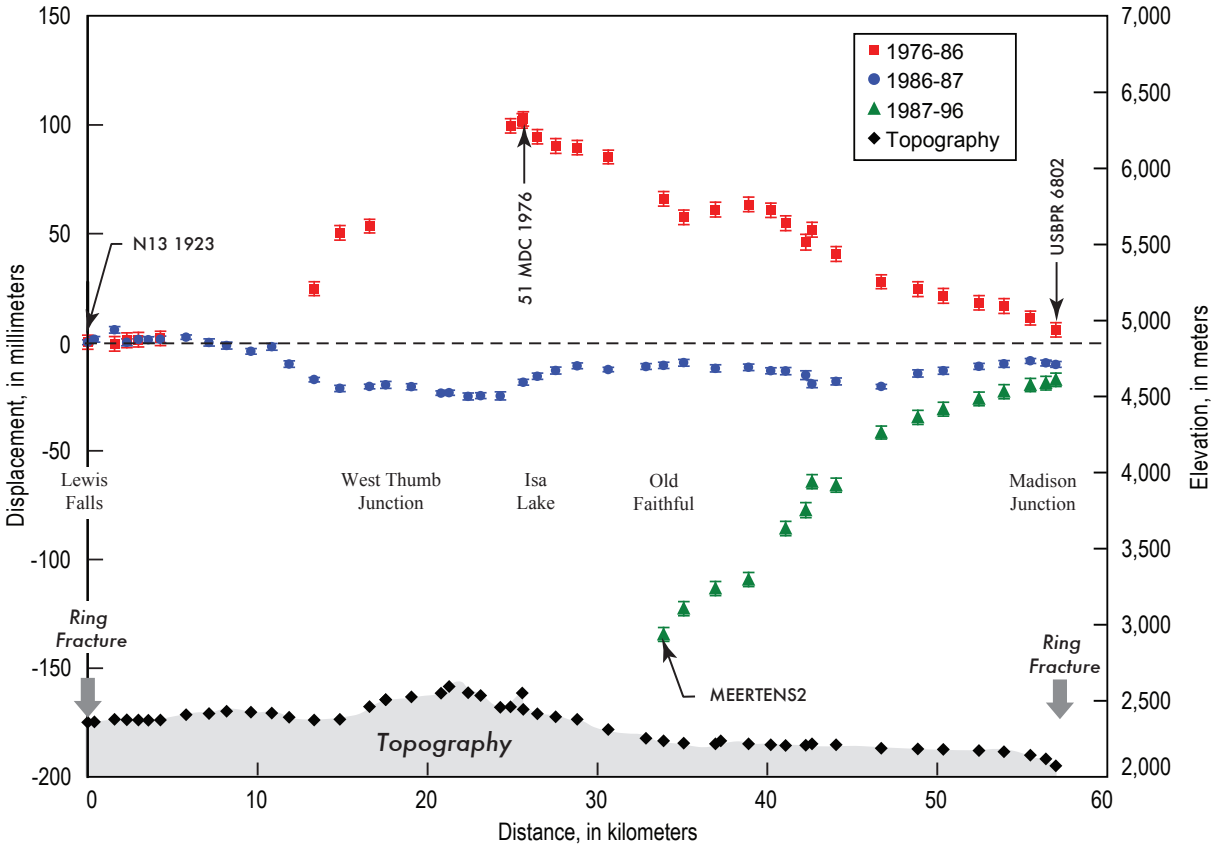

Figure 9. Diagram showing profiles of topography (black diamonds, bottom) and vertical displacements along the level line between Lewis Falls and Madison Junction by way of West Thumb Junction and the Old Faithful area in Yellowstone National Park from 1976 to 1986 (red squares), 1986 to 1987 (blue circles), and 1987 to 1996 (green triangles). Descriptions and photographs of benchmarks, which are indicated by arrows with labels, are included in appendix B in the interactive data files that accompany this report. The benchmark information is available online at http://pubs.usgs.gov/pp/1788/pp1788_benchmarks/.

interferogram showed an even greater amount of subsidence in the southwest part of the caldera, where no leveling had been done since 1987. This was a surprise because the pattern of uplift revealed by the complete surveys in 1923, 1975–77, and 1987 was nearly symmetric; that is, the northeast and southwest parts of the caldera floor moved similar amounts. The 1993–95 interferogram was the first clear indication of asymmetric uplift or subsidence within the caldera, although such a pattern could have escaped detection by sporadic leveling surveys.

InSAR images for the period August 1995–September 1996 produced the second surprise: the northeast part of the caldera floor rose about 20 mm, while the southwest part continued subsiding. Such a bimodal pattern had not been detected by any previous leveling surveys, although Hamilton (1987) had reported a similar pattern based on differential water-level records from gages along the shore of Yellowstone Lake. His analysis showed that at the time of the 1975 *M* 6.1 Yellowstone Park earthquake there was subsidence of the northeast part of the caldera and concurrent uplift of the southwest part (that is, the inverse of the pattern revealed by InSAR in the mid-1990s). By June 1997, InSAR observations showed that more than 30 mm of uplift had occurred throughout the central part of the caldera, in a pattern reminiscent of the 1923 to 1975–77 uplift as contoured by Pelton and Smith (1979, 1982; figs. 6 and 11). The onset of uplift was coincident with, or followed shortly after, a strong earthquake swarm during June–July 1995—the largest since the 1985 swarm that occurred in the same general area near the northwest caldera rim (USGS–University of Utah earthquake catalog). The InSAR results clearly showed that the caldera's two resurgent domes sometimes move in opposite directions and, in this instance, uplift began at the Sour Creek dome and spread southwestward to the Mallard Lake dome.

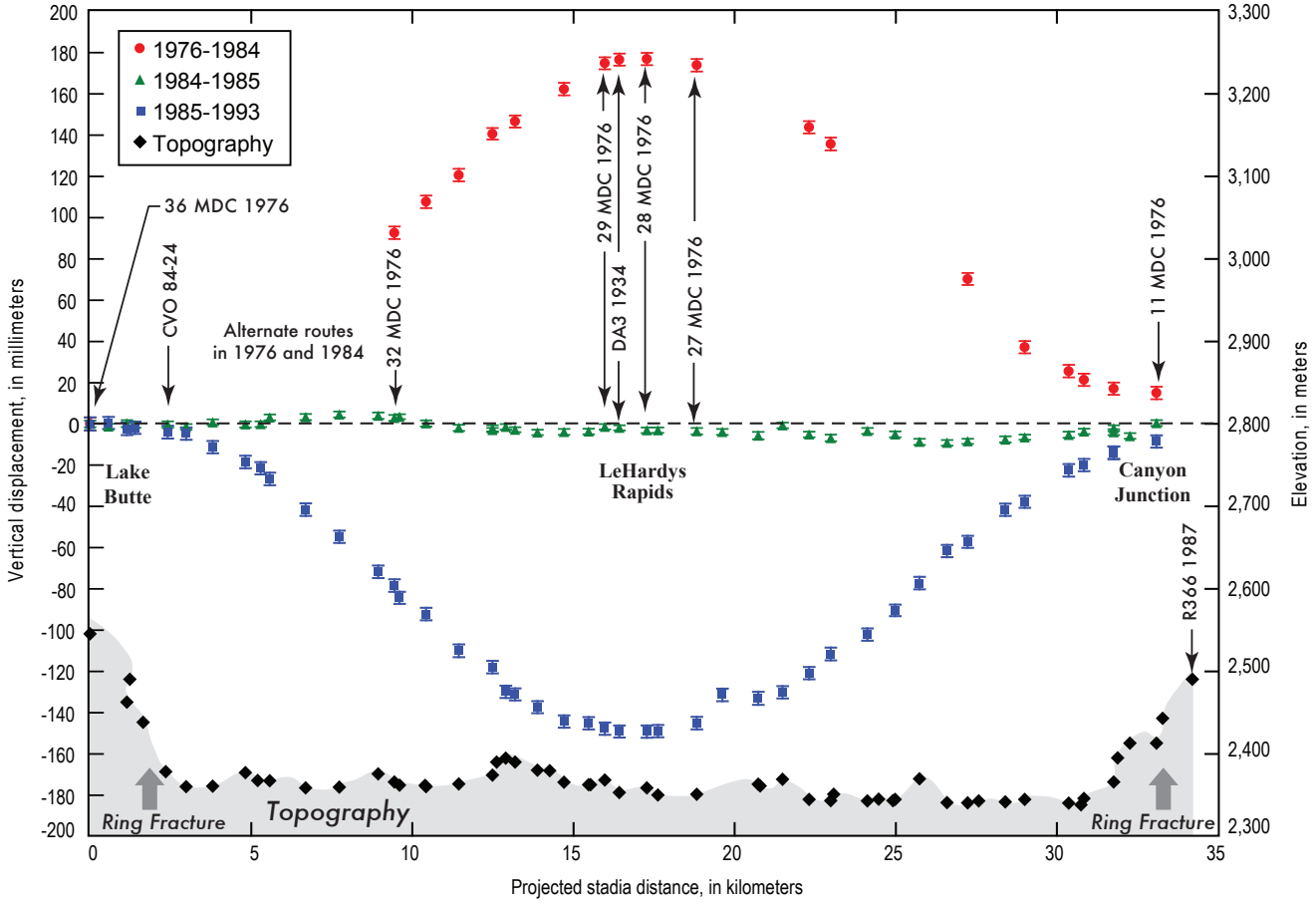

Figure 10. Diagram showing profiles of topography (black diamonds, bottom) and vertical displacements along the level line between Lake Butte and Canyon Junction by way of Le Hardys Rapids in Yellowstone National Park from 1976 to 1984 (red circles), from 1984 to 1985 (green triangles), and from 1985 to 1993 (blue squares). Descriptions and photographs of benchmarks, which are indicated by arrows with labels, are included in appendix B in the data files that accompany this report. The benchmark information is available online at http://pubs.usgs.gov/pp/1788/pp1788_benchmarks/. The subsidence profile for 1985–93 is nearly a mirror image of the uplift profile for 1976–84. No significant deformation occurred during the intervening year, 1984–85.

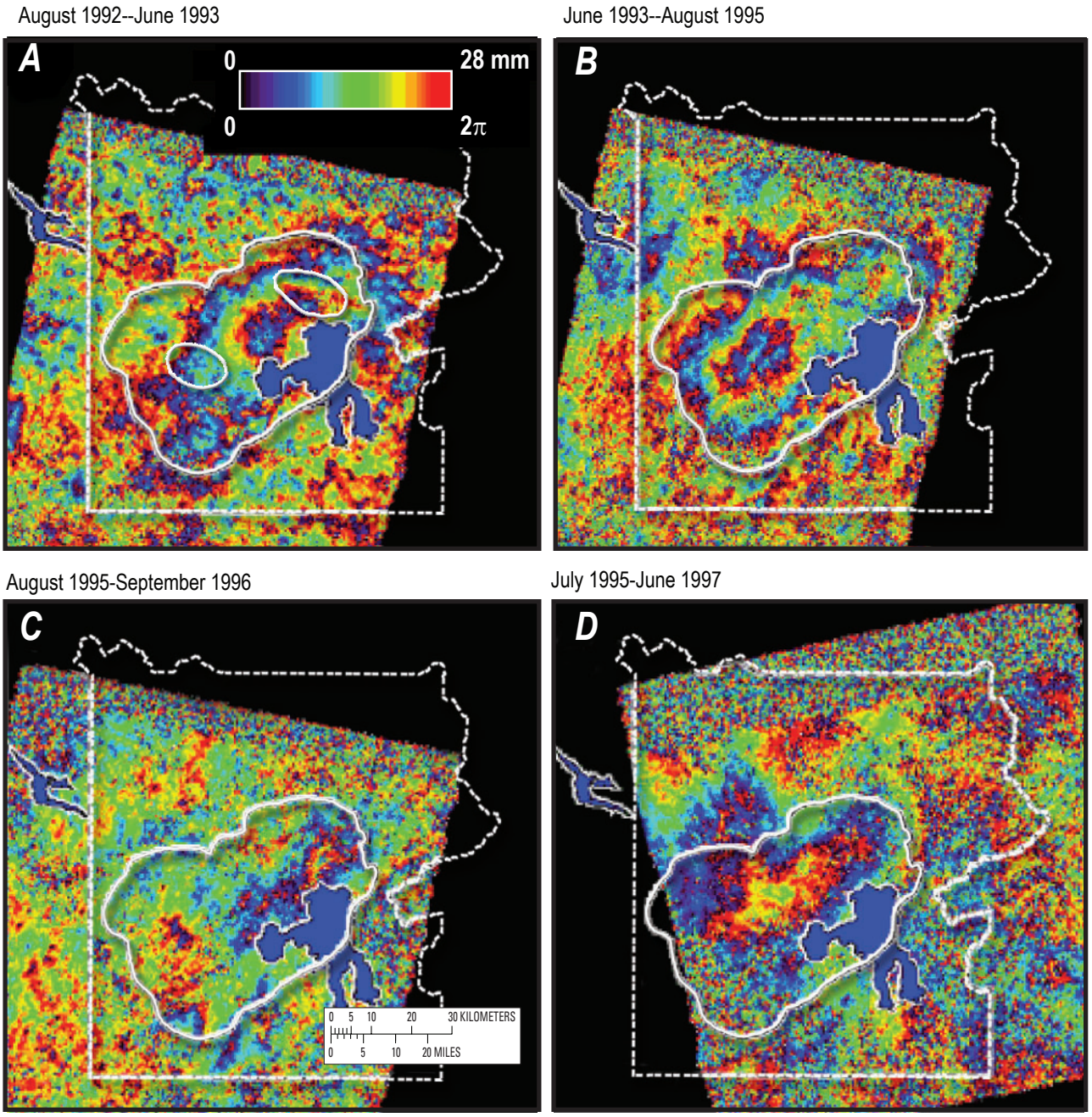

Figure 11. Four interferograms of the Yellowstone National Park region produced by Wicks and others (1998) from ERS-1 and ERS-2 radar images. The range of colors from violet to red, shown in the color bar, corresponds to one cycle of phase from 0 to 2π (one fringe). Each fringe represents 28.3 mm of range change (surface displacement) between a point on the ground and the satellite. Solid white lines, caldera rim and two resurgent domes (*A* only). Dashed white line, boundary of Yellowstone National Park. Figure modified slightly from Dzurisin and others (1999). The first three interferograms are sequential, whereas the time periods covered by the third and fourth overlap. Note the pixilated nature of these early Yellowstone interferograms compared to more recent ones elsewhere in this report (figs. 12–15)—a result of improved data processing techniques. *A*, August 1992 to June 1993. This image shows more than 30 mm of subsidence centered in the northeast half of Yellowstone caldera in the vicinity of the Sour Creek resurgent dome. *B*, June 1993 to August 1995. The center of subsidence (~40 mm maximum) has shifted in this image to the southwest half of the caldera near the Mallard Lake resurgent dome. *C*, August 1995 to September 1996. The fringe pattern in the northeast half of the caldera in this image corresponds to ~20 mm of uplift in the vicinity of the Sour Creek dome (note the reversed color sequence toward the center of the fringe pattern relative to *A* and *B*). *D*, July 1995 to June 1997. In this image, uplift extends throughout the central part of the caldera (maximum ~30 mm).

North Rim Uplift and Caldera-Floor Subsidence, 1997–2002

InSAR observations contributed another piece to the Yellowstone deformation puzzle when an ERS-2 interferogram for the period from September 1996 to September 2000 revealed a bulls-eye pattern of uplift centered along the north caldera rim in the vicinity of Norris Geyser Basin (Wicks and others, 2006, fig. 12). The uplifted area also had been identified by differencing results of GPS surveys made in 1995 and 2000 (Puskas and others, 2007). The maximum range change from the interferogram was about 80 mm during 1996–2000. Wicks and others (2006) noted that the 1996–2000 interferogram indicated only slight subsidence in the central part of the caldera, where ~30 mm of uplift had occurred during 1996–97 (Wicks and others, 1998). Therefore, the caldera floor between the two resurgent domes must have subsided more than 30 mm from 1997 to 2000, while the north rim was rising. If uplift of the north rim began in 1997, the average uplift rate there during 1997–2000 was about 27 mm/yr. The north rim source continued to inflate at a declining rate, while the caldera floor subsided, until 2002. An interferogram for the period from October 2002 to August 2003 showed slight subsidence of the north rim area, extending northward along the Norris–Mammoth corridor, and no measurable motion of the caldera floor. The second known pause in caldera deformation was underway.

Seeing the Yellowstone InSAR results for the first time was akin to switching from black-and-white to color television or from two-dimensional (2 D) to three-dimensional (3 D) movies—the effect was dramatic. Our repeated leveling surveys across the northeast part of the caldera had yielded a series of vertical displacement profiles (fig. 8) that we hoped were a good representation of the caldera deformation field as a whole. The August 1995–September 1996 interferogram showed in the blink of an eye that this was not the case, that is, the northeast part of the caldera had gone up, while the southwest part had gone down. Even more striking was the bulls-eye pattern of uplift along the north caldera rim that appeared in the September 1996–September 2000 interferogram. Suddenly the situation was much more complicated and intriguing than we had thought since the discovery of uplift in the mid-1970s. The InSAR results heralded the start of a new chapter in the Yellowstone deformation story, and this one was in color!

Creation of the Yellowstone Volcano Observatory, May 2001

It was during a brief respite in caldera deformation that scientists and managers of the USGS, University of Utah, and Yellowstone National Park came together to establish the Yellowstone Volcano Observatory (YVO) in May 2001 (http://volcanoes.usgs.gov/yvo/). YVO is an instrument-based monitoring facility designed for observing volcanic, hydrothermal, and earthquake activity in the Yellowstone National Park region. The monitoring primarily involves a seismic network operated by the University of Utah Seismograph Stations under a cooperative funding agreement with the USGS and with ancillary support from the National Science Foundation (NSF). YVO also operates a network of CGPS stations in the park that complements a network of CGPS stations and borehole strainmeters operated by the EarthScope Plate Boundary Observatory (PBO, http://pboweb.unavco.org/). In addition, campaign GPS, leveling, microgravity, and InSAR observations have been carried out by scientists of both the University of Utah and the USGS since YVO was created in 2001. Among these activities has been the study of ground deformation that we discuss here, a study which has evolved over time and is expected to continue under YVO auspices for the foreseeable future.

Rapid Uplift of the Sour Creek Dome and North Rim Subsidence, 2004–2008

The period of relative quiescence that began in 2002 ended in remarkable fashion less than two years later. Chang and others (2007) reported that, during the first 6 months of 2004, data from CGPS stations indicated 10–20 mm of subsidence of the Sour Creek dome and a similar amount of uplift of the north rim near Norris. Then, starting in July 2004, the caldera motion suddenly reversed to uplift at rates as high as ~70 mm/yr (an historically unprecedented value) at CGPS station WLWY near the eastern margin of the Sour Creek dome. The Norris area began to subside about 3 months later. Chang and others (2007) noted that the entire caldera floor began to rise nearly simultaneously in mid-2004. This is in contrast to the observation by Wicks and others (1998) that during 1995–96 uplift started at the Sour Creek dome—at a time when the Mallard Lake dome was subsiding—then spread to the entire caldera floor by 1996–97.

A stack of two ENVISAT IS2-mode[18] interferograms that collectively span the period from September 2004 to August 2006 depict more clearly the spatial pattern of caldera uplift and north rim subsidence (fig. 13). With reference to the stacked interferogram, Chang and others (2007, p. 953) wrote:

> The inflation increases symmetrically toward the caldera center about the long axis (northeast-southwest), with the highest rate of ~7 cm/year at the Sour Creek dome being three to five times faster than uplift rates in 1923–1984 and 1995–1997 * * *. The Norris

[18]The ASAR instrument aboard ENVISAT is capable of multiple, interleaved imaging modes. IS2 refers to one such mode, which is characterized by an incidence angle of 21.5 degrees from vertical and either HH or VV polarization. HH refers to a data acquisition mode in which radar pulses with horizontal polarization are transmitted and received by ASAR; VV refers to the case in which the pulses are transmitted and received with vertical polarization. Mode IS2, VV is suitable for interferometry and similar to the imaging mode of ERS-1 and ERS-2.

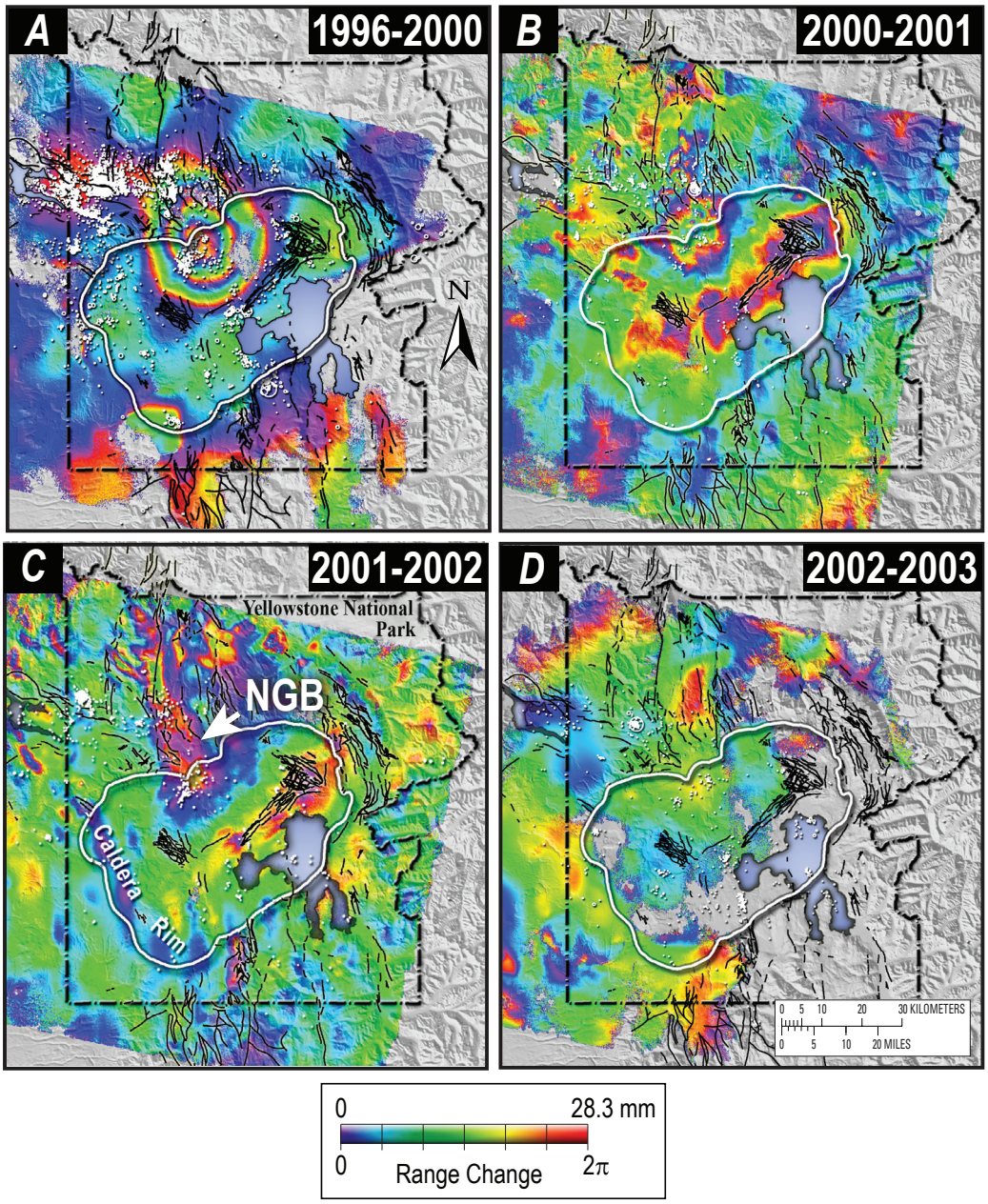

Figure 12. Four interferograms superimposed on digital terrain showing range changes (ground deformation) at the Yellowstone caldera, Yellowstone National Park, between 1996 and 2003. A color change from violet to blue to green to yellow to red, shown in the color bar, marks an increase in the range (distance from the satellite to points on the ground) of 28.3 mm. White dots represent epicenters of earthquakes recorded during the time interval spanned by each interferogram. White outline shows caldera rim. The interferograms were generated using European Space Agency ERS-2 data and the two-pass method of interferometry (Massonnet and Feigl, 1998). *A,* Summer 1996 to summer 2000 interferogram. Concentric pattern of fringes indicates uplift along the north caldera rim. Although the caldera floor appears to have subsided only slightly, this period includes about 30 mm of caldera-wide uplift from 1995 to 1997 (Wicks and others, 1998). Therefore, more than 30 mm of subsidence of the caldera floor occurred between the Mallard Lake and Sour Creek resurgent domes from 1997 to 2000, while the north rim rose about 80 mm. *B,* Summer 2000 to summer 2001 interferogram showing continuing uplift along the north caldera rim and subsidence of the caldera floor. *C,* Summer 2001 to summer 2002 interferogram. Uplift along the north rim continued and extended northward along the Norris–Mammoth corridor, while the caldera floor continued to subside at a declining rate. Arrow labeled NGB marks the location of Norris Geyser Basin. *D,* Summer 2002 to summer 2003 interferogram showing slight subsidence of the north rim area, extending northward along the Norris–Mammoth corridor, and no measurable motion of the caldera floor. Figure from Wicks and others (2006).

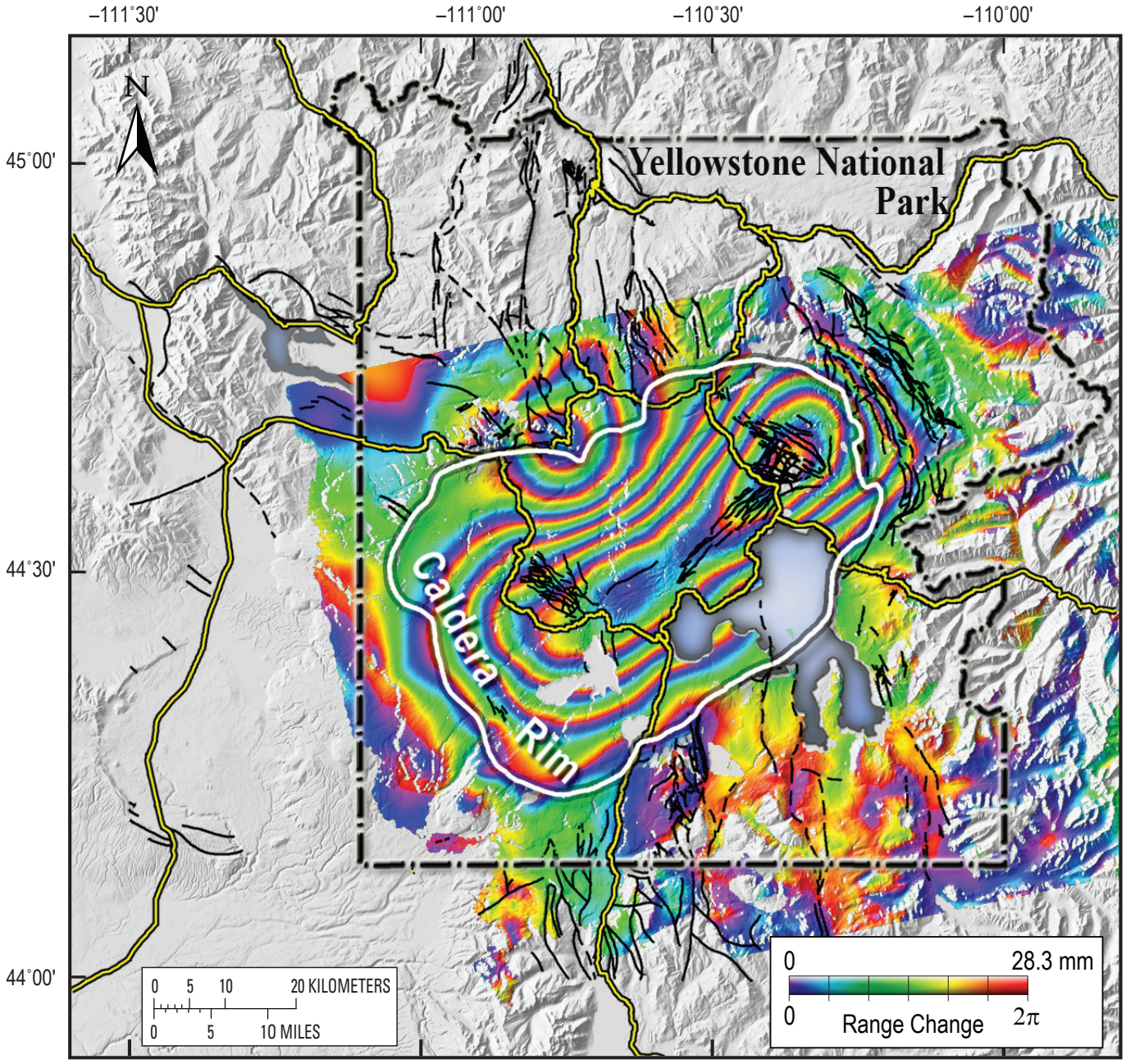

Figure 13. Stack of two deformation interferograms of the Yellowstone caldera, Yellowstone National Park, superimposed on digital terrain map, that collectively span the period from September 22, 2004, to August 23, 2006. The constituent interferograms were generated using European Space Agency Envisat IS2 mode data and the two-pass method of interferometry (Massonnet and Feigl, 1998). The range of colors from violet to red, shown in the color bar, corresponds to one cycle of phase from 0 to 2π (one fringe). Each fringe represents 28 mm of range change (surface displacement) between a point on the ground and the satellite. The line-of-sight (LOS) displacements represented by fringes in the interferogram indicate total uplift of about 110 mm in the west part of the caldera (Mallard Lake dome), uplift of about 150 mm in the east part of the caldera (Sour Creek dome), and subsidence of 60–70 mm near the Norris Geyser Basin. Yellow lines, major roads.

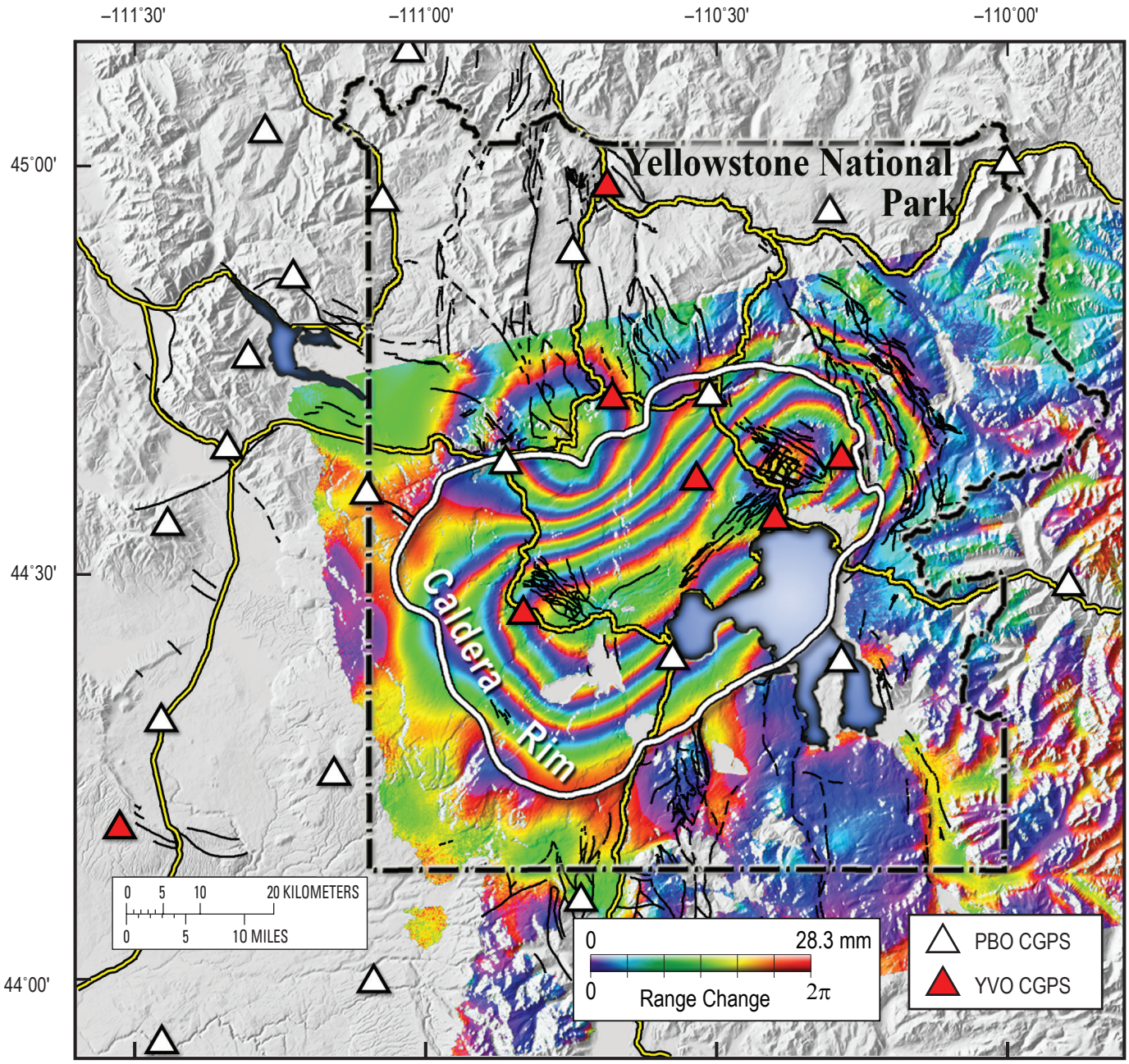

Figure 14. ENVISAT IS2 mode interferogram of the Yellowstone caldera, Yellowstone National Park, superimposed on digital terrain map. Interferogram was produced from images acquired on August 3, 2005, and July 4, 2007, showing uplift of the Yellowstone caldera (Sour Creek and Mallard Lake resurgent domes) and subsidence of the north rim in the vicinity of Norris Geyser Basin. The range of colors from violet to red, shown in the color bar, corresponds to one cycle of phase from 0 to 2π (one fringe). Each fringe represents 28 mm of range change (surface displacement) between a point on the ground and the satellite. Red triangles, continuous GPS (CGPS) stations operated by the Yellowstone Volcano Observatory (YVO). White triangles, continuous CGPS stations operated by the Plate Boundary Observatory (PBO). Yellow lines, major roads. Compare this figure to the 2004–6 interferogram in figure 13 and to the 2007–8 interferogram in figure 15. Caldera-floor uplift and north-rim subsidence continued at a slightly lower average rate during 2005–7 and 2007–8 than during 2004–6.

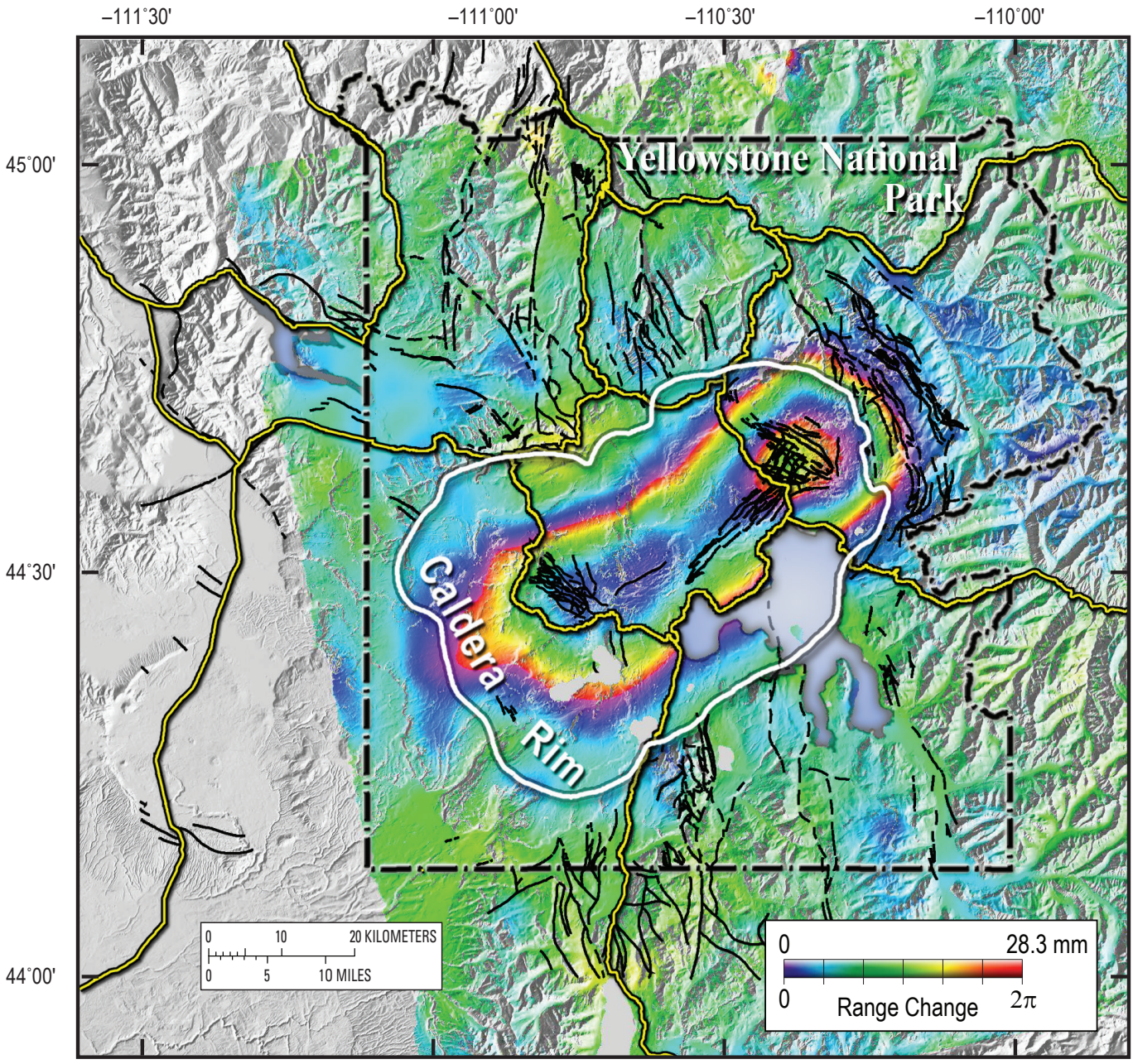

Figure 15. ENVISAT IS2 mode interferogram of the Yellowstone caldera, Yellowstone National Park, superimposed on digital terrain map. Interferogram was produced from images acquired on September 12, 2007, and August 27, 2008. The range of colors from violet to red, shown in the color bar, corresponds to one cycle of phase from 0 to 2π (one fringe). Each fringe represents 28 mm of range change (surface displacement) between a point on the ground and the satellite. Uplift during the period extended across most of the caldera floor, including the Mallard Lake and Sour Creek resurgent domes, and reached a peak value of about 50 mm at the Sour Creek dome. At the same time, an area along the north caldera rim in the vicinity of Norris Geyser Basin subsided about 8 mm. Yellow lines, major roads.

subsidence is ~3 cm/year, more than two times greater than the 1996–2002 uplift rate in this area.

The pattern of caldera-floor uplift and north-rim subsidence persisted at lower rates during 2006–7, as shown by comparison of figures 13 and 14 for 2004–6 and 2005–7, respectively. An Envisat IS2 interferogram for the interval September 12, 2007, to August 27, 2008, indicated ~50 mm of peak uplift centered on the Sour Creek dome and ~8 mm of subsidence along the north caldera rim (fig. 15). The uplift rate at CGPS station WLWY on the Sour Creek dome was 40–50 mm/yr during 2007–8; by September 2009, uplift there had slowed to the point that it may have stopped. The station had undergone a total of about 230 mm of uplift since mid-2004 (http://volcanoes.usgs.gov/yvo/activity/archive/2009.php). Minor subsidence in the Norris area also seemed to have stopped by the third quarter of 2009, as indicated by CGPS station NRWY. Up-to-date time-series data from CGPS stations in the Yellowstone network, including WLWY and NRWY, are available at http://www.uusatrg.utah.edu/ts_ysrp.html.

Results of leveling surveys conducted along the line between Lake Butte and Mount Washburn in 1998, 2005, and 2007 are consistent with the InSAR and CGPS observations described above (fig. 16). During 1995–98, DA3 1934 near Le Hardys Rapids rose 24±5 mm with respect to 36 MDC 1976. Recall that InSAR observations indicated more than 30 mm of uplift of the Sour Creek dome during 1995–7 and a slightly greater amount of subsidence during 1997–2000. The 1995–8 leveling results indicate that most of the subsidence near Le Hardys Rapids occurred after September 1998. Note from figure 16 that the shape of the 1995–98 uplift profile differs from all previous ones, in that the greatest amount of uplift occurred at the north end of the line near Canyon Junction—29±7 mm at 11 MDC 1976. About half of that amount reasonably could be attributed to leveling error, but the InSAR image for 1996–2000 (fig. 12) suggests another explanation. The north-rim uplift feature that was centered near Norris was extensive enough to have affected the northern half of the level line, which would account for some of the uplift at Canyon

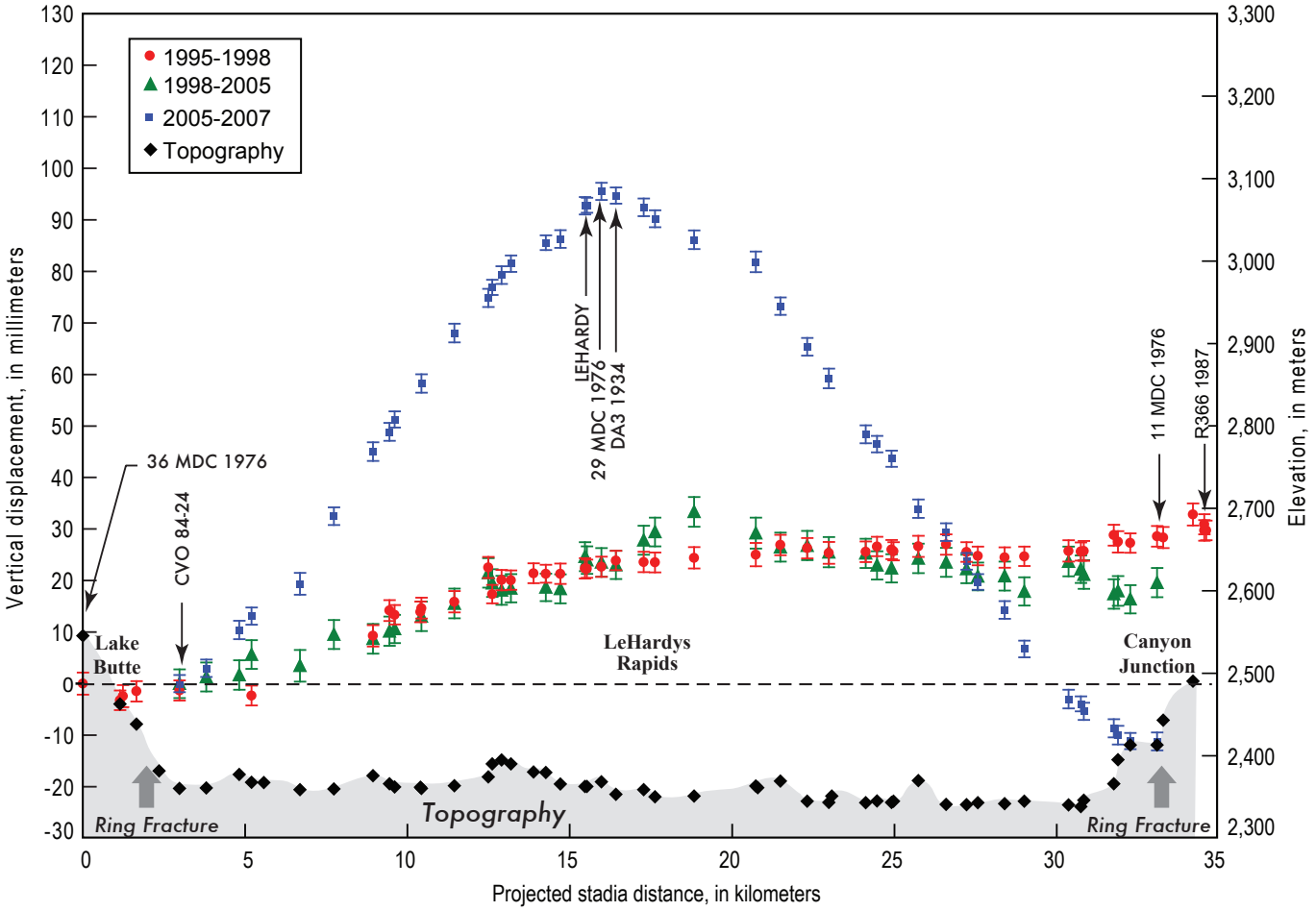

Figure 16. Diagram showing profiles of topography (black diamonds, bottom) and vertical displacements along the level line between Lake Butte and Canyon Junction by way of Le Hardys Rapids in Yellowstone National Park from 1995 to 1998 (red circles), from 1998 to 2005 (green triangles), and from 2005 to 2007 (blue squares). Descriptions and photographs of benchmarks, which are indicated by arrows with labels, are included in appendix B in the interactive data files that accompany this report. The benchmark information is available online at http://pubs.usgs.gov/pp/1788/pp1788_benchmarks/.

Junction. We suspect that the shape of the 1995–98 uplift profile reflects the combined effects of two inflation sources, one beneath the Sour Creek dome and the other beneath the north caldera rim.

The shape of the 1998–2005 uplift profile is nearly identical to that of the 1995–98 profile (fig. 16). InSAR observations indicate that the north-rim area rose as much as 80 mm from 1996 to 2000, while the Sour Creek dome subsided slightly. Uplift of the north rim area reached a maximum of about 120 mm during 2000–2002, while the area between both resurgent domes subsided as much as 40 mm (Wicks and others, 2006). The pattern changed to one of strong uplift of the Sour Creek dome starting in mid-2004, accompanied by subsidence of the north-rim area starting a few months later. From the 1998–2005 leveling results, we conclude that (1) the amount of uplift of the Sour Creek dome from mid-2004 to September 2005 exceeded the amount of subsidence there from September 1998 to mid-2004, which accounts for net uplift at Le Hardys Rapids during 1998–2005, and (2) net uplift in the Canyon Junction area during 1998–2005 reflects the combined effects of north-rim uplift during 1998–2002 and Sour Creek dome uplift starting in mid-2004.

The 1995–98 and 1998–2005 leveling results for the Canyon Junction area are reminiscent of the results for 1923 to 1975–77 as contoured by Pelton and Smith (1979, 1982). Note from figure 6 that Lake Butte and Canyon Junction are near the 0-mm and 200-mm uplift contours, respectively, and that uplift by 100–200 mm is shown extending well north of the north caldera rim. The only exception is a relative subsidence bowl centered near Norris Junction that might have been associated with the 1959 Hebgen Lake earthquake, the 1975 Yellowstone Park earthquake, or the north-rim deformation source identified by InSAR. Why such a broad area between Canyon Junction, Madison Junction, and Mammoth Hot Springs Junction should experience uplift relative to the south caldera rim remains an enigma and a topic worthy of further investigation.

The leveling results for 2005–7 are more straightforward, because they can be explained almost entirely by inflation of the Sour Creek dome source starting in mid-2004 (fig. 16). Uplift at DA3 1934 occurred at an average rate of 53±3 mm/yr during 2005–7, which is 3.8 times the average rate at nearby B11 1923 during 1923–76 (14±1 mm/yr) and 2.4 times the average rate at DA3 1934 during 1976–84 (22±1 mm/yr). Minor subsidence at the north end of the line (11±7 mm at 11 MDC 1976) could be a result of deflation of the north-rim source or leveling error.

It is interesting to note that the average uplift rate at B11 1923 near Le Hardys Rapids for 1976–2007, including the period of subsidence from 1985 to 1995, was 4±1 mm/yr. If caldera subsidence during 1985–95 had gone undocumented, we would know only that the average rate of caldera uplift had decreased markedly since the 1975–77 leveling survey. We actually know much more, thanks to frequent leveling surveys, CGPS monitoring, and repeated InSAR observations. Now the challenge is to translate that knowledge into better understanding of the causes and implications of ground motion at Yellowstone and other restless calderas.

Discussion

Considerable progress has been made in documenting the spatial and temporal patterns of ground deformation at the Yellowstone caldera since the first repeat leveling survey in 1975–77. The 1923 and 1975–77 surveys called attention to rapid crustal uplift at Yellowstone, but the surveys were separated by too many years and the leveling network was too sparse to provide a detailed picture of the deformation pattern. The first limitation was addressed by 15 leveling surveys between 1983 and 2007, which provided the first indication of caldera-floor subsidence and showed that uplift can reverse to subsidence in 2 years or less. However, those surveys were limited to two unconnected lines across the northeast and southwest parts of the caldera, so they could not shed much additional light on the spatial pattern of deformation. InSAR observations resulted in a breakthrough in that regard, first by identifying distinct deformation sources beneath the two resurgent domes and then by revealing temporal changes across the caldera over time scales too short to be captured by leveling. Another milestone was the discovery by InSAR of a third deformation source beneath the north rim of the caldera, which seems to interact with the other sources over time scales as short as a few months. Finally, CGPS stations have measured surface velocities two to three times greater than those captured by annual leveling surveys and have shown that changes in the deformation mode can occur across the entire caldera almost simultaneously (Chang and others, 2007, 2010).

Persistent snow cover at Yellowstone precludes leveling surveys or useful InSAR observations for more than 6 months each year, so the temporal resolution of these techniques is about 1 year. CGPS observations, on the other hand, provide temporal resolution on the order of 24 hours or less and represent a major step forward in monitoring ground deformation.

There has been parallel progress in understanding the causes of ground deformation at Yellowstone, but it has been less dramatic than the observational breakthroughs provided by leveling, CGPS, and InSAR. In a general way, Pelton and Smith (1979, 1982) anticipated the current view that the dominant uplift mechanism is basaltic intrusion into the mid-crust. They speculated that the intrusion responsible for historical uplift must have been "* * * recent (not more than 500 years ago) * * *" (Pelton and Smith, 1982, p. 2758). They also considered—and rejected as highly unlikely uplift mechanisms—glacio-isostatic rebound, tectonic horizontal compressive stress, and aseismic creep on an unmapped reverse fault. Rock dilatancy and coseismic deformation associated with the 1959 Hebgen Lake earthquake or the 1975 Yellowstone Park earthquake were regarded as speculative or impossible to confirm with available data.

The wealth of additional information concerning Yellowstone deformation that has been acquired by leveling, GPS,

and InSAR observations since the 1975–77 leveling survey generally supports the views expressed by Pelton and Smith (1979, 1982). However, we now know that the deformation field is more complicated and changeable than could be known from the 1923 and 1975–77 leveling surveys alone. These additional complexities call for some mechanism other than a single intrusive event to explain the situation fully. The next section outlines the salient facts about deformation at Yellowstone that must be accommodated in any successful model.

Observational Constraints on Deformation Models

The 1923–2007 leveling results and 1992–2008 InSAR observations impose several constraints on the mechanism(s) of uplift and subsidence at Yellowstone. The net elevation change at benchmark B11 1923 near Le Hardys Rapids from 1923 to 2007 was 828±23 mm, which corresponds to an average uplift rate of 10±1 mm/yr. This is the best estimate available for the long-term (century-scale) deformation rate and therefore is the appropriate value to use for models that seek to explain the caldera's background deformation mode. From the 1983 and 1984 leveling surveys, we know that uplift of the Sour Creek dome continued in the same basic pattern (that is, centered along the long axis of the caldera and extending approximately from rim to rim along the short axis) and at a somewhat greater average rate during 1976–84 (22±1 mm/yr) than during 1923–76 (14±1 mm/yr). We also know that uplift continued during 1983–84 at roughly the same rate (16±5 mm/yr), essentially stopped during 1984–85 (−2±5 mm/yr), and reversed to subsidence during 1985–86 (25±5 mm/yr). Therefore, if the 1923–84 uplift occurred as a single episode with a simple time history (1) the uplift probably started late in the 1923–76 interval, and (2) the uplift rate must have decayed rapidly from a value much higher than 22 mm/yr before 1976 to essentially zero in 1985. For example, if the uplift at Le Hardys Rapids began at the time of the 1959 Hebgen Lake earthquake, the average uplift rates at DA3 1934 were 43 mm/yr during 1959–76, 23 mm/yr during 1976–83, 16 mm/yr during 1983–84, and 0 mm/yr during 1984–85. The hypothetical uplift rate for 1959–76 is based on the assumption that all of the uplift at DA3 1934 that was measured by leveling surveys in 1923 and 1975–77 actually occurred during 1959–76 (726 mm/17 yr=43 mm/yr). Such a rate is plausible, given that the uplift rate from mid-2004 to 2008 was that high or higher. However, (1) no tectonic mechanism has been proposed to account for the shape of the 1923–84 uplift, (2) there is no evidence to support high uplift rates in the few years following the Hebgen Lake earthquake (Hamilton, 1987), and (3) the deformation pattern since 1985 requires a different explanation. Alternatively, if uplift began sometime before 1923, the higher average uplift rate during 1976–84, relative to 1923–76, requires a separate explanation. Neither scenario can be supported with available information, and neither can easily account for the abrupt onset of subsidence during 1985–86.

We know from the 1985–95 leveling surveys that the Sour Creek dome subsided progressively and without any pause lasting a full year during that entire interval. The 1-year subsidence rate at DA3 1934 varied between 35±5 mm/yr during 1986–87 and 9±5 mm/yr during 1987–88, but the average subsidence rate during 1985–93 (19±1 mm/yr) was nearly the same as the average uplift rate during 1976–84 (22±1 mm/yr). What's more, the 1976–84 uplift profile and 1985–93 subsidence profile are very similar in shape, which suggests a common source. The similarity in profile shapes is not definitive in this regard, because different sources can produce the same vertical or horizontal surface-deformation pattern. Distinguishing between such sources requires information about both vertical and horizontal surface displacements (Dieterich and Decker, 1975). Information about horizontal surface displacements at Yellowstone is available from two sources—trilateration and GPS surveys.[19] The Yellowstone trilateration network was established in 1984 and remeasured with a geodolite, a 1-mm-resolution electro-optical distance-measuring instrument, in 1985 and 1987 (Dzurisin and others, 1990). A regional network of GPS stations was established in 1987 and remeasured several times thereafter, most recently in 2010 (Smith and others, 1989; Puskas and others, 2007; Smith and others, 2009; R.B. Smith, University of Utah, written commun., November 2010). Neither dataset predates the change from uplift to subsidence during 1984–6, so it is not possible to distinguish between uplift and subsidence sources, if any distinction exists, on that basis.

The Occam's razor principle leads us to speculate that the similarity between uplift and subsidence profiles for 1976–84 and 1985–93, respectively, reflects a simple reversal in some process that can cause both uplift and subsidence at different times, rather than separate explanations for two opposite but otherwise similar outcomes. Furthermore, lacking horizontal surface-displacement data to indicate otherwise, we assume that uplift and subsidence are sourced in the same place beneath the caldera. From the 1976, 1986, 1987, and 1996 leveling surveys in the southwest part of the caldera, we know that the Mallard Lake dome moves mostly in the same direction as the Sour Creek dome during any given interval and at approximately the same rate.[20] The same inference was drawn from the 1923 and 1975–77 surveys, which showed similar amounts of net uplift at both domes. However, the greater than 50-year interval between those surveys left open the possibility of differential motion over shorter time scales. We conclude that whatever the deformation mechanism is, its reach includes both domes,

[19] InSAR measures range changes in the satellite-to-target direction and cannot separate the effects of vertical and horizontal surface displacements. The interferograms discussed here are about three times more sensitive to vertical displacements than to horizontal displacements, owing to the relatively steep incidence angles of the ERS-1, ERS-2, and ENVISAT radars (23 degrees at swath center for ERS-1 and ERS-2; 19–27 degrees for ENVISAT IS2 mode).

[20] An exception to this pattern occurred from August 1995 to September 1996. An InSAR image for that period showed uplift in the northeast part of the caldera and subsidence in the southwest part (Wicks and others, 1998).

and its effects are sometimes felt at both domes over time scales of 2 years or less. For the case of rapid caldera uplift starting in mid-2004, the onset was nearly simultaneous across the entire caldera (Chang and others, 2007, 2010). If lateral transport of magma or hydrothermal fluid is involved, this implies a high degree of connectivity within the magmatic or hydrothermal system beneath the caldera.

The discovery of subsidence during 1985–93 that mirrored the uplift during 1976–84 seemed to make a purely magmatic model for Yellowstone deformation less tenable. If surface uplift is caused by magma intrusion, then mirror-image subsidence could reasonably be attributed to magma withdrawal—but to where? Unlike many basaltic magma systems (for example, Kīlauea and Mauna Loa, Hawai‘i; Krafla, Iceland; Mount Etna, Italy; Piton de la Fournaise, and Réunion Island, Indian Ocean), the Yellowstone caldera does not have radiating rift zones to accommodate intrusions of magma from a deflating central reservoir. Conceivably, basaltic magma rises to the base of the silicic magma system, where it cools, densifies, and then sinks—a process that could account for both uplift and subsidence. This mechanism is akin to that proposed by Shaw and others (1971, p. 880–882) on a much larger scale to account for thermal circulation in the upper mantle. However, the time scale required for densification by cooling, crystallization, or volatile loss from basaltic magma beneath Yellowstone likely is too long to account for sudden reversals from uplift to subsidence, such as the one that occurred between 1984 and 1986. We revisit the magma-intrusion scenario in the Deformation Mechanisms and Models section of this paper, where we propose a variation of the concept that satisfies all of the observational constraints on deformation mechanisms.

An alternative explanation of mirror-image uplift and subsidence is that surface uplift-subsidence cycles reflect pressurization-depressurization episodes in Yellowstone's deep hydrothermal system (Dzurisin and others, 1990). We know from research drilling at Yellowstone and elsewhere, laboratory experiments, and theoretical considerations that the hydrothermal system consists of a deep, ductile zone in which pressure is near lithostatic and a shallow zone in which pressure is hydrostatic (Fournier and Pitt, 1985; Fournier, 1991, 1999). The two zones are separated by an impermeable, self-sealing layer created by mineral deposition and quasi-plastic flow, which at Yellowstone is thought to occur at depths of about 5 km (Fournier, 1999). The deep hydrothermal system beneath the self-sealing layer is near lithostatic pressure, so any change in pressure there has the potential to cause uplift or subsidence. Magmatic brine that forms during phase separation following cooling and crystallization of rhyolitic magma beneath the caldera would become trapped in horizontal lenses beneath the self-sealing layer, pressurizing it and potentially causing uplift (Fournier, 2007). Rupture of the self-sealing layer, likely during an earthquake swarm, would trigger fluid loss by upward transport, depressurization, and subsidence. If, as suggested by Fournier and Pitt (1985), a state of hydraulic equilibrium prevails throughout the deep hydrothermal system, subsidence would extend far beyond the epicentral area. Thus, rupturing of the self-sealing layer anywhere might cause the entire caldera floor to subside, as was the case during 1986–95.

Waite and Smith (2002) proposed such a mechanism to explain the October 1985 to early 1986 earthquake swarm near Madison Junction, which occurred between leveling surveys in September 1985 and September 1986 that bracketed the onset of subsidence inside the caldera. The swarm was noteworthy for several reasons: (1) it was the most energetic earthquake swarm ever recorded at Yellowstone; (2) seismic activity migrated at an average rate of 113 m/day to the northwest, away from the caldera rim, during the first month of the swarm, and thereafter it gradually migrated downward from depths of 2–5 km to more than 10 km; (3) the dominant focal mechanisms for the early part of the swarm were oblique-normal strike-slip instead of more typical normal-faulting mechanisms; (4) the maximum principal stress rotated from vertical to horizontal and subparallel to the axis of the swarm; and (5) the swarm was accompanied by two small steam explosions, increasing ground temperatures, and formation of new fumaroles and a mud volcano at three widely separated sites near the caldera rim (Dzurisin and others, 1994). Waite and Smith (2002, p. 2190 or ESE 1–14) concluded: "The most likely scenario [to account for the swarm and caldera subsidence] involves the rupture of a self-sealed hydrothermal layer and subsequent migration of hydrothermal fluid through a preexisting fracture zone out of the caldera." Before exploring this idea further, we move on to additional observational constraints on the role that hydrothermal fluid might play in Yellowstone deformation.

Starting in 1992, the most revealing information about ground deformation at Yellowstone came, not from leveling surveys, but from sequential InSAR observations. We learned from interferograms that spanned 1992–93 and 1993–95 that, although both domes subsided during both of those intervals, they did so differentially. That is, the area of maximum subsidence switched from the Sour Creek dome during 1992–93 to the Mallard Lake dome during 1993–95. This occurrence suggested either a lateral connection beneath the domes or separate deformation sources that might be connected at greater depth. An interferogram for 1995–96 captured what seems to be a relatively rare occurrence; that is, the Sour Creek dome rose while the Mallard Lake dome subsided. By 1997, uplift had spread southwestward across the caldera to include the Mallard Lake dome. These observations led Wicks and others (1998, p. 461) to conclude (1) that "interacting fluid reservoirs exist beneath the SC [Sour Creek] and ML [Mallard Lake] domes, with the inflation of each being regulated by flow through two conduits, one beneath SC * * * and the other connecting SC and ML* * *", and (2) that "* * * the driving pressure source may lie beneath the SC dome." The key bit of evidence for a lateral connection between the domes was the migration of the deformation front from one dome to the other within 2 years or less.

The Yellowstone deformation puzzle became even more complicated when InSAR images for 1996–2000 revealed a third deformation source beneath the north caldera rim (Wicks

and others, 2006). Recall that an earlier InSAR study and leveling surveys (Wicks and others, 1998; Dzurisin and others, 1999) indicated that following the period of caldera subsidence from 1985 to 1995 uplift began at the Sour Creek dome during 1995–96 and spread southwestward to the Mallard Lake dome during 1996–97. North-rim uplift began in 1997 and continued into 2002, while the caldera floor subsided. In this case, nearly simultaneous onset of north-rim uplift and caldera-wide subsidence suggested a connection among three sources—two beneath the resurgent domes and one beneath the north rim. The latter was centered near the structural intersection of the caldera ring fault, north-trending Norris–Mammoth corridor, and a west-northwest striking seismic belt east of the Hebgen Lake fault zone.

The most recent chapter in the Yellowstone deformation story is the near-simultaneous onset of uplift across the entire caldera in mid-2004, accompanied by north-rim subsidence. Chang and others (2007) jointly inverted GPS and InSAR observations, and wrote: "We thus suggest that the 2004–2006 episode of accelerated inflation occurred in response to a caldera-wide magma recharge of the Yellowstone volcanic system." Acknowledging that models of earlier deformation episodes are consistent with fluid pressurization in the upper part of the magmatic system, they concluded, "* * * magma intrusion and fluid pressurization should be considered as jointly operating processes to explain the accelerated caldera uplift reported here, although our estimate of large volume increase implies the former as a preferred source model." With regard to north-rim subsidence, Chang and others (2007) wrote: "We therefore propose that the 2004–2006 deflation near Norris Geyser Basin was in response to a redistribution of hydrothermal fluids as a consequence of caldera inflation."

To the extent that the model of Chang and others (2007, 2010) reflects current consensus, we can say that progress since the work of Pelton and Smith (1979, 1982) has been mainly in two areas: (1) documentation of the complexity—in both space and time—of the deformation field and (2) recognition of the likely role played by fluids in causing uplift and, especially, subsidence. Two remaining challenges are (1) to identify the fluids involved and (2) to improve understanding of the physical interactions among magma, fluids, heat, the hydrothermal system, and country rock that produce seismicity and surface deformation.

These challenges are being addressed in several ways. In addition to improved monitoring of deformation, gravity, seismic, and geochemical parameters, more realistic models are being developed to investigate the likely role of fluids and heat in causing ground deformation. For example, Hurwitz and others (2007a) carried out numerical simulations of hydrothermal-fluid flow and deformation in large calderas by coupling two numerical computer codes—TOUGH2 (Pruess and others, 1999) and BIOT2 (Hsieh, 1996). TOUGH2 is a three-dimensional (3-D) integrated finite difference simulator for nonisothermal, multicomponent (for example, H_2O-CO_2-NaCl), and multiphase flow in porous or fractured media. BIOT2 simulates axisymmetric or plane-strain deformation and fluid flow in a linearly elastic porous medium. To simulate the effects of fluids exsolving from a crystallizing magma body beneath a Yellowstone-size caldera, Hurwitz and others (2007a) used TOUGH2 to calculate the pressure and temperature distributions resulting from injection and flow of high-temperature (350ºC) water within a cylindrical volume with a radius of 50 km and a height (thickness) of 3–5 km. They used the output from TOUGH2 as input to BIOT2 to calculate the resulting elastic deformation field as a function of time. Their simulations showed that small differences in the assumed values of permeability and its anisotropy, shear modulus, and the depth and rate of fluid injection lead to large variations in the magnitude, rate, and geometry of surface deformation. Nonetheless, they were able to simulate the uplift rates observed at the Yellowstone, Long Valley, and Campi Flegrei calderas by using reasonable suites of parameter values. Todesco and others (2004) used a similar approach and showed that the temporal pattern of deformation at Campi Flegrei (that is, rapid uplift followed by slower subsidence) could be produced by poroelastic response of the shallow hydrothermal system to a pulse of magmatic fluid from depth. Hurwitz and others (2007a, p. 1) concluded that "* * * the injection of aqueous fluids into the shallow crust may explain some of the deformation observed in calderas."

Using a similar approach, Hutnak and others (2009) addressed an acknowledged limitation of the study by Hurwitz and others (2007a), that is, the assumption of single phase (liquid) and single component (pure water) fluid flow. In their simulations, Hutnak and others (2009) included two components (hot water and carbon dioxide, which are sourced into the overlying hydrothermal system from a crystallizing magma body) and two water phases (liquid and steam). For a range of plausible hydrologic parameters (permeability, injection rates, depths, and fluid compositions), they investigated effects of (1) high versus low permeability in rock hosting the hydrothermal system, (2) fluid injection from a point source versus a distributed source, (3) fluid saturation in water versus water + carbon dioxide systems, and (4) pulsed injection to simulate repeated rupturing of a self-sealing layer. Hutnak and others (2009) concluded:

(1) Numerical models are capable of generating ground surface deformation rates, magnitudes, and geometries similar to those observed in some large calderas,

(2) Simulated deformation (including subsidence) can be complex in time and space, even for homogenous property distributions and steady fluid sourcing,

(3) Gas formation in the shallow subsurface leads to broader radial extents and magnitudes of uplift, as well as increased uplift rates, and

(4) Hydrothermal circulation may explain periods of rapid surface deformation not followed by volcanic eruption.

Hutnak and others (2009, p. 10) summarized their findings as follows: "The potential for both rapid and gradual GSD

[ground-surface displacement] resulting from magma derived aqueous fluids, as demonstrated in this study, suggests that hydrothermal fluid circulation may help explain some occurrences of GSD that have not culminated in magmatic eruptions." In the future, this study could be extended to include other volatile components (sulfur, chlorine), hypersaline brine (a byproduct of crystallization of silicic magmas), and heterogeneous permeability (layers, fractures).

Complications that include heterogeneous and poorly known crustal properties are a problem for any type of deformation model, whether its approach is analytical or numerical and whether the assumed crustal rheology is elastic, plastic, or other. Some of these effects have been explored in recent publications by Masterlark (2007), Manconi and others (2007), Hurwitz and others (2007a), and Hutnak and others (2009). Such complexities might preclude a definitive result from modeling for the foreseeable future, but we believe nonetheless that modeling holds considerable promise for providing insights into caldera deformation processes and for guiding future observational and experimental studies.

More than three decades after the discovery of surface uplift at Yellowstone (Pelton and Smith, 1979; 1982), the understanding of its causes is still a work in progress. Consideration of poroelastic and thermoelastic effects, and of nonelastic rheology—which were ignored in most previous studies of Yellowstone but now are amenable to investigation—calls into question any conclusion about the causes of deformation (including our preferred model, see below). Future work, both experimental and theoretical, will reveal to what extent our current thinking reflects the real situation at Yellowstone.

Constraints from Deformed Shorelines and Microgravity Measurements

Two sets of observations that bear directly on the nature and causes of ground deformation at Yellowstone have yet to be discussed: (1) studies of deformed shorelines that extend the record of vertical surface displacements backward in time for several thousand years (Pierce and others, 2002), which provides important context for conceptual models; and (2) repeated microgravity observations, which when combined with height-change information from leveling and GPS, provide constraints on mass changes beneath the caldera and have the potential to distinguish between relatively low-density hydrothermal or magmatic fluids and higher-density magma as the primary deformation agent.

Evidence from Deformed Shorelines

The shorelines of Yellowstone Lake and its outlet stream, the Yellowstone River, record a rich Holocene deformation history, including at least two major inflation-deflation cycles that were thousands of years long and ~30 m in amplitude at Le Hardys Rapids relative to the caldera margin (Pierce and others, 2002, p. 2, 13; Locke and Meyer, 1994; Meyer and Locke, 1986). Between the lake outlet at Fishing Bridge and the bedrock knickpoint at Le Hardys Rapids, 5 km downstream, the river's surface drops only 0.25 m. As a consequence of this extremely low gradient, vertical motion of the knickpoint affects mean lake level. Uplift of Le Hardys Rapids causes mean lake level to rise, and subsidence causes the mean level to fall. These changes are superimposed on a long-term trend of falling lake level, as a result of erosion at the outlet (Pierce and others, 2002, p. 16). During relatively stable stands of the lake, terraces form in horizontal position along the shoreline. Subsequent vertical motion at Le Hardys Rapids affects preexisting terraces in two ways: (1) uplift or subsidence of the knickpoint cause terraces to submerge or emerge, respectively, as the lake level rises or falls, and (2) differential uplift or subsidence warps terrace surfaces that were initially planar and horizontal. Thus, tilting of the lake basin has resulted in terraces that range from about 30 m below the present shoreline to about 20 m above it. Each terrace records the cumulative effects of all uplift or subsidence episodes since the terrace formed. By measuring the tilts of a sequence of remnant terrace surfaces that surround the modern lake and determining the ages of terraces, it is possible to unravel the postglacial deformation history of the lake basin.[21]

Pierce and others (2002) deduced from their study of deformed terraces at Yellowstone Lake that twice during the past ~15,000 years Le Hardys Rapids has been uplifted ~8 m relative to the current lake outlet—most recently from 3,000–4,000 years ago to the present. Because those locations span only ~25 percent of the uplift measured by leveling surveys, they projected ~32 m of total uplift relative to the caldera margin. Nonetheless, subsidence has balanced or slightly exceeded uplift over the entire postglacial period, as shown by older shorelines that descend toward the caldera axis. Pierce and others (2002) inferred average uplift rates at Le Hardys Rapids over millennial time scales in the range 12–16 mm/yr, which is close to the average historical uplift rate from leveling surveys. Although the average uplift rates during parts of postglacial time and historical time are similar, the sheer magnitude of postglacial motions adds another dimension to considerations of deformation mechanisms. Pierce and others (2002) considered magma intrusion, crustal stretching, batholithic cooling, and hydrothermal pressure changes to be likely contributors. They concluded (Pierce and others, 2002, p. 2):

> We favor a hydrothermal mechanism for inflation and deflation because it provides for both inflation and deflation with little overall change. Other mechanisms such as inflation by magma intrusion and deflation by extensional stretching require two separate processes to alternate and yet result in no net elevation change.

[21] Terrace ages were established by radiocarbon dating of incorporated organic material, projectile-point ages obtained in archeological surveys, and geological studies (Pierce and others, 2002).

They clarified their use of the term "hydrothermal mechanism" as follows (Pierce and others, 2002, p. 24): "The mechanism of uplift by hydrothermal pressure buildup beneath a hydrothermal seal followed by subsidence due to rupture of the seal, and release of fluids * * *." It is important to note that the fluids to which they refer are most likely of magmatic origin, that is, released during intrusion or subsequent crystallization of basaltic or rhyolitic magma beneath the caldera (Fournier, 1989, 1999). Fluids of meteoric origin are limited to the hydrostatically pressured part of the hydrothermal system, above the self-sealing layer, where fracture permeability is high. Magmatic fluids that are trapped beneath, and eventually escape through, the self-sealing layer that caps the lithostatically pressured part of the hydrothermal system are the more likely deformation agent.

Evidence from Repeated Microgravity Surveys

Fluid connections among three separate but interacting deformation sources beneath the Yellowstone caldera are a plausible explanation for (1) migration of subsidence from the Sour Creek dome to the Mallard Lake dome during 1993–95, (2) migration of uplift from the Sour Creek dome to the Mallard Lake dome during 1995–97, (3) the near-simultaneous onset of north-rim uplift and caldera-wide subsidence in 1997, and (4) the reversal from north-rim uplift and caldera-wide subsidence during 1997–2002 to north-rim subsidence and caldera-wide uplift in mid-2004. A key question—What is the nature of the fluid?—is best addressed by repeat microgravity observations, which are sensitive to subsurface mass changes and to the density of the material added or lost. In the absence of any subsurface mass change, the ratio of gravity change to height change, $\Delta g/\Delta h$, is the average free-air gradient of −3.086 microgal per centimeter (μGal/cm). If height changes are accompanied by a change in mass (density) within a subsurface body of arbitrary shape, the value of $\Delta g/\Delta h$ varies with the body's shape and its density contrast with the surrounding rock (Telford and others, 1990; Turcotte and Schubert, 2002).

The Yellowstone gravity network consists of 160 stations along the level lines shown in figure 6, plus 40 additional stations in remote areas where height changes are measured by GPS observations (Hollis and others, 1987; Smith and others, 1989; Arnet and others, 1997). Each station comprises a benchmark and some means to precisely position a gravity meter either directly over the mark or adjacent to it (for example, three small, shallow holes ("dimples") in bedrock that align with the feet of a gravity-meter base plate). The gravity network was observed in 1977, 1983, 1987, 1991, and 1993, each time during late summer or early autumn to reduce the effect of water-table changes. Arnet and others (1997) reported that the gravity field decreased across the caldera from 1977 to 1983 by as much as 60±12 μGal along the caldera axis, then increased by the same amount from 1986 to 1993. The sense of the changes is consistent with leveling observations that indicated uplift from 1975–77 to 1984 and subsidence from 1985 to 1993. For stations along the level line between Lake Butte and Mount Washburn, Arnet and others (1997) found the weighted mean value of $\Delta g/\Delta h$=−1.7±0.7 μGal/cm for the 1977–83 period of uplift and $\Delta g/\Delta h$=−3.3±1.0 μGal/cm for the 1986–93 period of subsidence. Arnet and others (1997, p. 2743) wrote:

> Based on these results, we conclude that a mass increase occurred during the uplift episode. During the subsidence the gravity change followed almost the free-air gradient, thereby indicating that probably no mass change took place during this period.

To account for contemporaneous surface uplift and mass increase, Arnet and others (1997, p. 2744) called upon redistribution of hydrothermal fluid and magma input:

> We suggest that the most likely source of the gravity decrease, concomitant with the crustal uplift, is related to widespread hydrothermal fluid movement, which furthermore is related to input by magma. Basaltic intrusions into the mid or upper crust, pressurization of a deep hydrothermal system by magmatic gas, or brine released by crystallization of a rhyolitic melt, are also plausible sources for the uplift. It cannot have been caused solely by pressurization of the deep hydrothermal system, without any significant mass increase.

Regarding the mechanism for subsidence, which occurred without a detectable change in subsurface mass, Arnet and others (1997, p. 2744) wrote:

> For the episode of gravity increase – ground subsidence, the spatial synchroneity between the area of uplift (1923–1984) and the area of subsidence (1984–1994) suggests a common causative mechanism related to magmatic/hydrothermal intrusion followed by degassing from the same source. The fact that subsidence has not been accompanied by a measurable mass change is best explained by depressurization of the deep hydrothermal system as a result of fracturing and volatile loss to the shallow hydrothermal system or, less likely, reduced input of brine to the deep system. The first interpretation is preferred because it more easily explains the relatively abrupt change from uplift to subsidence during 1985–1986 (Dzurisin et al., 1990), which was also accompanied by sizable earthquake swarms originating in the upper crust.

Three factors weigh on the side of caution in interpreting the gravity results. First, the $\Delta g/\Delta h$ values for periods of uplift and subsidence are essentially the same within two standard deviations. Second, the $\Delta g/\Delta h$ value for a single station north of Fishing Bridge, where the gravity and height changes were greatest, was −3.3±0.7 μGal/cm for the entire period from 1977 to 1993, which included roughly equal amounts of uplift and subsidence (Arnet and others, 1997, p. 2743). Within uncertainty, this value is the same as the average free-air

gradient (−3.086 μGal/cm). Third, owing to a lack of suitable water-well data, no corrections were made to the gravity data for water-table differences between surveys. Although all of the surveys were conducted during the same time of year to reduce water-table effects, some unknown contribution to the gravity measurements is still possible. Uncorrected water-table variations would introduce noise of unknown magnitude to the gravity measurements and possibly bias $\Delta g/\Delta h$ values in an unpredictable way.

These reservations notwithstanding, the microgravity observations reported by Arnet and others (1997) provide support for the idea that surface uplift is caused, at least in part, by intrusion of magma—presumably basalt—in the mid-crust. Likewise, the evidence from microgravity observations that subsidence can occur with little or no subsurface mass change is consistent with the idea that fluid loss from magma—either as brine or gas and either from crystallizing rhyolite or degassing basalt—is a viable deformation mechanism. Additional microgravity observations, during periods of both uplift and subsidence and in areas affected by all three deformation sources, should provide additional constraints on deformation mechanisms. Scientists from the University of Utah now conduct microgravity surveys throughout Yellowstone National Park each autumn, most recently in 2010 (R.B. Smith, University of Utah, written commun., November 2010).

Deformation Mechanisms and Models

Previous Work

The discovery of caldera-floor subsidence starting in 1986, following a period of uplift, triggered a search for a deformation mechanism that could account for both of those deformation modes and also the relatively rapid switch between them. Subsequent observations—namely (1) deformation-front migration from the Sour Creek dome to the Mallard Lake dome, (2) alternating inflation-deflation cycles between the north-rim source and both caldera-floor sources, and (3) large but nearly offsetting amounts of uplift and subsidence within the caldera during postglacial time—led to general agreement that fluids of some sort are involved in the deformation mechanism (Dzurisin and others, 1990; Wicks and others, 1998, 2006; Pierce and others, 2002; Waite and Smith, 2002; Chang and others, 2007, 2010).

Two general classes of models have been proposed to explain surface deformation at Yellowstone since its discovery more than three decades ago, and both remain viable in various forms today. One class of models, commonly referred to as "hydrothermal" models, relies mainly on pressurization/depressurization of fluids other than magma to produce surface uplift/subsidence. Three variations on this theme are (1) supercritical fluid forms by phase separation from crystallizing magma and is trapped beneath a self-sealing layer at lithostatic pressure in ductile rock to produce uplift; episodic rupturing of the seal produces subsidence (for example, Dzurisin and others, 1990); (2) poroelastic deformation in the shallow hydrothermal system is induced by magmatic gas influx at the base of the hydrothermal system (for example, Todesco and others, 2004; Hurwitz and others, 2007a; Hutnak and others, 2009); and (3) precipitation recharge induces a poroelastic response of the shallow hydrothermal system (for example, Howle and others, 2003; Jahr and others, 2008; Westerhaus and others, 2005). In the first case, one might expect an increase in the surface flux of magmatic fluid associated with the onset of subsidence. This has not been observed, but there are reasons to think that the effect could be masked by the shallow hydrothermal system (Fournier, 2004) or so long-delayed as to be unrecognizable (Hurwitz and others, 2007b). The second type of hydrothermal model, involving poroelastic deformation in response to magmatic gas influx at the base of the hydrothermal system, requires a high rate of basaltic intrusions or convection of a large volume of basalt in the lower to mid-crust (Lowenstern and Hurwitz, 2008). Both processes would produce episodic releases of magmatic gases including CO_2—which could account for the very high surface flux of CO_2 observed at Yellowstone (Werner and Brantley, 2003). A third type of hydrothermal model, in which precipitation recharge induces a poroelastic response of the shallow hydrothermal system, has been invoked to explain surface motions at the Casa Diablo geothermal area in California (Howle and others, 2003) and at Merapi volcano, Indonesia, but as yet has not been applied to Yellowstone. In our opinion, all three of these "hydrothermal" mechanisms probably contribute in some measure and over various time scales to deformation at Yellowstone, and they merit further investigation through the use of numerical simulations or other modeling techniques.

The second class of models proposed to explain surface deformation at Yellowstone is generally referred to as "magmatic" for brevity. We will be explicit about our usage of the terms magma, magmatic fluid, and hydrothermal fluid later in this section, but for now the following distinction is sufficient. The primary deformation mechanism in magmatic models is injection of magma or fluid exsolved from magma at or below the base of the hydrothermal system, whereas in hydrothermal models the primary deformation mechanism is a pressure change within the hydrothermal system in response to some perturbation such as a gas pulse or precipitation recharge. Our preferred model is an amalgamation of ideas from recent studies by several authors, as summarized below.

Chang and others (2007) used joint inversion of InSAR and GPS data for 2004–6 to identify two deformation sources at Yellowstone: (1) an expanding, subhorizontal, sill-like source (that is, a tabular body) at a depth of 7–12 km beneath the caldera, and (2) a contracting volume at a depth of 8–16 km under the Norris area. These results are consistent with the earlier model of Wicks and others (2006) for 1996–2002, a period of north-rim uplift and caldera-floor subsidence. Their model included two subcaldera, contracting tabular bodies, one beneath the Sour Creek dome and the other beneath the central part of the caldera and Mallard Lake dome, both at

depths of 6–14 km. These correspond to the single, expanding tabular source at 7–12 km depth in the model of Chang and others (2007). For the north-rim source, Wicks and others (2006) proposed an expanding tabular source at 9–16 km depth, which corresponds to the contracting volume at 8–16 km depth in the model of Chang and others (2007). Both sets of authors called on fluid interactions between/among sources and regarded magma as the "fluid" most likely to be involved. However, both groups also mentioned the alternative possibility that hydrothermal or magma-derived fluids were the main deformation agent. In supplementary material for their manuscript, Wicks and others (2006) noted that a distributed, shallower source could be constructed to fit the north-rim uplift data for 1996–2002 equally well. A shallower source would be more permissive of the idea that deformation originates in the deep part of the hydrothermal system rather than in the underlying magmatic system. We note that the source depths indicated by these models are below the brittle-ductile transition, which is thought to occur at ~5 km depth beneath the Yellowstone caldera (Smith and Bruhn, 1984; Smith and Braile, 1994). Therefore, the models' assumption of linear elastic behavior is likely to be violated in rock surrounding the deformation sources, which adds uncertainty to any inferences drawn from the results.

Parallel studies by Puskas and others (2007) and Vasco and others (2007) produced results that are consistent with those of Wicks and others (2006) and Chang and others (2007, 2010) and offer additional insight into the configuration of deformation sources beneath the caldera. Puskas and others (2007) presented results of campaign-mode GPS and CGPS observations of the Yellowstone–Snake River Plain region for 1987–2004. For the Yellowstone caldera, including the northwest caldera boundary (equivalent to the north-rim source area discussed here), they divided the observations into three time windows of uniform ground motion. During 1987–95, the GPS observations indicate that the center of the caldera subsided 14±3 mm/yr. Leveling in the vicinity of Le Hardys Rapids gives essentially the same result for the same time period, that is, subsidence at an average rate of 16±1 mm/yr. For 1995–2000, Puskas and others (2007) reported from their analysis of GPS data that the north-rim area rose 15±4 mm/yr. That result is consistent in a qualitative sense with InSAR observations reported by Wicks and others (2006), which indicate about 100 mm of range decrease (mostly uplift) along the north-rim during 1996–2000. For 2000–3, the GPS and InSAR observations both indicate caldera-floor subsidence and north-rim uplift. Puskas and others (2007) found that the caldera floor subsided at an average rate of 9±6 mm/yr during that period, while the north-rim area rose at an average rate of 12±4 mm/yr. Wicks and others (2006) reported about 50 mm of range increase (mostly subsidence) in the central part of the caldera and about 40 mm of range decrease (mostly uplift) in the north-rim area during 2000–2002, and they also reported that both motions paused during 2002–3. Thus, the average displacement rates for 2000–3 from InSAR are about 17 mm/yr subsidence in the caldera and about 13 mm/yr uplift along the north rim. The GPS and InSAR results for this period are consistent qualitatively, although the measured caldera-floor subsidence rates differ by about a factor of 2.

Vasco and others (2007) used InSAR, GPS, and leveling observations to constrain deformation source models for the Yellowstone caldera for 1992–95, 1996–2000, 2000–2001, and 2001–2. Their modeling approach differed from those of Wicks and others (2006) and Chang and others (2007) in that Vasco and others (2007) allowed for an arbitrary, three-dimensional distribution of subsurface volume change rather than prescribing a specific source shape, such as a sphere, ellipsoid, or sill. To make the resulting mathematical problem tractable, they included penalty terms and inequality constraints in their formulation of the problem. Interested readers should consult Vasco and others (2002, 2007) for details. For 1992–95, Vasco and others (2007) concluded that caldera-floor subsidence was associated with decreases in source volume at depths of 6–10 km beneath the Elephant Back fault zone, that is, beneath a southwest-trending zone between the Sour Creek and Mallard Lake resurgent domes and extending northeast to Hot Springs Basin. The Elephant Back fault zone is approximately parallel to, and offset slightly to the southeast of, the long axis of the caldera (fig. 1). Both features are coincident with the area of maximum caldera-floor uplift from 1923 to 1975–77 as contoured by Pelton and Smith (1979, 1982). Another intriguing aspect of the source model for caldera-floor subsidence during 1992–5 is a linear trend of volume decrease extending north from the center of the caldera toward the north rim in the Norris area (fig. 17, reproduced from Vasco and others, 2007, fig. 5, p. 9). Vasco and others (2007) noted that the linear subsidence feature is located beneath an alignment of volcanic vents that fed post-caldera collapse (that is, younger than 0.64 Ma) lava flows, as mapped by Christiansen (2001).

We are struck by the similarity between the pattern of volume decreases inferred by Vasco and others (2007) and the "magma migration paths" interpreted by Wicks and others (2006) (compare figs. 17 and 18). Granted that both studies analyzed the same InSAR data, the similarity is nonetheless remarkable when one considers that Vasco and others (2007) also included GPS and leveling data in their analysis and used a different modeling approach. Wicks and others (2006) modeled InSAR data only, which do not provide the independent measurements of vertical and horizontal surface displacements that would greatly improve the constraints on source depth and shape (Dieterich and Decker, 1975). Accordingly, they considered only simple source shapes (prolate ellipsoid, sill) and showed that slightly dipping sills beneath the caldera (depth about 11 km, contracting) and north-rim (depth 9–16 km, expanding) provide the best fit to the 1996–2002 InSAR data. Their hypothesized magma migration paths (fig. 18) do not derive directly from modeling but instead derive from consideration of the relative timing of uplift and subsidence at different locations. Uplift of the Sour Creek resurgent dome started during 1995–96 and spread to the Mallard Lake dome during 1996–97. North-rim uplift began in 1997 and continued

into 2002, while the resurgent domes subsided. Wicks and others (2006) inferred from that pattern of deformation that a pulse of basaltic magma rose beneath the Sour Creek dome during 1995–96 and then migrated laterally to beneath the Mallard Lake dome and north rim area during 1996–97. They sketched their magma migration pathways accordingly.

Vasco and others (2007), on the other hand, included GPS and leveling data in their analysis, which together with the InSAR data provide a stronger constraint on the depth and shape of the source (although still subject to the limitation, noted above, imposed by assuming linear elastic rheology in the source region). Their result for the depth of the subcaldera source (6–10 km) differs slightly from that of Wicks and others (2006, about 11 km), but both results can be interpreted to coincide with the upper part of a crystallizing rhyolite body that has been hypothesized to exist beneath the caldera (for example, Eaton and others, 1975; Miller and Smith, 1999; Christiansen, 2001). Consistent with that idea, Husen and others (2004, p. 397) identified a low velocity zone for seismic P waves below 8 km depth that they interpreted as "* * * possibly representing hot, crystallizing magma." More important, in our opinion, than the exact source depth is the fact that Vasco and others (2007) were able to discern a connection among the deformation sources that underlie the Sour Creek dome, Mallard Lake dome, and north rim area. Their depiction of subsurface volume decreases during 1992–95 is reminiscent of the magma plumbing system sketched by Wicks and others (2006) on the basis of the chronology of caldera-floor subsidence and north-rim uplift during 1995–2002. Furthermore, Vasco and others (2007) claim to have detected an episode of lateral fluid intrusion from beneath the center of the caldera to the north-rim area during that period, which is consonant with the conceptual model of Wicks and others (2006). Vasco and others (2007, p. 15–18 of 19) concluded:

> Based upon contemporary Yellowstone deformation, we find that subsurface volume changes correlate with the resurgent domes and the Elephant Back fault zone, north-trending extensional faults related to a line of volcanic vents, and the extensive magma body beneath the caldera. These correlations suggest that such features control or at least influence deformation within the caldera, either as zones of mechanical weakness or as pathways for fluid flow or both. * * * We thus hypothesize that the observed surface deformation within and adjacent to the Yellowstone Caldera is due to the interaction of an underlying, large-scale crystallizing magmatic system and zones of weakness associated with crustal faults. In particular, large-scale pressure and mass changes within the magma body are focused into faults that act as narrow conduits or pathways for flow. The focused flow and pressure changes give rise to observable surface deformation. * * * We envision that the Yellowstone volcanic system involves the interaction of at least three subsystems: the shallow crustal hydrothermal system and seismogenic faults, the semisolid magmatic body, and a deeper underlying basaltic magma system. As yet, we cannot specify the exact nature of the interaction between these major components, and we can only draw very general conclusions about the influence of one component upon another. Specifically, the results here imply that crustal faults act as conduits for flow from within the Earth. Thus we are not proposing an encompassing model of the Yellowstone system, as given recently by Wicks et al. [2006].

Notwithstanding the qualification at the end of the preceding quotation, the general agreement between the conceptual model of Wicks and others (2006) and the numerical modeling results of Vasco and others (2007) is encouraging and, in our view, lends support to both studies.

Our Preferred Model

We are cognizant of the fact that geodetic data such as those presented here provide information only about displacements of the ground surface, which are but one manifestation of complex subsurface processes. To infer what those processes might be from such information, modelers generally must incorporate additional datasets and rely on assumptions or simplifications to make the modeling problem tractable. This introduces an additional level of uncertainty, which is best addressed by quantitative models that can test specific assumptions or hypotheses. The conceptual model outlined below does not meet that standard, nor is it intended to exclude other types of models that ultimately might prove to be correct. Instead, it describes our current thinking based on more than 25 years of deformation studies at Yellowstone and it offers some testable hypotheses for others to confirm or reject. Our preferred model is not an original contribution but rather an amalgam of ideas from earlier studies by several authors.

Taken together, the ideas put forward by Wicks and others (2006), Chang and others (2007, 2010), and Vasco and others (2007) can explain both the spatial and temporal patterns of deformation observed at Yellowstone. The leveling and InSAR results for 1983–2008 suggest an oscillatory pattern of uplift and subsidence within the caldera and along the north caldera rim (fig. 19). The northeast floor of the caldera rose during 1976–84, subsided during 1975–95, rose during 1995–97, subsided during 1997–2002, rose rapidly but at a declining rate during 2004–8, and had paused by late 2009. Meanwhile, the north rim area rose during 1997–2002, subsided during 2002–8, and also had paused by late 2009 (both 2009 results from CGPS observations). Generally speaking, the caldera floor rose while the north rim subsided and vice versa. Data for the Mallard Lake dome are not included in figure 19, owing to the paucity of leveling data there, but we know from leveling surveys in 1986 and 1987, and from InSAR observations since 1992, that the two domes tend to move up or down in unison. The only known exception occurred during

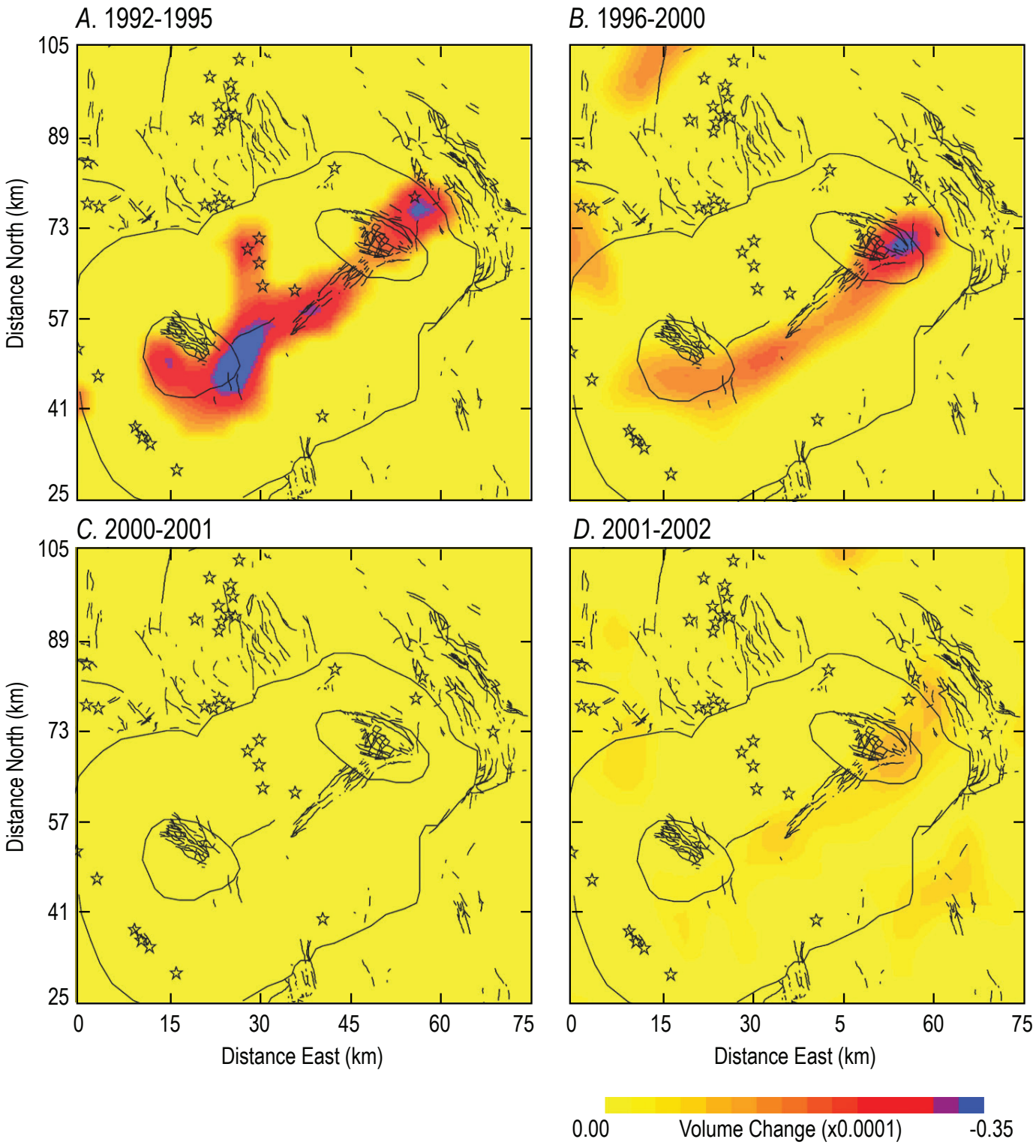

Figure 17. Diagrams of estimates of subsurface volume decrease at 6–8 km depth within the Yellowstone caldera, Yellowstone National Park, based on a best-fit model of GPS and InSAR observations. Time intervals shown are (*A*) 1992–1995, (*B*) 1996–2000, (*C*) 2000–2001, and (*D*) 2001–2002. For each time interval, the model layer at 6–8 km depth was the uppermost one containing volume decreases that the authors regarded as significant. Color scale is in terms of fractional volume change, which is unitless. Compare to figure 18 in this paper, which is based on an independent study by Wicks and others (2006). Figure reproduced from Vasco and others (2007, fig. 5).

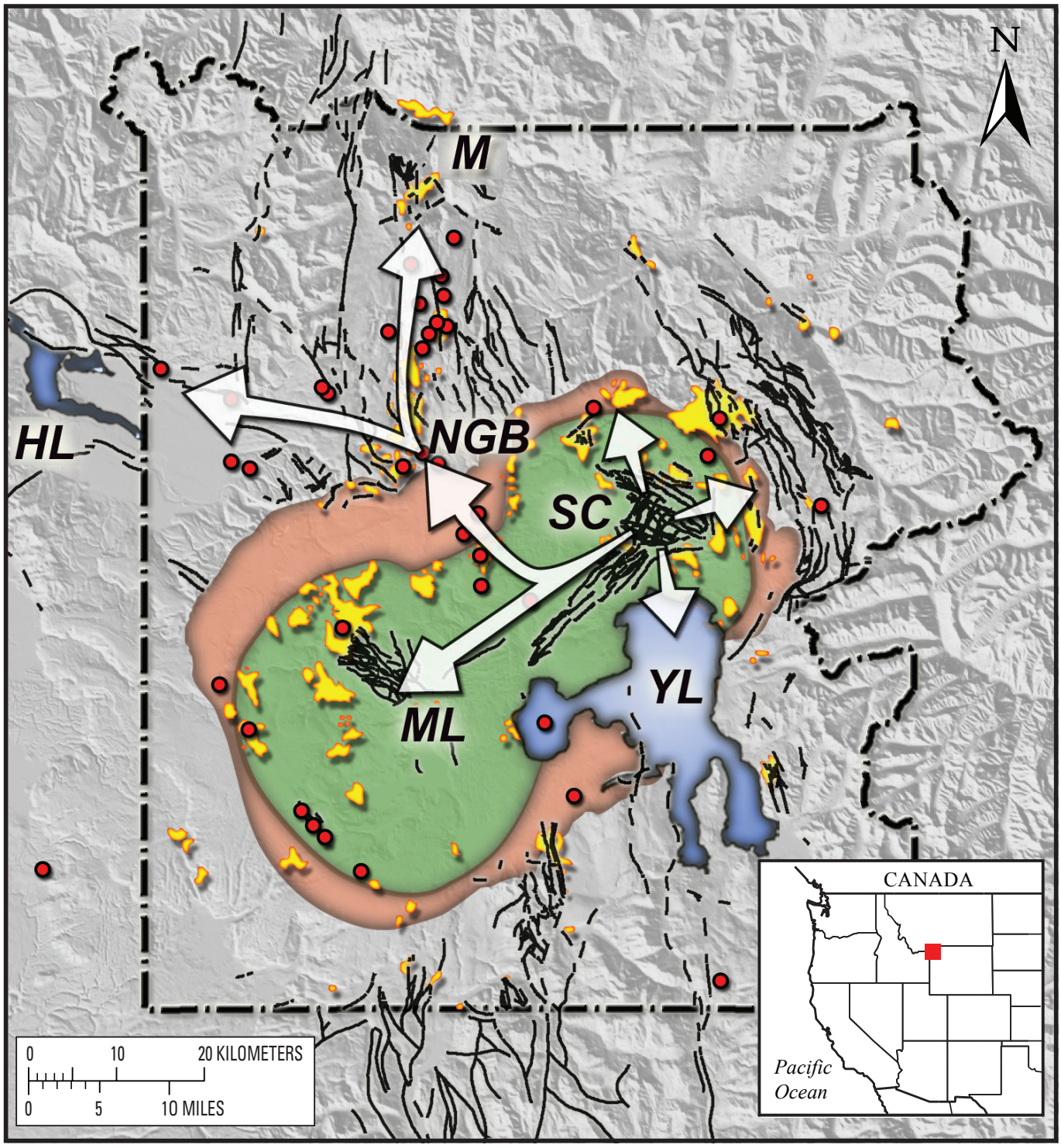

Figure 18. Map of structural, thermal and volcanic features in and around the Yellowstone caldera, Yellowstone National Park. Red circles mark locations of known volcanic vents that erupted after the caldera-forming event at 0.64 Ma (Christiansen, 2001). Areas of known past or present thermal activity are colored yellow. The part of the caldera bounded by ring-fractures is shown green, and the slumped zone between the ring-fracture zone and the best estimate of the caldera rim is shown in salmon. The National Park boundary is the dashed black line. Faults active in the Quaternary are marked with black lines. The labeled features are Norris Geyser basin (NGB), Mammoth Hot Springs (M), Sour Creek resurgent dome (SC), Mallard Lake resurgent dome (ML), Hebgen Lake (HL) and Yellowstone Lake (YL). White arrows show interpreted magma migration paths. Red square in the inset map (bottom right) shows the location of the study area. Compare to figure 17, which is based on an independent study by Vasco and others (2007). Figure from Wicks and others (2006).

1995–96, when the Sour Creek dome started to rise while the Mallard Lake dome was still subsiding slightly. However, by the following year, both domes were moving upward. We caution that the uplift and subsidence rates shown in figure 19 are not strictly comparable, for three reasons: (1) the periods of observation for leveling and InSAR differ in some cases; (2) the InSAR rates shown are average maximum values for the Sour Creek dome as a whole, whereas the leveling rates are for specific benchmarks near Le Hardys Rapids; and (3) InSAR measures line-of-sight range changes, whereas leveling measures vertical surface displacements. Nonetheless, the pattern described above generally has held since 1992, when InSAR data first became available.

The pattern of oscillatory, out-of-phase uplift and subsidence at the Sour Creek dome and north caldera rim can be explained by the models of Wicks and others (2006), Chang and others (2007, 2010), and Vasco and others (2007) as follows. A period of increased magma supply from a source beneath the northeast part of the caldera is expected to cause uplift first of the Sour Creek dome and then, as magma or an associated pressure pulse migrates southwestward across the caldera along subhorizontal pathways (sills or fluid-filled lenses), cause uplift of the Mallard Lake dome as well. For example, this scenario explains InSAR observations for the period 1995–97. If the migration rate is high enough, uplift of both domes might begin nearly simultaneously, as shown

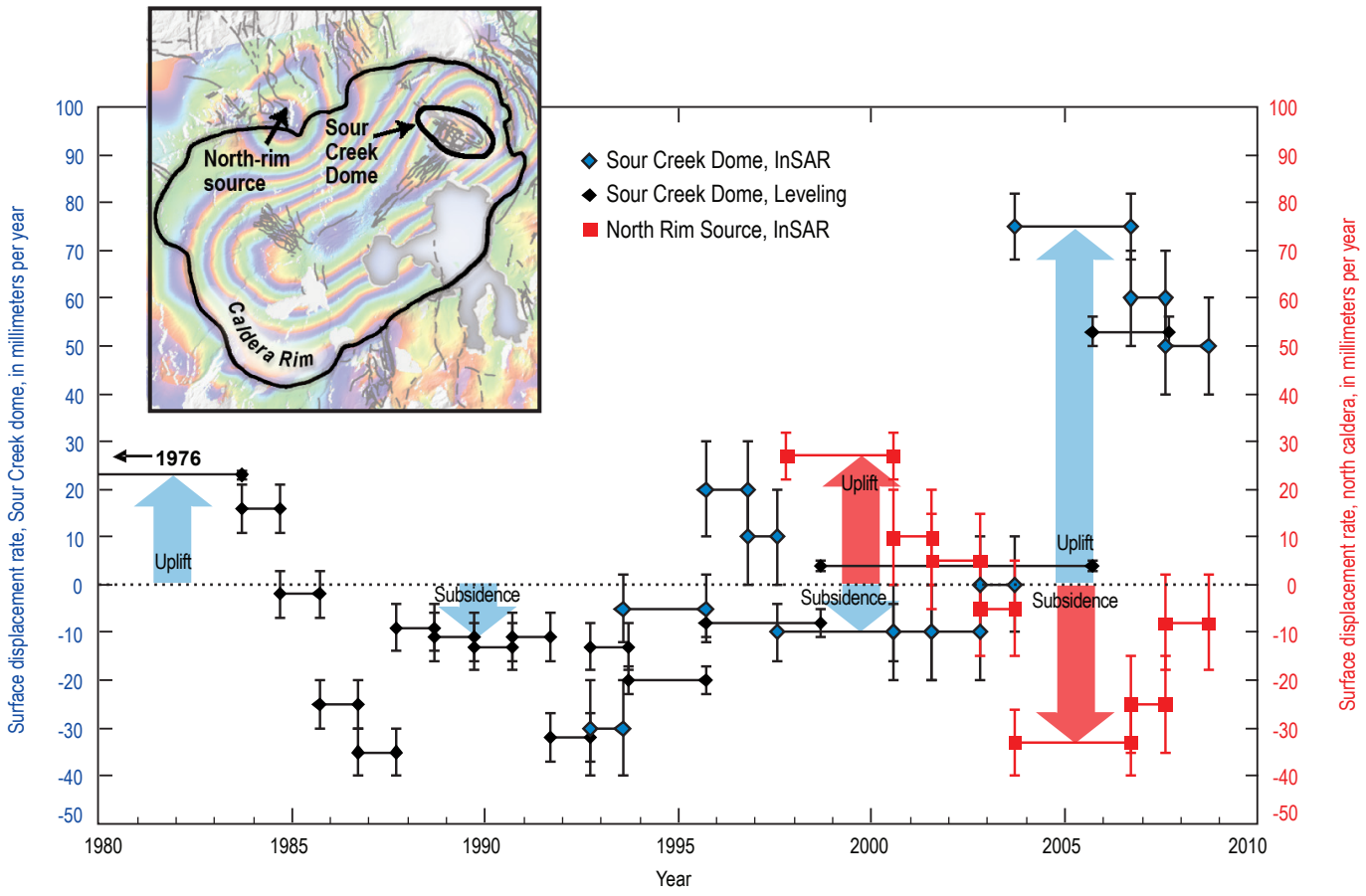

Figure 19. Diagram showing recent history of vertical surface displacements from leveling and line-of-sight surface displacements from InSAR at Yellowstone's Sour Creek resurgent dome (black and blue diamonds) and north caldera rim area (red squares). Inset, 2004–6 interferogram from figure 13, showing locations of north rim and Sour Creek dome deformation sources. For the Sour Creek dome, black diamonds represent leveling data and blue diamonds represent InSAR data. For both types of data, the average surface displacement rate during a time period spanned by two sequential observations is represented by a pair of symbols, with corresponding error bars, connected by a horizontal line that spans the time period. Since 1997–2000, when uplift of the north rim area was first detected using InSAR, there has been a tendency for uplift of the north rim to be accompanied by subsidence of the Sour Creek dome and vice versa—a pattern denoted here by blue and red arrows indicating the sense of motion of the Sour Creek dome and north caldera rim, respectively. Before 1997, there is insufficient information to reconstruct the displacement history of the north rim area. See text for discussion.

by CGPS observations in mid-2004. During periods of lower magma supply, exsolution of volatiles from magma beneath the caldera results in subsidence of the caldera floor if those volatiles are lost to the shallow hydrothermal system or to the surface. If volatiles are trapped temporarily beneath a self-sealing layer, resulting pressurization contributes to surface uplift; subsidence ensues when the seal eventually ruptures (Dzurisin and others, 1994; Fournier, 1999, 2004, 2007). An example of the latter process might be the decade-long subsidence episode that followed an intense earthquake swarm near the caldera rim starting in October 1985. Accumulation of magma and volatiles beneath the north caldera rim causes uplift there until the resulting pressure increase initiates an injection into the Norris–Mammoth corridor or into the southeastward extension of the Hebgen Lake fault zone. The sequence begins again with the next episode of increased magma supply beneath the Sour Creek dome. We caution that the same patterns might be explained equally well or better by other models. Clearly, additional investigation into the cause(s) of surface deformation at Yellowstone is needed.

Before moving on to a discussion of current and future research topics, we first assess and discount the possibility that thermal contraction of solidified intrusions beneath the caldera—rather than depressurization as a result of fluid loss—is a primary subsidence mechanism at Yellowstone. Dzurisin and others (1990) based their assessment of potential subsidence mechanisms on the thermal energy output from Yellowstone's hydrothermal system, which they took to be about 4×10^{16} cal/yr. Subsequent estimates are in the range 4.5–6.0 gigawatts (Fournier 1989; Friedman and Norton, 2007), which corresponds to 3.4×10^{16}–4.5×10^{16} cal/yr, so the calculations by Dzurisin and others (1990) remain valid. A typical value for the specific heat capacity, C, of rock is 800 Joules/kg·ºC or 190 cal/kg·ºC. Following Dzurisin and others (1990), we attribute Yellowstone's entire thermal energy flux to cooling rock from T=800ºC (near the liquidus temperature of rhyolite) to T=450ºC (maximum estimated temperature within the deep hydrothermal system). Using 2,500 kg/m^3 for the average density ρ of intrusive rock and ΔT=350ºC, we can compute the volume of rock V needed to supply Yellowstone's thermal energy flux dQ/dT:

$$V = \frac{dQ/dt}{C \cdot p \cdot \Delta T} = 2\times10^{8}\ \text{m}^3 = 0.2\ \text{km}^3/\text{yr}. \qquad (1)$$

What is the volume change ΔV associated with cooling 0.2 km^3 of rock by 350ºC? The coefficient of thermal expansion α for granite is about 8×10^{-6}/ºC, so the answer is:

$$\Delta V = \alpha \cdot \Delta T \cdot V = -0.0006\ \text{km}^3/\text{yr}. \qquad (2)$$

Dzurisin and others (1990, p. 260–263) characterized this result as "negligible" compared to their best-fit model result based on leveling and trilateration data for the period 1985–7. No additional trilateration data are available for the period of caldera subsidence from 1985 to 1995, but leveling surveys across the northeast part of the caldera each year from 1985 to 1995, except 1994, show that the average 1985–87 subsidence rate of 30±2 mm/yr is representative (within a factor of 2) of the entire period (19±3 mm/yr for 1985–95). The model result for 1985–87 mentioned above was contraction of a tabular body located 10±5 km beneath the caldera floor by 0.019±0.002 km^3, which corresponds to about -0.01 km^3/yr. So, even allowing for substantial uncertainties in the values used for the calculation above and in the model result, thermal contraction of crystalline rock beneath the caldera alone is inadequate by more than an order of magnitude to explain historical subsidence rates observed at Yellowstone.

Dzurisin and others (1990, p. 263–264) went on to consider magmatic fluid loss during crystallization of rhyolitic magma as a potential subsidence mechanism and came to a much different conclusion. In this case, they assumed that the entire heat flux at the surface is extracted by crystallizing without cooling rhyolitic magma near the top of the magmatic system. The latent heat of crystallization L for rhyolitic magma is about 75 cal/g (75×10^3 cal/kg), so the volume of magma required to supply the known heat flux dQ/dt=4×10^{16} cal/yr is:

$$V = \frac{dQ/dt}{L \cdot \rho} = 2\times10^{8}\ \text{m}^3 = 0.2\ \text{km}^3/\text{yr}. \qquad (3)$$

What is the volume change ΔV associated with crystallizing 0.2 km^3 of rhyolitic magma, assuming that all the exsolved fluid produced escapes into the shallow, hydrostatically pressured part of the hydrothermal system? Dzurisin and others (1990, p. 263–264) assumed a 7-percent decrease in volume associated with crystallization of the magma, which corresponds to 0.014 km^3 in this case. This is of the same order as the best-fit model result of Dzurisin and others (1990) for the decrease in source volume during 1985–87 (0.019±0.002 km^3). To verify this result, we checked the assumption of a 7-percent volume decrease during crystallization in the following way.

A water-saturated rhyolite melt having a temperature of about 850°C and a pressure of 250 MPa (consistent with the depths of deformation sources at Yellowstone) would have a density of about 2,200 kg/m^3, as calculated using the thermodynamic relations of Ghiorso and Sack (1995) and the program Conflow (Mastin, 2002). By contrast, the density of the main crystal phase expected from such a melt, an albite-rich plagioclase, at the same temperature and pressure calculated using the thermodynamic relations of Berman (1988) with Conflow would be about 2,520 kg/m^3 (L. Mastin, written commun., 2009). The difference in these densities is about 14 percent, which is twice the value assumed by Dzurisin and others (1990). Given this range in values (7 to 14 percent volume decrease), it is clear that deriving the known heat flux at Yellowstone from the crystallization of 0.2 km^3/yr of rhyolite magma would result in a subsurface volume decrease on

the order of 0.01 km^3/yr, which is comparable to the surface volume change rate measured during periods of caldera-floor subsidence. Conversely, deriving the heat flux by cooling the same volume of rhyolite magma from typical melt temperature to near its solidus temperature would produce a volume contraction 1–2 orders of magnitude smaller, which is insufficient to caused the observed subsidence rate.

Current and Future Research Topics

Among the issues raised by recent studies (for example, Wicks and others, 2006; Chang and others, 2007, 2010; Puskas ansd others, 2007; Vasco and others, 2007; Fournier, 2007) are (1) the nature of the fluid(s) involved in caldera deformation (magma, brine, gas, multiphase mixtures); (2) the nature of the interactions among the basaltic magma system, overlying rhyolitic magma body, hydrothermal system (deep and shallow components), and structural elements such as the Elephant Back fault zone, Norris–Mammoth corridor, postcaldera vent alignments, two resurgent domes, and caldera ring fracture system; and (3) the rate at which such interactions occur, which in turn raises the issue of the mobility of various types of fluids in the subcaldera environment. These frontier issues are being addressed by long-term, time-series measurements of deformation, gravity, seismicity, and magmatic-volatile flux (chloride, CO_2), and by numerical simulations, laboratory experiments, and theoretical studies. A few lines of investigation that seem particularly promising are highlighted below.

Nature of Fluids Involved in Surface Deformation

What fluids are likely to exist at depths of 6–16 km beneath the three known deformation sources at Yellowstone, that is, beneath both resurgent domes and the north rim of the caldera near Norris? What characteristics of that depth range at those locations are conducive to the observed patterns of ground deformation? Are there testable hypotheses to be addressed with future experiments that might shed additional light on the causes and implications of ongoing deformation? Before addressing those questions, some clarification of terminology is necessary. By "magma," we mean a mixture of molten or partially molten rock that generally comprises four phases—residual melt, hypersaline brine, gas, and crystals. At Yellowstone, the dominant magmas are of basaltic or rhyolitic composition. The basaltic magma system extends from the mantle upward to the mid-crust, probably to a depth of about 12 km. A large body of partially molten, but mostly crystallized, rhyolite magma capping the basaltic magma system at depths of 6–12 km has been inferred from seismic results (Miller and Smith, 1999; Husen and others, 2004). Chu and others (2010) analyzed first-arrival waveforms from broadband seismometers and concluded that the melt fraction is much greater than previously thought; that is, they hypothesized a subcaldera magma body with a volume greater than 4,300 km^3 and a porosity of about 32 percent—the latter filled with at least 90 percent rhyolite melt and 8 percent water-CO_2 by volume. Their interpretation is controversial, but nonetheless there is consensus that heat from the rhyolite body, and ultimately from the basaltic system as well, is extracted to the surface through an extensive hydrothermal system (Lowenstern and Hurwitz, 2008). A self-sealing layer near the base of the hydrothermal system, at about 5 km depth, separates fluids at lithostatic pressure from fluids at hydrostatic pressure (Fournier and Pitt, 1985; Fournier, 1991, 1999). We use the term "magmatic fluid" to describe hypersaline brine and magmatic gas that exsolve from the melt as it cools and crystallizes. These are mostly confined to the upper part of the magmatic system and lower part of the hydrothermal system, beneath the self-sealing layer, except at times when the seal is ruptured. At those times, magmatic fluid mixes with fluid from the shallow part of the hydrothermal system, which is mostly of meteoric origin. We avoid using the term "hydrothermal fluid," which has been applied to fluids of both magmatic and meteoric origin. Instead, we distinguish between magmatic fluid in the deep part of the hydrothermal system and mainly meteoric fluid in the shallow part.

All of the deformation sources proposed by Wicks and others (2006) and Chang and others (2007, 2010) are in the depth range 6–16 km, which puts them either in the crystallizing rhyolite body or near the top of the underlying basaltic system. The magma fluxes required to explain deformation rates observed in the caldera and along the north rim (0.01–0.1 km^3/yr; Wicks and others, 2006; Chang and others, 2007) are a factor of 3 to 30 times less than the long-term average intrusion rate of basalt required to account for the observed flux of CO_2 gas at the Yellowstone caldera (0.3 km^3/yr, Lowenstern and Hurwitz, 2008). Lowenstern and Hurwitz (2008, p. 37) point out that an intrusion rate of 0.3 km^3/yr (1) would create a maximum power output of 22 gigawatts (GW) (assuming full crystallization and further cooling of 300°C), which is 3 to 5 times greater than the observed convective heat flow at Yellowstone (4.5–6.0 GW, Fournier, 1989; 6.4 GW, Friedman and Norton, 2007), and (2) is comparable to, though slightly higher than, those estimated for Kilauea and the Columbia River Basalts (Gerlach and others, 2002; Lange, 2002). We infer that the basaltic magma system beneath Yellowstone is both well situated and sufficiently dynamic to host Yellowstone's three known deformation sources and that basalt is the primary "fluid" responsible for deformation. We suspect, but cannot prove, that apparent discrepancies between (1) the basaltic intrusion rate required to explain historical deformation rates, (2) the intrusion rate required to account for the observed CO_2 flux, and (3) the measured convective heat flow at Yellowstone result from time variability of several factors. For example, a long-term average intrusion rate of 0.1 km^3/yr of basalt is consistent with both the average deformation rate measured during historical time and the observed convective heat flow. The somewhat greater intrusion rate required to explain the observed CO_2 flux can be explained by time variability in the intrusion rate, the CO_2 flux, or both. Changes in these rates

would not necessarily occur in lockstep, owing to differences in the depth of basalt intrusion and to subsurface complexities that affect the transit time of CO_2 through the upper crust—complexities which themselves change with time as a result of sporadic earthquake swarms and processes occurring in the deep hydrothermal system. Within measurement uncertainties and allowing for time variability of processes that are occurring in a manifestly dynamic system, we conclude that the models proposed by Wicks and others (2006) and Chang and others (2007, 2010) do a reasonably good job of explaining the recent deformation history at Yellowstone.

The conceptual model proposed by Wicks and others (2006) involves nearly continuous movement of basaltic magma into and out of the mid-crust beneath the Yellowstone caldera, through fluid connections among three interacting magma-storage zones—one beneath each resurgent dome and a third beneath the north rim near Norris (fig. 18). Magma flux into the system from a deep source beneath the Sour Creek dome is allowed to vary with time, as is the flux out of the caldera toward two extensional "sinks"—the Norris–Mammoth corridor and a seismic belt east of the Hebgen Lake fault zone—by way of the north-rim deformation source. The seismic belt is coincident with a zone of crustal extension between Hebgen Lake and the Norris area, which was hypothesized by Savage and others (1993) to explain the results of trilateration measurements from 1974 to 1987. The model of Wicks and others (2006) is flexible enough to explain the full range of observed deformation patterns. For example, Wicks and others (1998) reported that uplift started at the Sour Creek dome during 1995–96 and migrated toward the Mallard Lake dome during 1996–97, whereas Chang and others (2007, 2010) noted that the entire caldera began to rise nearly simultaneously in mid-2004 following a period of subsidence. The difference can be explained with the model of Wicks and others (2006) by invoking differential time histories of magma input from a source beneath the Sour Creek dome and magma/fluid output to the Norris–Mammoth corridor or Hebgen Lake area. Similarly, the model can explain an otherwise counterintuitive fact—that the hottest and most active thermal areas at Yellowstone (Norris Geyser Basin and Hot Springs Basin)—are located outside the caldera (Werner and others, 2008). Hot Springs Basin is located above the model's proposed source of basaltic magma, and Norris Geyser Basin is above a proposed injection site for magma and exsolved fluid along the Norris–Mammoth corridor. A third example is the association between notable earthquake swarms and changes in caldera-floor deformation mode, such as during 1984–86 (onset of subsidence and October 1985–early 1986 swarm) and during 1995–96 (onset of uplift and June–July 1995 swarm). Both swarms occurred just outside the northwest caldera rim. Wicks and others (2006, p. 74) wrote:

> The flux of magma out of the Yellowstone system is controlled by extra-caldera tectonic activity acting on fractured rock bordering the northern caldera boundary. Tectonic strain can either enhance or restrict the flow of magma out of the caldera. In so doing, strain along the north caldera rim might initiate either subsidence or uplift of the caldera floor, triggering an earthquake swarm in either case.

We acknowledge that the relationship between earthquake swarms and deformation at Yellowstone is not straightforward. Swarms are common occurrences and most swarms are not accompanied by a change in the rate or mode of deformation (Smith and others, 2009; Farrell and others, 2009). Nonetheless, we are struck by the fact that the two largest swarms ever recorded in the Yellowstone area, the 1985–86 swarm and the 2010 Madison Plateau swarm (http://volcanoes.usgs.gov/yvo/publications/2010/10swarm.php, accessed September 14, 2011), were accompanied by a change from uplift to subsidence within the caldera. Furthermore the June–July 1995 swarm, which at the time was the largest one to occur since the 1985–86 swarm, was accompanied by a change from caldera-floor subsidence to uplift during 1995–97. All three of these notable swarms occurred near the northwest caldera rim, which suggests to us that the area is an important structural element that episodically influences deformation modes within the caldera.

The model proposed by Wicks and others (2006) is consistent with other observations, including (1) sill-like sources of inflation and deflation in the depth range 6–16 km, which corresponds to the top of a low-velocity zone for seismic P waves that was identified by Husen and others (2004); (2) basalt flux beneath the caldera in the range 0.01–0.1 km^3/yr to account for observed deformation rates (see below); and (3) coequal amounts of uplift and subsidence during postglacial time, which would be expected if, over long time scales, magma influx beneath the Sour Creek dome is balanced by efflux to the Norris–Mammoth corridor and to the Norris–Hebgen Lake seismic belt and extension zone. Such a balance does not preclude substantial heat input to the hydrothermal system from basalt that transits the caldera. We point out that the basalt-flux estimate of 0.01–0.1 km^3/yr in the depth range 6–16 km by Wicks and others (2006) to account for deformation rates does not preclude a greater flux into the lower to mid-crust, as proposed by Lowenstern and Hurwitz (2008) to account for CO_2 flux and heat flow (0.3 km^3/yr).

As noted by Wicks and others (2006), a viable alternative to the magma-transit model is a shallower, distributed deformation source that corresponds to the deep hydrothermal system. Pierce and others (2002) favored such a model, in which magmatic fluid alternately accumulates within and escapes from the deep hydrothermal system, to explain the postglacial deformation record. Referring to the offsetting amounts of uplift and subsidence during postglacial time, Pierce and others (2002, p. 24) concluded: "The inflation-deflation cycles seem to represent an essentially zero sum process with little net subsurface volume change, which seems most readily explained by buildup and release of hydrothermal fluids [magmatic fluids, in the nomenclature used here]." We note that the magma-transit model produces a zero sum by balancing magma influx and efflux, whereas the magmatic fluid model does so by alternately accumulating and dispersing brine and

gas. A hybrid model, in which uplift is caused primarily by magma intrusion and subsidence is caused by injection of exsolved magmatic fluid into the Norris–Mammoth corridor or into the eastward extension of the Hebgen Lake fault zone, is consistent with the isostatic gravity map for Yellowstone National Park and vicinity (Carle and others, 1991). Repeated intrusion of basalt into one or both of those extensional zones likely would produce an isostatic gravity high, which has not been observed. Intrusion of relatively low-density magmatic fluid into those zones would produce no such gravity high outside the caldera, and the gravity high associated with residual basalt intruded beneath the caldera could be masked by the gravitational effect of low-density caldera fill, as interpreted by Carle and others (1991, p. 12).

We favor the hybrid model because it explains more readily some of the complexities of the observed deformation pattern. We envision fluid exsolution from a stagnant, cooling rhyolitic magma body beneath the caldera as a steady, gradual process that is unlikely to produce the short-term changes in deformation mode and rates that have been observed during the past decade. Likewise, we would expect self-sealing of a layer near the base of the hydrothermal system to be a slow process that would result in a more gradual onset of uplift than was observed, for example, in mid-2004. These concerns are lessened if the source of magmatic fluid is basalt rising and accumulating beneath or within a crystallizing rhyolite body. In that case, any variation in the rate of magma intrusion would be reflected in the rate of fluid production, and a discrete intrusion beneath the Sour Creek dome might result in an uplift episode with a rapid onset (assuming rapid bubble growth and ascent). The rate at which basaltic magma, or fluid derived from that magma, migrated southwestward beneath the caldera might vary over time, depending on the state of tectonic stress or on conditions in the deep hydrothermal system that affect permeability. In this scenario, a time-varying supply of basaltic magma to mid-crustal levels beneath the Sour Creek dome is necessary, and even sufficient, to explain rapid-onset uplift episodes. In other words, to call on a time-varying rate of fluid accumulation beneath the Sour Creek dome as the primary uplift mechanism, we require a time-varying supply of basaltic magma that, by itself, could account for uplift. The situation is less clear elsewhere in the caldera. Presumably, lateral intrusion of magmatic fluid alone could account for uplift of the Mallard Lake dome and, as a result of temporary reductions in the rate of fluid outflow beneath the north rim, of that area as well. Subsequent intrusion of magmatic fluid into the Norris–Mammoth corridor or into the extension of the Hebgen Lake fault zone would result in subsidence. As mentioned earlier, this is the mechanism proposed by Waite and Smith (2002) to explain some unusual characteristics of the 1985–6 earthquake swarm near Madison Junction, a swarm which was associated with the onset of subsidence in the caldera.

Recent basaltic intrusions beneath the northeast part of the caldera are plausible for two reasons—(1) continued northeastward migration of the Yellowstone hotspot since the last caldera-forming eruption and (2) uplift that began at the Sour Creek dome in 1995–96, which Wicks and others (2006) attributed to a pulse of basaltic magma from a deep source beneath the dome. At an average migration rate of 4.5 cm/yr, the hotspot has moved approximately 30 km farther northeast since the Yellowstone caldera formed 0.64 Ma—toward the Sour Creek dome and the northeast caldera rim in the vicinity of Hot Springs Basin. This is the area where uplift began in 1995–96. If we accept that a time-variable supply of basaltic magma from a mantle source beneath the Sour Creek dome is a likely cause of uplift there, either directly or as a result of fluid-phase separation, then we can account for deformation elsewhere in the caldera through lateral migration of magma, a fluid phase, or both. Either could accumulate in fractured zones beneath the Mallard Lake dome and along the north caldera rim, causing uplift, and then migrate into one or more sinks outside the caldera, causing subsidence. Magma would be less mobile than the fluid phase, so we would expect the proportion of magma/fluid to decrease "downstream"—that is, from the source beneath the Sour Creek dome, to accumulation zones beneath the Mallard Lake dome and north caldera rim, to sinks along the Norris–Mammoth corridor and Hebgen Lake fault zone. The absence of postcaldera basalt flows inside the caldera is explained by the presence of a partly molten body of rhyolite that impedes the buoyant rise of basalt (Miller and Smith, 1999; Husen and others, 2004; Chu and others, 2010). Outside the caldera, we might expect to see basalt escaping to the surface along the Norris–Mammoth corridor or in the vicinity of the Hebgen Lake fault zone. Christiansen (2001) mapped the postcaldera Swan Lake Flat Basalt and the Madison River Basalt in those two areas, respectively. However, postcaldera basalts also occur elsewhere around the periphery of the Yellowstone Plateau (Christiansen, 2001, p. G48–G49).

Structural Control of Deformation Sources

The second issue raised above (What is the nature of the interactions among the basaltic magma system, overlying rhyolitic magma body, hydrothermal system (deep and shallow components), and structural elements such as the Elephant Back fault zone, Norris–Mammoth corridor, postcaldera vent alignments, two resurgent domes, and caldera ring fracture system?) deals with the locations of deformation sources in structurally distinctive areas, that is, beneath each resurgent dome and at the three-way intersection of the caldera ring fault, the Norris–Mammoth corridor, and the Norris–Hebgen Lake seismic belt. How might these structural elements interact with Yellowstone's magmatic and hydrothermal systems to produce the spatial and temporal deformation patterns described above? We hypothesize that enhanced fracture permeability at all three locations facilitates fluid storage and migration, which is a prerequisite for inflation-deflation cycles that produce surface deformation. This is true regardless of the nature of the fluid involved (magma or brine), so the observation does not favor either model. Likewise, either model can

account for the existence of porous, gas-filled rock at depths of less than 2 km between Norris and Hebgen Lake, which Husen and others (2004) inferred from anomalously low values of V_p and V_p/V_s in that area.[22] The close spatial correlation between the anomaly and the epicentral area of the 1985–86 earthquake swarm, which had several characteristics that Waite and Smith (2002) attributed to fluid migration, led Husen and others (2004, p. 409) to propose "* * * a model in which CO_2 as part of magmatic fluids exsolved from a large crystallizing magma body beneath the Yellowstone caldera and occasionally migrated outwards * * *." We concur, but suggest that any CO_2 that migrated out of the caldera during the 1985–86 earthquake swarm could have exsolved instead, or in part, from basalt that intruded beneath the northeast part of the caldera.

We acknowledge a counterpoint to this idea made by Evans and others (2006), who conducted a geochemical survey of springs outside the northwest margin of the caldera in 2003 and 2004. The survey was designed specifically to look for increased CO_2 flux that might be associated with the onset of caldera subsidence in 1985–86 or with the 1985–86 earthquake swarm. Evans and others (2006, p. 169) found: "* * * no evidence to associate the ten-year period of caldera deflation that began in 1985 with expulsion of magmatic fluids through the caldera rim in this area.[22] They went on to say (p. 179):

> Our results are compatible with the involvement of pressurized hydrothermal fluids in the 1985 swarm, but they suggest that if caldera subsidence resulted from large-scale fluid leakage, the fluid mostly escaped elsewhere. An intense but short-lived geochemical anomaly cannot be ruled out, given the timing of sampling surveys, but other potential fluid flow paths that might be active during caldera subsidence at Yellowstone need further investigation. We suggest that intracaldera CO_2 efflux, which is currently unmonitored apart from the one-time survey of Werner and Brantley (2003), might track caldera deformation cycles even if riverine Cl does not.

Lack of a "smoking gun" in the form of increased CO_2 flux in the 1985–86 epicentral area in 2003–4 does not preclude the mechanism proposed by Waite and Smith (2002) and Husen and others (2004), but neither does it lend support to this aspect of our preferred model.

Temporal Gravity Observations as a Means to Distinguish Between Magma and Other Fluids

The third issue raised above deals with the relative mobilities of various fluids (gas, brine, magma) beneath the Yellowstone caldera and with testable hypotheses or observations that might distinguish between the magma-transit and magmatic fluid models. Both models predict the episodic release of magmatic fluid into the shallow part of the hydrothermal system or into fracture zones north of the caldera. A temporal correlation between earthquake swarms, periods of subsidence, and increased surface flux of magmatic volatiles such as chloride and CO_2 would favor the magmatic fluid model, because subsidence and rupture of the self-sealing layer are directly linked in that model but not in the magma-transit model. In the latter case, subsidence might occur whenever the magma flux is relatively low, as a result of volatile loss from crystallizing magma, even without rupture of a self-sealing layer.

The most convincing observations to date of a link between seismicity and fluid flow at Yellowstone were reported by Pitt and Hutchinson (1982) and Waite and Smith (2002) for two notable earthquake swarms. The first occurred during May–November 1978 beneath the Mud Volcano hydrothermal area, a vapor-dominated, acid-sulfate system located at the intersection of the Elephant Back fault zone and the Sour Creek resurgent dome (fig. 1). The area produced fewer than 10 located earthquakes from 1973 to April 1978, but starting in May 1978 numerous earthquakes began occurring there at 1–5 km depth. Activity culminated with intense swarms of about 100 events/hour on October 23 and November 7; the largest event (M 3.1) occurred on November 13 and at least 8 events were M 2.5 or larger. By December 1978, heat flux in the area had increased sufficiently to kill lodgepole pine trees and other vegetation. From January to May 1979, existing mud volcanoes became more active with increased turbidity, surging activity, and explosive ejection of mud; and new mud volcanoes and fumaroles formed. Activity began to decline in July 1979 and had returned to preswarm levels by June 1980. Pitt and Hutchinson (1982, p. 2765) concluded that fluids were involved in the event but declined to speculate whether they were sourced in the hydrothermal system or magmatic system:

> The spatial and temporal association of earthquakes and increased heat flux at Mud Volcano is the best defined so far in Yellowstone. The earthquakes preceded the increase in heat flux and may have occurred on faults that control the convective fluid flow into the area. The entire hydrothermal area was affected, not only selected features, and the increase in heat flux lasted for over a year. Accumulated tectonic strain in the Mud Volcano area could have caused the earthquakes, which in turn expanded the plumbing system of the hydrothermal area, permitting a temporary increase in the normal convective fluid flow. Alternatively, if the uplift in the eastern caldera is due to pressure and temperature variations within a magma chamber, as suggested by Pelton and Smith [1979], hot fluids migrating upward in the crust as a result of the pressure in the uplift could have entered

[22] V_p is P-wave velocity, V_s is S-wave velocity. Husen and others (2004) proposed that the combination of low V_p and low V_p/V_s is indicative of a change in pore fluid from liquid to gas, likely CO_2, at shallow crustal depths.

the seismogenic zone and triggered the earthquake sequence. If the uplift and the high $^3He/^4He$ ratio at Mud Volcano are at least partly due to the injection of new magma into the eastern caldera, the seismic heat flux variation in the hydrothermal area may provide a sensitive monitor of this process.

A case can be made for similar but more widespread responses of Yellowstone's hydrothermal system to the October 1985–early 1986 earthquake swarm near Madison Junction (Waite and Smith, 2002). The timing of that swarm was roughly coincident with the onset of caldera subsidence sometime between leveling surveys in September 1985 and September 1986 (Dzurisin and others, 1990, 1994). The swarm was preceded in ~July 1985 by an explosion near Pelican Cone, about 5 km east of the east caldera rim (fig. 1), that formed a 20 m^3 crater, killed mature trees, and gave rise to a new superheated fumarole. About 6 months later and 3 months after the start of the swarm, an explosion in mature forest 3 km west of Norris Junction and 10 km north of the north caldera rim formed a 750 m^3 crater, knocked down trees, and threw debris 35 m laterally. Although the swarm was over by the end of 1986, subsidence of the caldera floor continued for a decade until uplift resumed in 1995–96. During 1990–93, ground temperatures increased in part of Hot Springs Basin thermal area near the northeast caldera rim and both a new superheated fumarole and mud volcano emerged (Hutchinson, 1993).

If the primary cause of caldera subsidence is depressurization and loss of magmatic fluid from the deep hydrothermal system as a result of a self-sealing zone rupturing during an earthquake swarm, then we might expect to observe an increase in the surface flux of magmatic gases shortly after the swarm and the onset of subsidence. Concurrent changes in hydrothermal basins, such as those described above, might also occur if hot, upwardly mobile magmatic fluid were to encounter the shallow hydrothermal system. There is as yet no evidence for increased emission of magmatic gases or chloride flux during subsidence episodes, and the changes in hydrothermal activity associated with the 1978 and 1985–86 earthquake swarms, although unusual, are not unique during historical time at Yellowstone. In the first case, uncertainties in the chloride-flux measurements combined with the buffering effect of the shallow hydrothermal system tend to downplay the significance of the negative result (Fournier, 2004). Furthermore, Hurwitz and others (2007b, p. 168) argue that any correlation between the onset of subsidence and increased chloride flux is highly unlikely, because transport of chloride to the surface could take thousands of years. Nonetheless, we suggest that monitoring of chloride and CO_2 fluxes be continued and improved, to the extent possible, through multiple inflation-deflation cycles. Chloride flux estimates have been made each year since 1983, except 1995 and 1996, by combining water discharge measurements at streamgaging stations with chloride concentrations in samples obtained at the gaging stations (Friedman and Norton, 2007). Surface CO_2 flux has been estimated by Werner and Brantley (2003) using a painstaking sampling and statistical approach. Neither measurement is easy to automate or obtain in real time, but progress in this regard would be extremely important. With regard to the incompletely understood relationship between earthquake swarms and changes in hydrothermal activity, we urge continued documentation of Yellowstone's unparalleled hydrothermal features, in the tradition established by park geologist Rick Hutchinson before his untimely death in 1997. Fortunately, park managers and staff have seen fit to continue that important work in his absence.

An obvious difference between the magma-transit and magmatic fluid models for caldera deformation is the density of the fluid involved—a factor of 2–3 between hypersaline brine and magma. For that reason, among others, the two models predict different gravity signatures through time, suggesting another testable hypothesis. Battaglia and others (2003) modeled changes in gravity, surface height, and water-table level at the Long Valley caldera, California, to constrain the density of fluid responsible for surface inflation during 1980–99. They interpreted their result, 1,713 kg/m^3 (best fit) or 1,180–2,330 kg/m^3 at 95-percent confidence, as evidence for intrusion of low-density magma or a combination of magma and low-density fluid. By adding additional constraints on the deformation model from InSAR observations, Tizzani and others (2009) revised the density estimate for the intrusion to 2,509 kg/m^3 (best fit) or 2,192–3,564 kg/m^3 at 95-percent confidence. They noted that the estimate is strongly dependent on the shape and location of the source model, but argued that these parameters were sufficiently well constrained to conclude: "* * * inflation of the resurgent dome from 1982 through 1999 was the result of an intrusion of basaltic to silicic magma" (Tizzani and others, 2009, p. 66).

A recent microgravity study at Kīlauea Volcano, Hawai'i, provides additional evidence for the technique's unique capability to detect subsurface mass changes. Johnson and others (2010) reported a net increase in residual gravity (that is, after free-air correction) of 521 μGal during 1975–2008 at a benchmark near the east rim of Halema'uma'u Crater in the volcano's summit area. The change, which is a factor of about 20 times greater than the combination of measurement uncertainty plus any plausible water-table effect, occurred progressively between gravity surveys in 1975, 1981, 1998, 2003, and 2008. Concurrent leveling surveys show that the mark subsided progressively by a total of nearly 2 m from 1975–2008, a period that included nearly continuous lava extrusion from vents along Kīlauea's East Rift Zone starting in January 1983. The combination of net subsidence and positive residual gravity is unambiguous evidence for an increase in subsurface mass, which Johnson and others (2010) interpret as magma accumulation at 0.5–1.0 km depth. On 19 March 2008, a new eruptive vent formed along the southeast margin of Halema'uma'u Crater, within 1 km of the surface projection of

the gravity anomaly source model. Johnson and others (2010, p. 1142) concluded: "The eruptive activity was apparently preceded by decades of magma accumulation that gradually filled void space, and that was detected by gravity measurements but unknown from deformation monitoring alone."

Arnet and others (1997) used a similar approach, that is, microgravity and leveling surveys, to infer a subsurface mass increase at Yellowstone during 1977–83, a period of net surface uplift. However, in this case, a lack of water-table data made it impossible to estimate the density of the intruding material. Short of monitoring water-table fluctuations in a network of newly drilled wells within Yellowstone National Park, which is impractical, the next best approach would be to install a small network of continuously recording gravity meters and GPS stations at key locations throughout the park and to monitor gravity and height changes during several inflation-deflation cycles. Such a network might be cost prohibitive and would raise serious permitting and logistics issues. A more viable alternative for the time being is to make repeated, very precise, absolute gravity measurements using a portable gravity meter, then estimate and remove the effects of water-table changes using a groundwater model constrained by precipitation and lake-level records. Hurwitz and others (2007a, p. 12), on the basis of the results of their numerical simulations of fluid flow, suggested: "Continuous, high-precision microgravity measurements may discriminate between magma intrusion and hydrothermal injection at shallow depths, because the density of magma differs by a factor of 3 or more from the density of superheated vapor or gas * * *." We believe this approach, combined with continued improvement of four-dimensional (4-D) (X,Y,Z, time) subsurface imaging methods, holds the greatest promise for ultimately indentifying the correct deformation mechanism(s) at Yellowstone and for assessing the implications for associated hazards.

Four-Dimensional Numerical Simulations and Modeling—A Way Forward

Numerical simulations of heat and mass flow in porous, nonisotropic, nonelastic media (for example, Hurwitz and others, 2007a; Hutnak and others, 2009) are an essential step toward better understanding of ground deformation at Yellowstone and other large calderas. Only process-oriented models such as these can provide insight into the mechanism of ground deformation, in addition to insight into the geometrical parameters of the source. Knowing with confidence that a lens-shaped deformation source exists 8 km beneath a caldera's floor is useful. Knowing whether such a source represents magma, brine, gas, or some combination thereof is essential for improved understanding and hazards assessments. Even idealized models of deformation in a homogeneous, semi-infinite, elastic half-space might give reasonable estimates of source depth, size, and shape in spite of the unrealistic assumptions involved, but full confidence in those results awaits verification by models that account for known complexities in the real Earth. The studies by Hurwitz and others (2007a) and Hutnak and others (2009) address such complexities in a theoretical sense and provide a framework for additional advances. The next step is to incorporate more detailed information about the actual 3-D distribution of mechanical properties in the crust beneath Yellowstone. Such information can be gleaned from multidisciplinary investigations such as one by DeNosaquo and others (2009), who combined gravity and heat-flow data with tomographic seismic velocity models, GPS-derived strain rates, earthquake locations, and chemical analyses of volcanic rocks to constrain models of density and lithospheric strength for the Yellowstone-Snake River Plain system.

Laboratory experiments to investigate processes of bubble nucleation, growth, and migration in magmas of mafic and silicic composition, under pressure and temperature conditions that prevail in the crust beneath calderas, are another important piece to the Yellowstone deformation puzzle. Also needed is a better means to incorporate experimental results into physical models of deformation processes at caldera scale. In numerical simulations by Hurwitz and others (2007a) and Hutnak and others (2009), volatiles are "sourced" from a crystallizing magma body to the base of a hydrothermal system—without consideration of processes by which volatiles exsolve, migrate upward, and eventually escape into the overlying hydrothermal system. In an ongoing series of piston-cylinder decompression experiments, Mangan and Sisson (2000, 2005) are exploring the relative importance of decompressional expansion, coalescence, and Ostwald ripening[23] as processes of bubble growth and migration in rhyolitic magma. Working along similar lines, Lensky and others (2004) developed a theoretical model of bubble growth during decompression of supersaturated melt and used decompression experiments to verify essential elements of the model. Together with heat and mass transport through porous media, the mechanisms and time scales of gas escape from magmas are important aspects of any comprehensive explanation of ground deformation at Yellowstone.

Also important is better characterization of the subcaldera crust in terms of structure (faults, fractures, layering), temperature, permeability, pore pressure, strength (shear modulus), and gas content. These characteristics are amenable to study by ever-improving seismic (for example, Waite and others, 2005; 2006; DeNosaquo and others, 2009) and electromagnetic techniques.

[23]In this context, Ostwald ripening refers to a process in which larger bubbles in a magma grow at the expense of smaller ones. Large bubbles have a lower surface to volume ratio, which results in a lower energy state. As the system tries to lower its overall energy, gas molecules tend to diffuse out of small, energetically unfavorable bubbles and into larger ones. As a result, smaller bubbles continually shrink, while larger bubbles grow

As more accurate and diverse geophysical and geochemical datasets are acquired, the need for more detailed numerical models will increase. Finite-element models can be used to account for nonhomogeneous Earth structure and properties, and they have the potential to incorporate all relevant information in a flexible, extensible, and updatable system. For example, a finite-element model for Yellowstone could include information—measured, inferred from modeling, or assumed—about the 3-D distributions of such parameters as temperature, permeability, rheology, and gas content. The model could be used to investigate the system's deformational response to various time-varying inputs, such as earthquake swarms (permeability increase), a temperature pulse (for example, heating by magmatic gases), or mass influx (intrusion of magma or other fluid). Such a model could continually be updated as new or better observational and experimental data are acquired. This "system in a box" or "virtual volcano" approach has been applied to subduction zones (Masterlark, 2003) and to volcanic centers in the Aleutian Arc, Hawaii, and Iceland (for example, Masterlark, 2007); a similar effort for the Long Valley caldera system is underway (M. Mangan, oral commun., 2009).

In the Yellowstone region, a 3-D finite-element model was used to explore the relationship between inflation/deflation cycles in the caldera and anomalous slip on the nearby Teton normal fault (Hampel and Hetzel, 2008). Leveling surveys across the fault were carried out between 1988 and 2001 and revealed two phases of hanging-wall uplift relative to the foot wall (that is, reverse slip), alternating with two phases of normal slip (Sylvester and others, 1991, 2001). Hampel and Hetzel (2008) showed that the motion is explained by modification of the tectonic-displacement field by inflation/deflation cycles in the caldera. Inflation causes enhanced horizontal extension across the north-trending Teton fault to the south, which favors accelerated normal slip on the fault. Conversely, caldera deflation causes horizontal contraction across the fault and favors reverse slip. Hampel and Hetzel (2008, p. 1 of 5) concluded: "Our findings imply a strong coupling between magmatism and tectonic faulting, which requires coordinated monitoring of both processes to improve our understanding of the resulting spatial and temporal strain pattern." Such effects are another aspect of the Yellowstone deformation story that is amenable to theoretical and numerical investigations.

Hurwitz and others (2007a, p. 14) used numerical simulations to investigate the effects of fluids on ground-surface deformation, and concluded: "On the basis of the numerical experiments, and a growing number of observations which indicate a causal link between GSD [ground surface displacement] and dynamics of hydrothermal fluids and/or gases, we propose that future studies should focus on resolving the nature of the fluid causing GSD (for example, magma or aqueous fluid and gas)." Hutnak and others (2009) extended that work by including multicomponent, multiphase flow in their simulations, which confirmed the likely importance of thermoelastic and poroelastic effects in causing ground deformation at large calderas.

Conclusions

Even though crustal uplift at the Yellowstone caldera was discovered more than 30 years ago, the causes of rapid ground motions there are not fully understood. Subsequent work has revealed periods of subsidence that mirrors the pattern of uplift, identified three interacting deformation sources, and explored the likely roles played by magma and exsolved magmatic fluid in causing surface deformation. A definitive measurement or experiment to determine the relative importance of magma and fluid (magmatic or meteoric) in the deformation process as a function of time remains to be done. An expanded program of microgravity measurements using both relative and absolute gravity meters is especially promising in this regard. Also lacking at this time is a comprehensive, 4-D model that accounts for heterogeneous structure and physical properties of the crust beneath Yellowstone, characteristics of multiphase flow through porous media, and the effects of magmatic volatiles in addition to water and carbon dioxide (that is, sulfur, chlorine, hypersaline brine). In this regard, numerical simulations of heat and mass flow in porous, nonisotropic, nonelastic media (for example, Hurwitz and others, 2007a; Hutnak and others, 2009) point the way for future studies.

Although acknowledging that many questions concerning deformation at Yellowstone are yet to be posed and answered, we suggest that the conceptual model offered by Wicks and others (2006)—which is generally in agreement with numerical models by Chang and others (2007), Puskas and others (2007), and Vasco and others (2007), among others—is a useful framework for future studies. The essential elements of the Wicks and others (2006) model that can serve as testable hypotheses are the following: (1) caldera-floor uplift is caused mainly by a variable but nearly continuous supply of basaltic magma beneath the northeast part of the caldera (Sour Creek dome); (2) basalt and exsolved fluid migrate laterally along a subhorizontal boundary, probably near the transition from ductile to brittle behavior within a mostly crystalline body of rhyolite, and accumulate beneath the southwest part of the caldera (Mallard Lake dome) and north rim (Norris area); (3) discrete deformation sources beneath the two domes interact in such a way that they mostly inflate or deflate in unison, but there can be brief exceptions—in such cases, uplift starts earlier at the Sour Creek dome because it is closer to the deep source of basalt; (4) basalt or fluid exsolved during ascent, migration, cooling, and crystallization of basalt is injected episodically into the Norris–Mammoth corridor or Hebgen Lake fault zone; and (5) interplay between uplift and subsidence at three sites within the caldera is controlled by the relative rates of magma input, magma migration, fluid exsolution, and injection of magma/fluid outside the caldera—which vary as a function of time. The net result of these processes, as documented here and in numerous other studies, is one of the most dynamic caldera systems on Earth.

Acknowledgments

The CVO leveling surveys at Yellowstone from 1983 to 2007 would not have been possible without the efforts of dozens of staff members and volunteers—including crew chiefs John Estrem, Gene Iwatsubo, Jack Kleinman, Maurice Sako, Dave Wieprecht, and Ken Yamashita—who braved fickle weather, wildlife, wildfires, and Winnebagos to ensure that the data are of high quality. Numerous colleagues from USGS, University of Utah, and Yellowstone National Park—notably Bob Christiansen, Bob Fournier, Hank Heasler, Jake Lowenstern, and Bob Smith—contributed through thoughtful discussions and written comments that shaped our thinking and corrected our mistakes. Hank Heasler, Wayne Hamilton, and Rick Huthchinson—current and former Yellowstone National Park geologists—contributed many helpful ideas and acted as liaisons between us and park managers to ensure that our research was both scientifically sound and consistent with park management principles. Two of those managers, former Chief of the Yellowstone Center for Resources Tom Olliff and his predecessor John Varley, served at the nexus of numerous special-interest groups with competing demands for park resources, including us, and successfully accommodated most, while adhering to the principles of stewardship that keep Yellowstone a special place for future generations.

Larry Mastin helped with calculations of density changes during crystallization of a rhyolite magma using his open-source numerical model Conflow. Megan McLay meticulously organized a mountain of information concerning more than 500 benchmarks in Yellowstone National Park for appendix B. She created the interactive version for the data files that accompany this report and also an on-line version, which will ensure that information about this important geodetic resource is available to future researchers. Lisa Faust made major improvements to early versions of the illustrations in this report and used her artistic skills to portray complicated data graphs in ways that are both intuitive and precise.

Reviewers Shaul Hurwitz, Evelyn Roeloffs, and Cynthia Gardner provided thorough and constructive reviews of the manuscript, which significantly improved the final product. Christie Hendrix and Stacey Gunther in the Yellowstone Research Permit Office guided us through the permitting process and provided essential logistical support. Stephanie Tubman, Liz Juers, and Heidi Anderson helped in our search for back-country benchmarks. Radar images from European Space Agency (ESA) satellites ERS-1, ERS-2, and ENVISAT were acquired through ESA Category-1 Project 2765, through an ENVISAT Announcement of Opportunity, and through the WInSAR consortium (supported by NASA, the National Science Foundation, and USGS; administered by UNAVCO, http://winsar.unavco.org/main.php).

This research was supported by the USGS Volcano Hazards Program at the USGS David A. Johnston Cascades Volcano Observatory, Washington, USGS Hawaiian Volcano Observatory, Hawai‘i, and USGS Menlo Park, California, offices. In recent years, our research was conducted under the auspices of the Yellowstone Volcano Observatory (YVO)—a collaboration among USGS, Yellowstone National Park, and the University of Utah, which was formed in 2001 to strengthen long-term monitoring of volcanic and earthquake unrest in the Yellowstone National Park region.

References

Allen, E.T., and Day, A.L., 1935, Hot Springs of the Yellowstone National Park: Carnegie Institution of Washington Publication 466, Washington, D.C., 1935.

Arnet, F., Kahle, Hans-Gert, Klinglé, Emile, Smith, R.B., Meertens, C.M., and Dzurisin, D., 1997, Temporal gravity changes and height changes of the Yellowstone caldera, 1977–1994: Geophysical Research Letters, v. 24, no. 22, p. 2741–2744.

Battaglia, M., Segall, P., and Roberts, C., 2003, The mechanics of unrest at Long Valley caldera, California, 2—Constraining the nature of the source using geodetic and micro-gravity data: Journal of Volcanology and Geothermal Research, v. 127, no. 3–4, p. 219–245.

Berman, R.G., 1988, Internally consistent thermodynamic data for minerals in the system Na_2O-K_2O-CaO-MgO-FeO-Fe_2O_3-Al_2O_3-SiO_2-TiO_2-H_2O: Journal of Petrology, v. 29, p. 445–522.

Bradley, F.H., 1873, Report, *in* Hayden, F.V., Sixth annual report of the United States Geological Survey in the Territories: U.S. Geological and Geographical Survey of the Territories Sixth Annual Report [for 1872], p. 191–271.

Carle, S.F., Glen, J.M., Langenheim, V.E., Smith, R.B., and Oliver, H.W., 1991, Isostatic gravity map and principal facts for 694 gravity stations in Yellowstone National Park and vicinity, Wyoming, Montana and Idaho: U.S. Geological Survey, Open-File Report 90–649A and B, 1 over-sized sheet, scale 1:125,000 map, and 1 5 1/4 inch diskette.

Chang, W-L., Smith, R.B., Wicks, C., Farrell, J.M., and Puskas, C.M., 2007, Accelerated uplift and magmatic intrusion of the Yellowstone caldera, 2004 to 2006: Science, v. 318, no. 5852, p. 952–956, doi:10.1126/science.1146842.

Chang, W-L., Smith, R.B., Farrell, J.M., and Puskas, C.M., 2010, An extraordinary episode of Yellowstone caldera uplift, 2004–2010, from GPS and InSAR observations: Geophysical Research Letters, v. 37, L23302, doi:10.1029/2010GL045451.

Christiansen, R.L., 1984, Yellowstone magmatic evolution—its bearing on understanding large-volume explosive volcanism, *in* Explosive Volcanism—Inception, Evolution, and Hazards: Washington, D.C., National Academy Press, National Research Council Studies in Geophysics, p. 84–95.

Christiansen, R.L., 2001, The Quaternary and Pliocene Yellowstone Plateau volcanic field of Wyoming, Idaho, and

Montana: U.S. Geological Survey Professional Paper 729-G, 145 p., 3 plates, scale 1:125,000.

Christiansen, R.L., Foulger, G.R., and Evans, J.R., 2002, Upper-mantle origin of the Yellowstone hotspot: Bulletin of the Geological Society of America, v. 114, no. 10, p. 1245–1256.

Christiansen, R.L., Lowenstern, J.B., Smith, R.B., Heasler, H., Morgan, L.A., Nathenson, M., Mastin, L.G., Muffler, L.J.P., and Robinson, J.E., 2007, Preliminary assessment of volcanic and hydrothermal hazards in Yellowstone National Park and vicinity: U.S. Geological Survey Open-File Report 2007–1071, 94 p.

Chu, R., Helmberger, D.V., Sun, D., Jackson, J.M., and Zhu, L., 2010, Mushy magma beneath Yellowstone: Geophysical Research Letters, v. 37, p. L01306, doi:10.1029/2009GL041656.

DeNosaquo, K.R., Smith, R.B., and Lowry, A.R., 2009, Density and lithospheric strength models of the Yellowstone-Snake River Plain volcanic system from gravity and heat flow data: Journal of Volcanology and Geothermal Research, v. 188, 108–127, doi:10.1016/j.jvolgeores.2009.08.006.

Dieterich, J.H., and Decker, R.W., 1975, Finite element modeling of surface deformation associated with volcanism: Journal of Geophysical Research, v. 80, p. 4095–4102.

Dzurisin, D., 2007, Volcano Deformation—Geodetic Monitoring Techniques, Berlin, Springer, Springer-Praxis Books in Geophysical Sciences, 441 p.

Dzurisin, D., and Yamashita, K.M., 1986, Preliminary results of precise leveling and trilateration surveys in Yellowstone National Park, Wyoming, 1983–1984: U.S. Geological Survey, Open-File Report 86-265-A, 33 p.

Dzurisin, D., and Yamashita, K.M., 1987, Vertical surface displacements at Yellowstone Caldera, Wyoming, 1976–1986: Journal of Geophysical Research, v. 92, no. B13, p. 13753–13766.

Dzurisin, D., Yamashita, K.M., and Johnson, D.J., 1986, Preliminary results of precise leveling and trilateration surveys in Yellowstone National Park, Wyoming, 1985: U.S. Geological Survey, Open-File Report 86-265-B, 28 p.

Dzurisin, D., Savage, J.C., and Fournier, R.O., 1990, Recent crustal subsidence at Yellowstone Caldera, Wyoming: Bulletin of Volcanology, v. 52, p. 247–270.

Dzurisin, D., Yamashita, K.M., and Kleinman, J.W., 1994, Mechanisms of crustal uplift and subsidence at the Yellowstone caldera, Wyoming: Bulletin of Volcanology, v. 56, p. 261–270.

Dzurisin, D., Wicks, C. Jr., and Thatcher, W., 1999, Renewed uplift at the Yellowstone caldera measured by leveling surveys and satellite radar interferometry: Bulletin of Volcanology, v. 61, no. 6, p. 349–355.

Eaton, G.P., Christiansen, R.L., Iyer, H.M., Pitt, A.M., Blank, H.R., Jr., Zietz, I., Mabey, D.R., and Gettings, M.E., 1975, Magma beneath Yellowstone National Park: Science, v. 188, p. 787–796.

Evans, W.C., Bergfeld, D., van Soest, M.C., Huebner, M.A., Fitzpatrick, J., and Revesz, K.M., 2006, Geochemistry of low-temperature springs northwest of Yellowstone caldera—Seeking the link between seismicity, deformation, and fluid flow: Journal of Volcanology and Geothermal Research, v. 154, p. 169–180.

Farrell, J., Husen, S., and Smith, R.B., Earthquake swarm and b-value characterization of the Yellowstone volcano-tectonic system: Journal of Volcanology and Geothermal Research, v. 188, p. 260–276.

Federal Geodetic Control Committee, Bossler, J.D. (chairman), 1984, Standards and specifications for geodetic control networks: Rockville, Maryland, National Oceanic and Atmospheric Administration.

Fenner, C.N., 1936, Borehole investigations in Yellowstone Park: Journal of Geology, v. 44, no. 2, p. 225–315.

Floyd, R.P., 1978, Geodetic bench marks: Rockville, Maryland, National Geodetic Survey, NOAA Manual NOS NGS 1, accessed October 21, 2010, at *http://www.ngs.noaa.gov/PUBS_LIB/GeodeticBMs/*.

Fournier, R.O., 1989, Geochemistry and dynamics of the Yellowstone National Park hydrothermal system: Annual Reviews of Earth and Planetary Science, v. 17, p. 13–53.

Fournier, R.O., 1991, The transition from hydrostatic to greater than hydrostatic fluid pressure in presently active continental hydrothermal systems in crystalline rock: Geophysical Research Letters, v. 18, no. 5, p. 955–958.

Fournier, R.O., 1999, Hydrothermal processes related to movement of fluid from plastic into brittle rock in the magmatic-epithermal environment: Economic Geology, v. 94, p. 1193–1212.

Fournier, R.O., 2004, Yellowstone caldera inflation-deflation and hydrothermal Cl flux revisited, *in* Wanty, R.B., and Seal, R.R., II, eds., Proceedings of the 11th International Symposium on Water–Rock Interaction: Leiden, A.A. Balkema, p. 53–58.

Fournier, R.O., 2007, Hydrothermal systems and volcano geochemistry, *in* Dzurisin, D., Volcano deformation—Geodetic monitoring techniques: Berlin, Springer-Praxis Books in Geophysical Sciences, 441 p.

Fournier, R.O., and Thompson, J.M., 1993, Composition of steam in the system NaCl–KCl–H_2O–quartz at 600ºC: Geochimica et Cosmochimica Acta, v. 57, p. 4365–4375.

Fournier, R.O., and Pitt, A.M., 1985, The Yellowstone magmatic-hydrothermal system, U.S.A., *in* Stone, C., ed., Geothermal Resources Council 1985 International Symposium on Geothermal Energy International Volume: Geothermal Resources Council, p. 319–327.

Friedman, I., and Norton, D.R., 2007, Is Yellowstone losing its steam? Chloride flux out of Yellowstone National Park, *in* Morgan, L.A., ed., Integrated geoscience studies in the greater Yellowstone area—Volcanic, hydrothermal and tectonic processes in the Yellowstone geoecosystem: U.S. Geological Survey Professional Paper 1717, p. 271–298, available at *http://pubs.usgs.gov/pp/1717/*.

Gerlach, T.M., McGee, K.A., Elias, T., Sutton, A.J., Doukas, M.P., 2002, Carbon dioxide emission rate of Kilauea Volcano—Implications for primary magma and the summit reservoir: Journal of Geophysical Research, v. 107, p. 2189, doi:10.1029/2001JB000407.

Ghiorso, M.S., and Sack, R.O., 1995, Chemical mass transfer in magmatic processes IV—A revised and internally consistent thermodynamic model for the interpolation and extrapolation of liquid-solid equilibria in magmatic systems at elevated temperatures and pressures: Contributions to Mineralogy and Petrology, v. 119, p. 197–212.

Hamilton, W.L., 1987, Water level records used to evaluate deformation within the Yellowstone caldera, Yellowstone National Park: Journal of Volcanology and Geothermal Research, v. 31, p. 205–215.

Hampel, A., and Hetzel, R., 2008, Slip reversals on active normal faults related to the inflation and deflation of magma chambers—Numerical modeling with application to the Yellowstone-Teton region: Geophysical Research Letters, v. 35, p. L07301, doi:10.1029/2008GL033226.

Hayden, F.V., 1872, Preliminary report of the United States Geological Survey of Montana and Portions of Adjacent Territories: U.S. Geological and Geographical Survey of the Territories Fifth Annual Report [for 1871], p. 13–165.

Hayden, F.V., 1873, Sixth annual report of the United States Geological Survey in the Territories: U.S. Geological and Geographical Survey of the Territories Sixth Annual Report [for 1872], p. 13–85.

Hildreth W., 1981, Gradients in silicic magma chambers—Implications for lithospheric magmatism: Journal of Geophysical Research, v. 86, p. 10153–10192.

Hildreth, W., Halliday, A.N., and Christiansen, R.L., 1991, Isotopic and chemical evidence concerning the genesis and contamination of basaltic and rhyolitic magma beneath the Yellowstone Plateau volcanic field: Journal of Petrology, v. 32, p. 63–138.

Hill, D.P., 1984, Monitoring unrest in a large silicic caldera, the Long Valley–Inyo Craters volcanic complex in east-central California: Bulletin of Volcanology, v. 47, p. 371–395.

Hill, D.P., Bailey, R.A., and Ryall, A.S., 1985a, Active tectonic and magmatic processes beneath Long Valley caldera, eastern California—An overview: Journal of Geophysical Research, v. 90, p. 11111–11120.

Hill, D.P., Wallace, R.E., and Cockerham, R.S., 1985b, Review of evidence on the potential for major earthquakes and volcanism in the Long Valley–Mono Craters–White Mountains regions of eastern California: Earthquake Prediction Research, v. 3, p. 571–594.

Holdahl, S.R., and Dzurisin, D., 1991, Time-dependent models of vertical deformation in the Yellowstone-Hebgen Lake region, 1923–1987: Journal of Geophysical Research, v. 96, no. B2, p. 2465–2483.

Hollis, J.R., Klingele, E.E., Schlinger, C.S., and Smith, R.B., 1987, Precision gravity reobservations of crustal deformation in the Yellowstone caldera: EOS Transactions of the American Geophysical Union, v. 68, p. 1452.

Howle, J.F., Langbein, J.O., Farrar, C.D., and Wilkinson, S.K., 2003, Deformation near the Casa Diablo geothermal well field and related processes Long Valley caldera, Eastern California, 1993–2000: Journal of Volcanology and Geothermal Research, v. 127, p. 365–390.

Hurwitz, S., Christiansen, L.B., and Hsieh, P.A., 2007a, Hydrothermal fluid flow and deformation in large calderas—Inferences from numerical simulations: Journal of Geophysical Research, v. 112, p. B02206, doi:10.1029/2006JB004689.

Hurwitz, S., Lowenstern, J.B., Heasler, H., 2007b, Spatial and temporal geochemical trends in the hydrothermal system of Yellowstone National Park—Inferences from river solute fluxes: Journal Volcanological and Geothermal Research, v. 162, p. 149–171.

Husen, S., Smith, R.B., and Waite, G.P., 2004, Evidence for gas and magmatic sources beneath the Yellowstone volcanic field from seismic tomographic imaging: Journal of Volcanology and Geothermal Research, v. 131, p. 397–410.

Hsieh, P.A., 1996, Deformation-induced changes in hydraulic head during ground-water withdrawal: Ground Water, v. 34, p. 1082–1089.

Hutchinson, R.A., 1993, Precursors to emergence of a major new mud volcano—Continuing unrest in the Yellowstone Plateau [abs.]: EOS Transactions of the American Geophysical Union, v. 74, no. 43, p. 592.

Hutnak, M., Hurwitz, S., Ingebritsen, S.E., and Hsieh, P.A., 2009, Numerical models of caldera deformation—Effects of multiphase and multicomponent hydrothermal fluid flow: Journal of Geophysical Research: v. 114, p. B04411, doi:10.1029/2008JB006151.

Jahr, T., Jentzsch, G., Gebauer, A., and Lau, T., 2008, Deformation, seismicity, and fluids—Results of the 2004/2005 water injection experiment at the KTB/Germany: Journal of Geophysical Research, v. 113, B11410, doi:10.1029/2008JB005610.

Johnson, D.J., Eggers, A.A., Bagnardi, M., Battaglia, M., Poland, M.P., and Miklius, A., 2010, Shallow magma accumulation at Kīlauea Volcano, Hawai'i, revealed by microgravity surveys: Geology, v. 38, no. 12, p. 1139–1142.

Jónsson, S., Zebker, H., Segall, P., and Amelung, F., 2002, Fault slip distribution of the 1999 M_w 7.1 Hector Mine, California, earthquake, estimated from satellite radar and GPS measurements: Bulletin of the Seismological Society of America, v. 92, p. 1377–1389.

Langbein, J., and Johnson, H., 1997, Correlated errors in geodetic time series—Implications for time-dependent deformation: Journal of Geophysical Research, v. 102, no. B1, p. 591–603.

Lange, R.A., 2002, Constraints on the preeruptive volatile concentrations in the Columbia River flood basalts: Geology, v. 30, p. 179–182.

Lensky, N.G., Navon, O, and Lyakhovsky, V., 2004, Bubble growth during decompression of magma—Experimental and theoretical investigation: Journal of Volcanology and Geothermal Research, v. 129, no. 1, p. 7–22.

Lipman, P.W., and Mullineaux, D.R., eds., 1981, The 1980 eruptions of Mount St. Helens, Washington: U.S. Geological Survey Professional Paper 1250, 844 p.

Locke, W.W., and Meyer, G.A., 1994, A 12,000-year record of vertical deformation across the Yellowstone caldera margin—The shorelines of Yellowstone Lake: Journal of Geophysical Research, v. 99, no. B10, p. 20,079–20,094.

Lohman, R.B., and Simons, M., 2005, Some thoughts on the use of InSAR data to constrain models of surface deformation—Noise structure and data downsampling: Geochemistry, Geophysics, Geosystems, v. 6, p. Q01007, doi:10.1029/2004GC000841.

Lowenstern, J.B., 2001, Carbon dioxide in magmas and implications for hydrothermal systems: Mineralium Deposita, v. 36, no. 6, p. 490–502.

Lowenstern, J.B., and Hurwitz, S., 2008, Monitoring a supervolcano in repose—Heat and volatile flux at the Yellowstone caldera: Elements, Special Issue on Supervolcanoes, v. 4, p. 35–40, doi:10.2113/GSELEMENTS.4.1.35.

Lowenstern, J.B., Smith, R.B., and Hill, D.P., 2006, Monitoring super-volcanoes—Geophysical and geochemical signals at Yellowstone and other caldera systems: Philosophical Transactions of the Royal Society A, v. 264, no. 1845, p. 2055–2072.

Lu, Z., Mann, D., Freymueller, J., and Meyer, D., 2000, Synthetic aperture radar interferometry of Okmok volcano, Alaska 1—Radar observations: Journal of Geophysical Research, v. 105, p. 10791–10806.

Manconi, A., Walter, T.R., and Amelung, F., 2007, Effects of mechanical layering on volcano deformation: Geophysical Journal International, v. 170, no. 2, p. 952–958, doi:10.1111/j.1365-246X.2007.03449.x.

Mangan, M., and Sisson, T., 2000, Delayed, disequilibrium degassing in rhyolite magma—Decompression experiments and implications for explosive volcanism: Earth and Planetary Science Letters, v. 183, no. 3–4, p. 441–455.

Mangan, M., and Sisson, T., 2005, Evolution of melt-vapor surface tension in silicic volcanic systems—Experiments with hydrous melts: Journal of Geophysical Research, v. 110, no. B1, 9 p.

Massonnet, D., and Feigl, K.L., 1998, Radar interferometry and its application to changes in the Earth's surface: Reviews of Geophysics, v. 36, no. 4, p. 441–500.

Masterlark, T., 2003, Finite element model predictions of static deformation from dislocation sources in a subduction zone—Sensitivities to homogeneous, isotropic, Poisson-solid, and half-space assumptions: Journal of Geophysical Research, v. 108, no. B11, p. 2540, doi:10.1029/2002JB002296.

Masterlark, T., 2007, Magma intrusion and deformation predictions—Sensitivities to the Mogi assumptions: Journal of Geophysical Research, v. 112, doi:10.1029/2006JB004860, 17 p.

Mastin, L.G., 2002, Insights into volcanic conduit flow from an open-source numerical model: Geochemistry, Geophysics, Geosystems, v. 3, no. 7, doi:10.1029/2001GC00019210.

Meyer, G.A., and Locke, W.W., 1986, Origin and deformation of Holocene shoreline terraces, Yellowstone Lake, Wyoming: Geology, v. 14, no. 8, p. 699–702.

Miller, C.D., 1985, Holocene eruptions at the Inyo volcanic chain, California—Implications for possible eruptions in Long Valley caldera: Geology, v. 13, p. 14–17.

Miller, C.D., 1989, Potential hazards from future volcanic eruptions in California: U.S. Geological Survey Bulletin 1847, 17 p.

Miller, C.D., Mullineaux, D.R., Crandell, D.R., and Bailey, R.A., 1982, Potential hazards from future volcanic eruptions in the Long Valley-Mono Lake area, east-central California

and southwest Nevada—A preliminary assessment: U.S. Geological Survey Circular 877, 10 p.

Miller, D.S., and Smith, R.B., 1999, P and S velocity structure of the Yellowstone volcanic field from local earthquake and controlled source tomography: Journal of Geophysical Research, v. 104, p. 15105–15121.

Morgan, W.J., 1971, Convective plumes in the lower mantle: Nature, v. 230, p. 42–43.

Morgan, W.J., 1972a, Deep mantle convection plumes and plate motions: Bulletin of the American Association Petroleum Geology, v. 56, p. 203–213.

Morgan, W.J., 1972b, Plate motions and deep mantle convection, *in* Shagam, R., Hargraves, R.B., Morgan, W.J., Van Houten, F.B., Burk, C.A., Holland, H.D., and Hollister, L.C., eds, Studies in earth and space sciences: Geological Society of America Memoir, v. 132: p. 7–22.

Morgan, L.A., Cathey, H.E., and Pierce, K.L., eds., 2009, The track of the Yellowstone hot spot—Multi-disciplinary perspectives on the origin of the Yellowstone-Snake River Plain volcanic province: Journal of Volcanology and Geothermal Research Special Volume, v. 188, issues 1–3, 304 p.

Myers, W.B., and Hamilton, W., 1964, Deformation accompanying the Hebgen Lake earthquake of August 17, 1959: U.S. Geological Survey Professional Paper 435–I, p. 55–138.

Muffler, L.J.P., White, D.E., and Truesdell, A.H., 1971, Hydrothermal explosion craters in Yellowstone National Park: Bulletin of the Geological Society of America, v. 82, p. 723–740.

Newhall, C.G., and Dzurisin, D., 1988, Historical unrest at large calderas of the world: U.S. Geological Survey Bulletin 1855, 1108 p.

Peale, A.C., 1873, Report, *in* Hayden, F.V., Sixth annual report of the United States Geological Survey in the Territories: U.S. Geological and Geographical Survey of the Territories Sixth Annual Report [for 1872], p. 99–187.

Pelton, J.R., and Smith, R.B., 1979, Recent crustal uplift in Yellowstone National Park: Science, v. 206, p. 1179–1182.

Pelton, J.R., and Smith, R.B., 1982, Contemporary vertical surface displacements in Yellowstone National Park: Journal of Geophysical Research, v. 87, p. 2745–2761.

Pierce, K.L., and Morgan, L.A., 1992, The track of the Yellowstone hotspot—Volcanism, faulting, and uplift, *in* Link, P.K., Kuntz, M.A., and Platt, L.B., eds., Regional Geology of Eastern Idaho and Western Wyoming: Geological Society of America Memoir 179, p. 1–53.

Pierce, K.L., Cannon, K.P., Meyer, G.A., Trebesch, M.J., and Watts, R., 2002, Post-glacial inflation-deflation cycles, tilting, and faulting in the Yellowstone caldera based on Yellowstone Lake shorelines: U.S. Geological Survey Open-File Report 02–0142, 30 p.

Pitt, A.M., and Hutchinson, R.A., 1982, Hydrothermal changes related to earthquake activity at Mud Volcano, Yellowstone National Park, Wyoming: Journal of Geophysical Research, v. 87, p. 2762–2766.

Pitt, A.M., Weaver, C.S., and Spence, W., 1979, The Yellowstone Park earthquake of June 30, 1975: Bulletin of the Seismological Society of America, v. 69, no. 1, p. 187–205.

Pruess, K. Oldenburg, C., Moridis, G., 1999, TOUGH2 user's guide, version 2.0: Berkeley, California, Lawrence Berkeley National Laboratory, Paper LBNL-43134, 197 p.

Puskas, C., Smith, R.B., Meertens, C.M., and Chang, W.L., 2007, Crustal deformation of the Yellowstone–Snake River Plain volcano-tectonic system—Campaign and continuous GPS observations, 1987–2004: Journal of Geophysical Research, v. 112, p. B03401, doi:10.1029/2006JB004325.

Rampino, M.R., Self, S., and Stothers, R.B., 1988, Volcanic winters: Annual Review of Earth and Planetary Sciences, v. 16, p., 73–99.

Reilinger, R.E., 1986, Evidence for postseismic viscoelastic relaxation following the 1959 M=7.5 Hebgen Lake, Montana, earthquake: Journal of Geophysical Research, v. 91, p. 9488–9494.

Reilinger, R.E., Citron, G.P., and Brown, L.D., 1977, Recent vertical crustal movements from precise leveling data in southwestern Montana, western Yellowstone National Park, and the Snake River Plain: Journal of Geophysical Research, v. 82, p. 5349–5359.

Savage, J.C., and Cockerham, R.S., 1984, Earthquake swarm in Long Valley caldera, California, January 1983—Evidence for dike inflation: Journal of Geophysical Research, v. 89, p. 8315–8324.

Savage, J.C., Lisowski, M., Prescott, W.H., and Pitt, A.M., 1993, Deformation from 1973 to 1987 in the epicentral area of the 1959 Hebgen Lake, Montana, earthquake (M_s=7.5): Journal of Geophysical Research, v. 98, p. 2145–2153.

Self, S., Gertisser, R., Thordarson, T., Rampino, M.R., and Wolff, J.A., 2004, Magma volume, volatile emissions, and stratospheric aerosols from the 1815 eruption of Tambora: Geophysical Research Letters, v. 31, no. 20, L20608, 4 p., doi:10.1029/2004GL020925.

Shaw, H.R., 1971, Kistler, R.W., and Evernden, J.F., 1971, Sierra Nevada plutonic cycle—Part II, tidal energy and a hypothesis for orogenic–epeirogenic periodicities: Geological Society of America Bulletin, v. 82, p. 869–895.

Sholly, D.R., and Newman, S.M., 1991, Guardians of Yellowstone—An intimate look at the challenges of protecting America's foremost wilderness park: New York, William Morrow and Company, Inc., 317 p.

Simons, M., Fialko, Y., and Rivera, L., 2002, Coseismic deformation from the 1999 M_w 7.1 Hector Mine, California, earthquake as inferred from InSAR and GPS observations: Bulletin of the Seismological Society of America, v. 92, p. 1390–1402.

Smith, R.B., and Arabasz, W.J., 1991, Seismicity of the Intermountain seismic belt, *in* Slemmons, D.B., Engdahl, E.R., Zoback, M.L., and Blackwell, D.D., eds., Neotectonics of North America, decade map volume 1: Geological Society of America, p. 185–228.

Smith, R.B., and Braile, L.W., 1984, Crustal structure and evolution of an explosive silicic volcanic system at Yellowstone National Park, *in* Studies in geophysics; explosive volcanism—Inception, evolution, and hazards: National Academy Press, p. 96–111.

Smith, R.B., and Braile, L.W., 1994, The Yellowstone Hotspot: Journal of Volcanology and Geothermal Research, v. 61, p. 121–188.

Smith, R.B., and Bruhn, R.L., 1984, Intraplate extensional tectonics of the western U.S. Cordillera—Inferences on structural style from seismic-reflection data, regional tectonics and thermal-mechanical models of brittle ductile deformation: Journal of Geophysical Research, v. 89, p. 5733–5762.

Smith, R.B., and Siegel, L.J., 2000, Windows into the Earth—The geologic story of Yellowstone and Grand Teton National Parks: Oxford University Press, Oxford, 242 p.

Smith, R.B., Braile, L.W., Schilly, M.M., Ansorge, J., Prodehl, C., Baker, M., Healey, J.H., Mueller, S., and Greensfelder, R., 1982, The Yellowstone-eastern Snake River Plain seismic profiling experiment—Crustal structure of Yellowstone: Journal of Geophysical Research, 84, p. 2583–2596.

Smith, R.B., Reilinger, R.E., Meertens, C.M., Hollis, J.R., Holdahl, S.R., Dzurisin, D., Gross, W.K., and Klingele, E.E., 1989, What's moving at Yellowstone!—The 1987 crustal deformation survey from GPS, leveling, precision gravity and trilateration: EOS Transactions of the American Geophysical Union, v. 70, no. 8, p. 113–125.

Smith, R.B., Jordan, M., Steinberger, B., Puskas, C.M., Farrell, J., Waite, G.P., Husen, S., Chang, W.-L., and O'Connell, R., 2009, Geodynamics of the Yellowstone hotspot and mantle plume—Seismic and GPS imaging, kinematics, and mantle flow: Journal of Volcanology and Geothermal Research, v. 188, p. 26–56, doi:10.1016/j.jvolgeores.2009.08.020.

Stoopes, G.S., and Yamashita, K.M., 1988, Preliminary results of a precise leveling survey in Yellowstone National Park, Wyoming, September 1986: U.S. Geological Survey, Open-File Report 88-24, 33 p.

Stothers, R.B., 1984, The great Tambora eruption in 1815 and its aftermath: Science, v. 224, no. 4654, p. 1191–1198. doi:10.1126/science.224.4654.1191.

Sylvester, A.G., Byrd, J.O.D., and Smith, R.B., 1991, Geodetic evidence for aseismic reverse creep across the Teton fault, Teton Range, Wyoming: Geophysical Research Letters, v. 18, p. 1083–1086.

Sylvester, A.G., Smith, R.B., Chang, W.L., Hitchcock, C.S., and Byrd, J.O.D., 2001, First-order leveling reveals anomalous, interseismic, contractile, transient strain across Teton normal fault, 1988–2001, Grand Teton National Park, Wyoming, *in* Harlow, H.J., and Harlow, M., 25th Annual Report: Laramie, Wyoming, University of Wyoming, p. 104–110.

Sylvester, A.G., Smith, R.B., Chang, W.L., Hitchcock, C.S., and Byrd, J.O.D., 2001, First-order leveling reveals anomalous, interseismic, contractile, transient strain across Teton normal fault, 1988–2001, Grand Teton National Park, Wyoming: EOS Transactions of the American Geophysical Union, v. 82, no. 47, Fall Meeting Suppl. Abstract, F263.

Telford, W.M., Geldart, L.P., Sheriff, R.E., and Keys, D.A., 1990, Applied geophysics (2nd ed.), Cambridge University Press, Cambridge, 770 p., ISBN 0-521-33938-3.

Tizzani, P., Battaglia, M., Zeni, G., Atzori, S., Berardino, P., Lanari, R., 2009, Uplift and magma intrusion at Long Valley caldera from InSAR and gravity measurements: Geology, v. 37, p. 63–66, doi:10.1130/G25318A.

Todesco, M., Rutqvist, J., Chiodini, G., Pruess, K., and Oldenburg, C.M., 2004, Modeling of recent volcanic episodes at Phlegraean Fields (Italy)—Geochemical variations and ground deformation: Geothermics, v. 33, p. 531– 547, doi:10.1016/j.geothermics.2003.08.014.

Turcotte, D.L., and Schubert, G., 2002, Geodynamics (2nd ed.): Cambridge University Press, 456 p., ISBN 0521661862.

Vanicek P., Castle, R.O., and Balazs, E.I., 1980, Geodetic leveling and its applications: Reviews of Geophysics, v. 18, p. 505–524.

Vasco, D.W., Wicks, C., Jr., Karasaki, K., and Marques, O., 2002, Geodetic imaging—Reservoir monitoring using satellite interferometry: Geophysical Journal International, v. 149, no. 3, p. 555–571.

Vasco, D.W., Puskas, C.M., Smith, R.B., and Meertens, C.M., 2007, Crustal deformation and source models of the Yellowstone volcanic field from geodetic data: Journal of Geophysical Research, v. 112, p. B03401, doi:10.1029/2006JB004325.

Waite, G.P., and Smith, R.B., 2002, Seismic evidence for fluid migration accompanying subsidence of the Yellowstone caldera: Journal of Geophysical Research, v. 107, no. B9, p. 2177, doi:10.1029/2001JB000586.

Waite G.P., Schutt, D.L., and Smith, R.B., 2005, Models of lithosphere and asthenosphere anisotropic structure of the Yellowstone hot spot from shear wave splitting: Journal of Geophysical Research, v. 110, p. B11304, doi:10.1029/2004JB003501.

Waite, G.P., Smith, R.B., and Allen, R.M., 2006, V_p and V_s structure of the Yellowstone hot spot from teleseismic tomography—Evidence for an upper mantle plume: Journal of Geophysical Research, v. 111, p. B04303. doi:1029/2005JB0003867.

Werner, C., and Brantley, S., 2003, CO_2 emissions from the Yellowstone volcanic system: Geochemistry Geophysics Geosystems, v. 4, no. 7, p. 1061. doi:10.1029/2002GC000473.

Werner, C., Hurwitz, S., Evans, W.C., Lowenstern, J.B., Bergfeld, D., Heasler, H., Jaworowski, C., and Hunt, A., 2008, Volatile emissions and gas geochemistry of Hot Spring Basin, Yellowstone National Park, USA: Journal of Volcanology and Geothermal Research, v. 178, 751–762, doi:10.1016/j.jvolgeores.2008.09.016.

Westerhaus, M., Lühr, B.-G., and Zschau, J., 2005, Local deformation and internal pressure changes due to annual recharge of ground water at Merapi Volcano: 2nd General Assembly European Geosciences Union, (Vienna, Austria, 2005), accessed September 14October 1, 2011, at *http://www.cosis.net/abstracts/EGU05/05172/EGU05-J-05172.pdf.*

White, D.E., Fournier, R.O., Muffler, L.J.P., and Truesdell, A.H., 1975, Physical results of research drilling in thermal areas of Yellowstone National Park, Wyoming: U.S. Geological Survey Professional Paper 892, 77 p.

White, D.E., Muffler, L.J.P., Truesdell, A.H., 1971, Vapor-dominated hydrothermal systems compared with hot-water systems: Economic Geology, v. 66, p. 75–97.

White, D.E., Hutchinson, R.A., and Keith, T.E.C., 1988, The geology and remarkable thermal activity of Norris Geyser Basin, Yellowstone National Park, Wyoming: U.S. Geological Survey Professional Paper 1456, 84 p., 1 plate, scale 1:2,400, available at *http://pubs.usgs.gov/pp/1456/*.

Wicks, C. Jr., Thatcher, W., and Dzurisin, D., 1998, Migration of fluids beneath Yellowstone caldera inferred from satellite radar interferometry: Science, v. 282, p. 458–462.

Wicks, C.W., Thatcher, W., Dzurisin, D., and Svarc, J., 2006, Uplift, thermal unrest and magma intrusion at Yellowstone caldera, observed with InSAR: Nature, v. 440, no. 7080, p. 72–75. doi:10.1038/nature04507.

Wooton, K.M., and Spell, T.L., 2007, Latest Yellowstone volcanism—Roaring Mountain rhyolites, Yellowstone Volcanic Field, Wyoming [abs.]: Geological Society of American Denver Annual Meeting, October 28–31, 2007, accessed September 14October 1, 2011, at *http://gsa.confex.com/gsa/2007AM/finalprogram/abstract_125441.htm*.

Wyatt, F.W., 1989, Displacement of surface monuments—Vertical motion: Journal of Geophysical Research, v. 94, p. 1655–1664.

Yamashita, K.M., Endo, E., Sako, M., and Wieprecht, D., 1997, Descriptions and elevations for first-order, class II leveling bench marks, and Global Positioning System (GPS) coordinates and elevations between West Yellowstone, Montana and Old Faithful, Yellowstone National Park, Wyoming: U. S. Geological Survey Open-File Report 97-0057.

Appendixes A–B

Appendix A. Uncertainties in Surface Displacement Measurements from Repeated Leveling Surveys and InSAR

Uncertainty in Leveling Surveys

Throughout this report, uncertainties in vertical displacement measurements are expressed as one standard deviation from the combination of random leveling error and long-term benchmark instability. For two first-order, class-II leveling surveys, these error sources are approximated by:

$$\sigma = \sqrt{\left(1.0\ \text{mm}\cdot\text{km}^{-1/2}\cdot\sqrt{\Delta L}\right)^2 + \left(1.0\ \text{mm}\cdot\text{yr}^{-1/2}\cdot\sqrt{\Delta t}\right)^2},$$

where ΔL is stadia distance in kilometers along the level line and Δt is time in years between surveys (Vanicek and others, 1980; Wyatt, 1989). When a first-order, class-II survey and second-order, class-II survey are combined, the coefficient of the first term, 1.0 mm·km$^{-1/2}$, is replaced by 2.2 mm·km$^{-1/2}$. This is the case, for example, when the second-order 1923 survey in Yellowstone National Park is combined with any of the subsequent, first-order surveys. The coefficient of the second term, 1.0 mm·yr$^{-1/2}$ in this case, depends on the quality of the benchmark. For geodetic marks set in bedrock or on deeply anchored rods, it is generally in the range 0.2–1.0 mm·yr$^{-1/2}$ (Wyatt, 1989) or, more conservatively, 0.5–2.0 mm·yr$^{-1/2}$ (Langbein and Johnson, 1997). The marks used for leveling along the Lake Butte–Mount Washburn line at Yellowstone are of variable quality. Approximately two-thirds of the marks are set on bedrock, on substantial structures such as bridge abutments, or on deeply anchored rods. These types are considered to be high quality marks (Floyd, 1978). Most of the others are set on large boulders or culvert headwalls; they are of lower quality for long-term deformation studies, but useful as recoverable points between marks of higher quality. Our choice of 1.0 mm·yr$^{-1/2}$ in the expression above is thought to be conservative for the high-quality marks in Yellowstone and to be generally reflective of the stability of the other marks as well.

The uncertainties in vertical displacement measurements from repeated leveling surveys are reported here in one of two ways, depending on the context. When the intent is to express the uncertainty associated with a height-change measurement at a given mark with respect to a reference mark, the value of ΔL is the cumulative stadia distance between the given mark and the reference mark. For example, the uncertainty in a vertical displacement measurement at DA3 1934 near Le Hardys Rapids relative to 36 MDC 1976 near Lake Butte based on comparison of two first-order, class-II surveys is ±4.9 mm if the surveys were separated by one year (ΔL=23.4 km, Δt=1 year) or ±5.8 mm if the surveys were separated by 10 years (ΔL=23.4 km, Δt=10 years). Uncertainties reported in the text were calculated this way. To calculate the error bars for vertical-displacement profiles shown in several of the figures, we used a different approach. In that case, a more useful indicator is the uncertainty in tilt measured between adjacent marks. This is because the uncertainty calculated as described above grows with distance from the reference mark, even though height differences measured between adjacent marks that are far from the reference mark are no less precise than those measured between marks closer to the reference mark. To calculate the error bars shown on vertical-displacement profiles, we used the incremental distance between adjacent marks for ΔL in the expression above. It might be useful to think of these error bars as an uncertainty envelope for the shape of a profile, which can move up or down by a greater amount that corresponds to the uncertainty value reported in the text. Uncertainties reported earlier in the literature, including those by other authors, are replaced here by values that were calculated as described above; any resulting discrepancies are minor.

Uncertainty in InSAR Measurements

The measurement of surface displacements using radar interferometry is inherently much more complicated than the same measurement made by repeating leveling surveys, and therefore specifying the uncertainty in InSAR measurements is much more difficult. The fundamental measurement depicted in a deformation interferogram is the phase difference between two radar pulses backscattered to the SAR from the same resolution element on the ground at two different times. For a C-band SAR such as the ASAR instrument onboard Envisat, which operates at a wavelength λ=56.3 mm, each full fringe in a deformation interferogram represents a pulse round-trip travel distance of $n\cdot\lambda$, where n=1, 2, 3… . Ignoring all other effects for the time being, this corresponds to a line-of-sight (LOS) range change (surface displacement) of $\frac{n\cdot\lambda}{2}$, or about 28 mm for the Envisat ASAR if n=1. Radar phase-difference measurements can be made with a precision of better than 1 percent, so in theory InSAR is capable of submillimeter accuracy. However, several factors make it impossible to achieve such high accuracy in practice.

In the preceding discussion, we ignored the effects of noise in SAR images on the accuracy attainable with InSAR measurements. For our purposes “noise” refers to any signal other than that resulting from displacement of Earth’s surface.

Potential noise sources include sensor noise, satellite orbital errors, errors in the digital elevation model (DEM) used to produce a deformation interferogram, and propagation delays caused by inhomogeneity in the troposphere and ionosphere. The last factor arises because the speed of radar waves depends on the refractive index of the medium through which they travel, which in this case is a function of water-vapor content in the troposphere and electron density in the ionosphere. In general, the net effect of various noise sources is to limit the range-change accuracy of C-band interferometry to 1–10 mm under favorable conditions.

Spatial covariance in the noise structure of InSAR data is another factor that increases the uncertainty of surface displacement measurements made with InSAR. A typical interferogram comprises tens of millions of data points, but nearby data points are not independent of one another—they result from similar paths through the ionosphere and troposphere, and therefore the noise components in the information they represent are correlated. Lu and others (2000) have shown that propagation delays commonly produce as many as two to three fringes in interferograms of Aleutian volcanoes. This might be an extreme case, because the Aleutian Islands are subject to notoriously dynamic and wet weather. Even so, the effect of propagation delays can be mitigated if several radar images of the same area that span similar time intervals are available. Imagine, for example, that we form three coherent interferograms, AB, BC, and AC, from radar images A, B, and C. Assume that B includes a large propagation delay anomaly in part of the image. The anomaly will manifest itself as a closed pattern of fringes in interferograms AB and BC, but will be absent from AC. We can reasonably associate the fringe pattern with image B and dismiss the possibility that it represents surface deformation. By extending this approach to a larger suite of interferograms we can partly eliminate spurious effects.

Lohman and Simons (2005) studied the covariance structure of noise in InSAR data by comparing several independent interferograms with GPS observations of tropospheric delay in the same target area. They concluded that downsampling InSAR data by spatial averaging can be an effective means to reduce the number of highly correlated data points and proposed a resolution-based resampling method as an alternative to the approaches used by Jónsson and others (2002) and Simons and others (2002). Regardless of the resampling algorithm used, Lohman and Simons (2005) stressed the importance of using the full noise covariance matrix to estimate the uncertainty in model parameters obtained from inversions of InSAR data.

It should be obvious from the preceding discussion that it is not yet possible to specify in a rigorous way the uncertainty in displacement measurements made with InSAR. How large are propagation delay anomalies in the SAR images used to produce the interferograms? Were their effects correctly identified in the interferograms and eliminated from the displacement measurements? Which spatial averaging algorithm was used to downsample the InSAR data? How was the covariance structure of noise in the InSAR data estimated? These questions cannot be answered in a uniform way for a set of interferograms, even if all of the interferograms were produced from images acquired by the same SAR. On the basis of our own experience and consultations with colleagues who specialize in InSAR, we assign an uncertainty to the InSAR displacement measurements reported here of ±10 mm. We report InSAR results to one significant figure in units of millimeters, rather than centimeters, for ease of comparison with leveling and CGPS results. Even if our uncertainty estimate is too small by a factor of two, which seems unlikely, it does not invalidate the InSAR results reported here because most of the displacements are larger than 20 mm and corroborated by leveling results.

Appendix B. Descriptions, Coordinates, and Photographs of Benchmarks in Yellowstone National Park

This section is intended as an enduring repository for information concerning more than 500 benchmarks in Yellowstone National Park that have been used primarily for leveling surveys from 1923 to 2007 and also used for more recent gravity and GPS surveys. In compiling this information, we included many more benchmarks than are available in the National Geodetic Survey (NGS) online database (http://www.ngs.noaa.gov/cgi-bin/datasheet.prl), including marks than have not been used for any NGS- or USGS-led surveys (for example, a large number of Federal Highway Administration (FHWA) marks along paved roads). Also included are many benchmarks, most of them away from roads, that have been used by the USGS and University of Utah for GPS surveys that are not discussed in this report. Nonetheless, we are aware that this compilation is not comprehensive for all benchmarks in Yellowstone National Park. Rather, it includes all marks in close proximity to roads that have been used for leveling or gravity surveys (or could be used in future surveys) plus a selection of backcountry marks that we were able to visit on foot. We hope that the availability of these descriptions will facilitate the design and execution of future geophysical surveys, especially using gravity and GPS.

We searched for benchmarks along Yellowstone National Park roads during the summers of 2002, 2003, 2004, and 2008. Information included in these descriptions is current as of October 2008. More than 300 benchmarks were recovered in good condition. A significant number (approximately 40) that were searched for and not found probably still exist but are obscured by vegetation, soil, or other debris. Another approximately 30 marks that were not found are presumed destroyed, based on evidence for roadwork that probably disturbed the mark (for example, removal of a culvert headwall into which a mark was set). Only a handful of benchmarks (about 5) could be confirmed destroyed based on evidence including broken concrete piers, empty drill-holes, or the marks themselves lying on the ground. At the time of this writing, a segment of the highway between Madison Junction and Norris Junction was under construction. Realignment will make several benchmarks difficult to access and might result in the destruction of at least one mark in the headwall of a bridge. Similar work has occurred previously elsewhere in the park, where some marks can still be found along abandoned road segments that have been remediated to their original state. The National Park Service (NPS) and FHWA have demonstrated commendable awareness of the historical importance of benchmarks throughout the park and try to avoid disturbing them or, in cases when disturbance is unavoidable, to reset replacement marks nearby. Such was the case near Mount Washburn, where several marks were reset in 2002 before extensive road construction between Canyon Junction and Tower-Roosevelt Junction.

The locations of all benchmarks included in this compilation are shown on the maps in figures B1–B15, which are color coded according to the status of the marks (found; searched for, not found; presumed destroyed; destroyed; not searched for). Interactive versions of the maps are included in the data files that accompany this report, together with descriptive information for each of the marks. The same information is available online at http://pubs.usgs.gov/pp/1788/pp1788_benchmarks/.

In addition to the interactive maps of figures B1–B15, the following information is included in the data files for this appendix. Each benchmark description includes a standard set of information. The benchmark name is assigned by the organization that installed the mark, generally NGS, USGS, FHWA, or NPS. The "STAMPING" field gives the exact stamping that is on the face of the mark, and the "USGS QUAD MAP" indicates the USGS 7.5-minute quadrangle map name that covers the location of the mark. "NGS PID" refers to the Permanent Identifier (PID) of the mark if it is included in the NGS database. Using this unique identifier, one can easily locate the mark in the online NGS database (http://www.ngs.noaa.gov/cgi-bin/datasheet.prl). If this field is empty, then the benchmark is not included in the NGS database. The "LATITUDE," "LONGITUDE," and "ELEVATION" fields show the most precise WGS84 coordinates available for the mark. The locations were established by (1) rapid-static GPS measurements by E. Endo of the USGS Cascades Volcano Observatory (CVO) in 1996, (2) differential GPS measurements during 2002, 2003, and 2004 using equipment owned by NPS, or (3) handheld GPS measurements in 2008. Coordinates are accurate to within 10 m but are much better in most cases.

Below the fields described above is the benchmark description ("DESCRIPTION") and the year in which the mark was located or searched for most recently ("DATE OF DESCRIPTION"). The text of the descriptions and history of the marks are drawn from the online NGS database, from USGS descriptions by Dzurisin and Yamashita (1986), Dzurisin and others (1986), Stoopes and Yamashita (1988), and Yamashita and others (1997), or from information provided by Jeff Place (written commun., 2002) of the FHWA Western Federal Lands Highway Division in Vancouver, Washington. Each description has been modified to account for differences between the original description and current road configuration, mileages, distances to landmarks, or other details as determined during reconnaissance work in 2002, 2003, 2004, and 2008. In addition to the text, photographs of each mark, usually including one closeup and two oblique views from opposing vantage points, are provided to aid with locating and identifying the mark. For additional information, please contact Dan Dzurisin (dzurisin@usgs.gov).

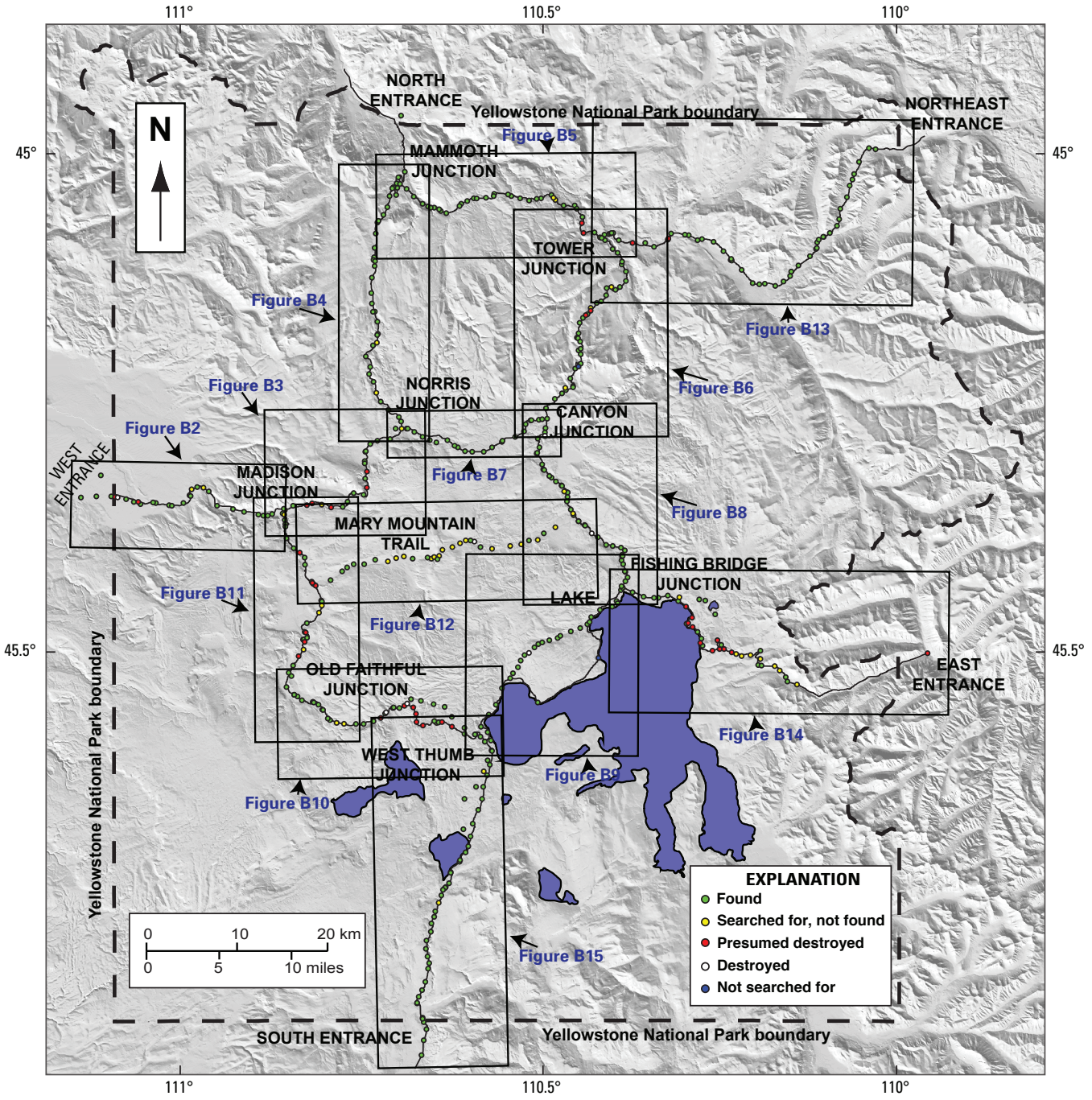

Figure B1. Location and status of benchmarks in Yellowstone National Park and vicinity. Benchmarks that were found in good condition during reconnaissance work in 2002–8 are green. Several of the marks shown as "searched for, not found" (yellow) probably exist but might be buried or obscured; they likely could be found with a concerted effort (this includes several marks along the Mary Mountain Trail in areas not likely to have been disturbed since the marks were set). Marks shown as "presumed destroyed" (red) were set in areas known to have been disturbed by subsequent roadwork and are unlikely to have survived. Benchmarks that could be confirmed destroyed (either because the benchmark itself was found out of place or because the mounting itself, usually either a drill hole or the base of a concrete pier, was found but the benchmark was absent) are shown in white. Time constraints or lack of an adequate description precluded searches for a few marks shown as "not searched for" (blue). An interactive version of this map is included on the data files that accompany this report, together with descriptive information for each of the benchmarks. The information is available online at http://pubs.usgs.gov/pp/1788/pp1788_benchmarks/. Figures B2–B15 show enlarged sections of this map that can be used to locate benchmark descriptions in the data files or online. The one-page descriptions are arranged by benchmark name in numerical order, followed by alphabetical order.

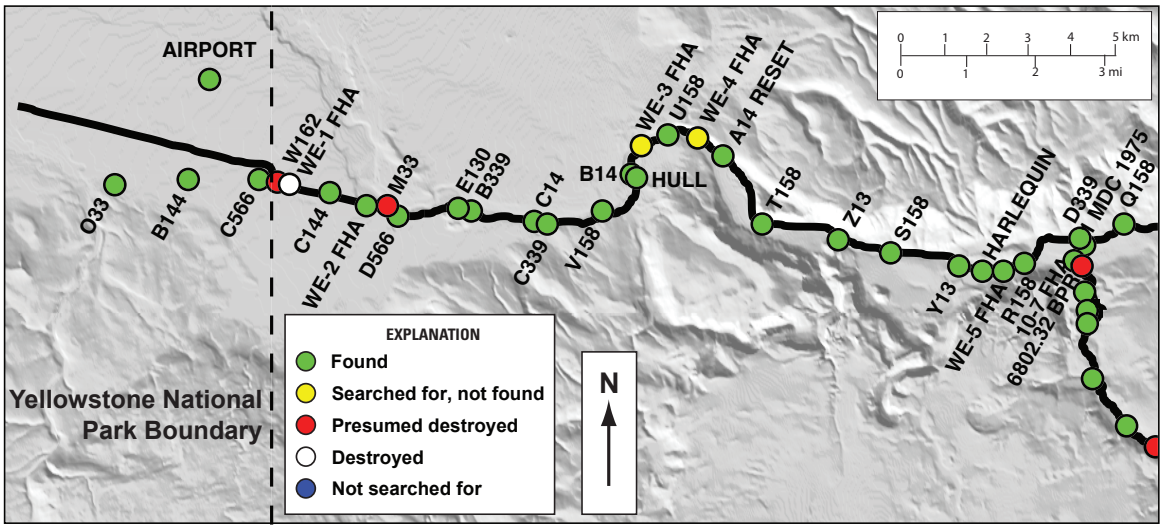

Figure B2. Location and status of benchmarks between the West Entrance of Yellowstone National Park and Madison Junction. Status is indicated by color code shown in the explanation. See appendix B text and figure B1 caption for additional information.

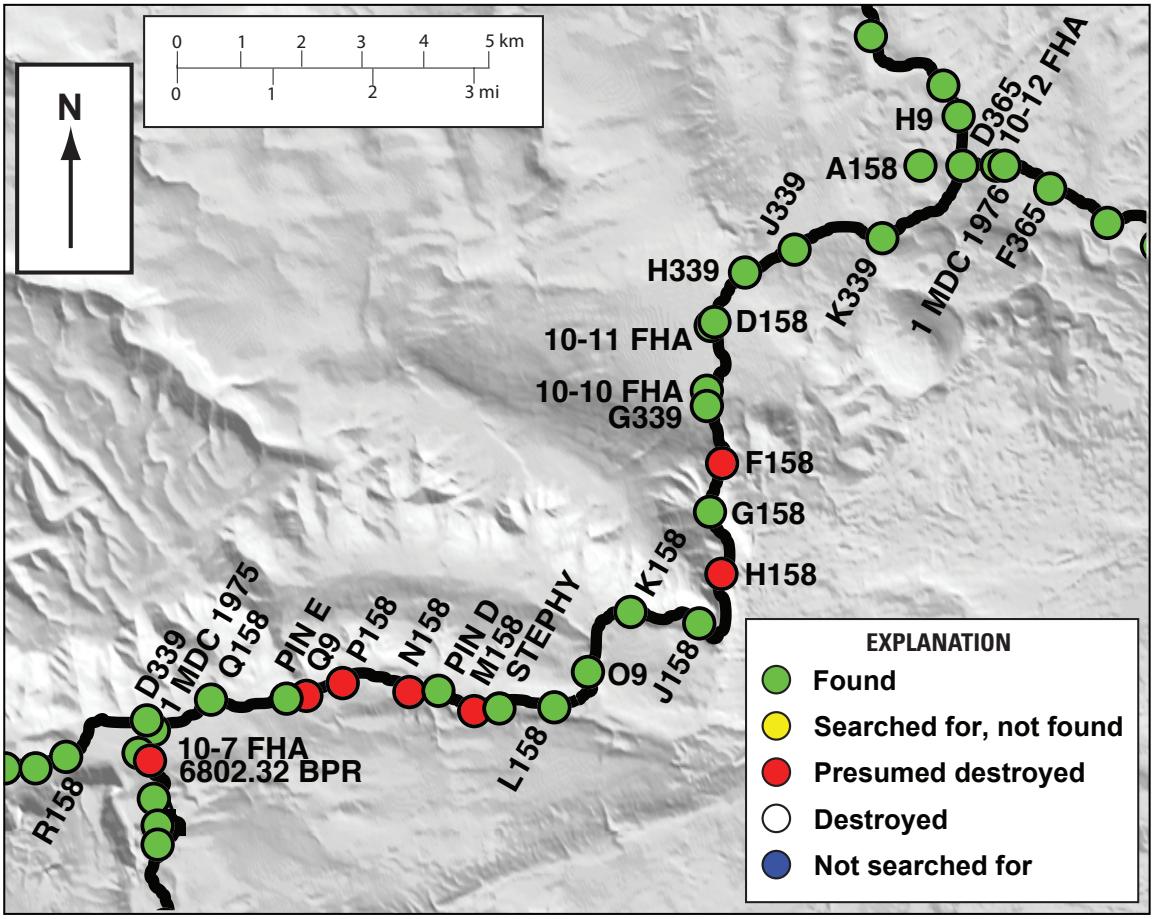

Figure B3. Location and status of benchmarks between Madison Junction and Norris Junction. Status is indicated by color code shown in the explanation. See appendix B text and figure B1 caption for additional information.

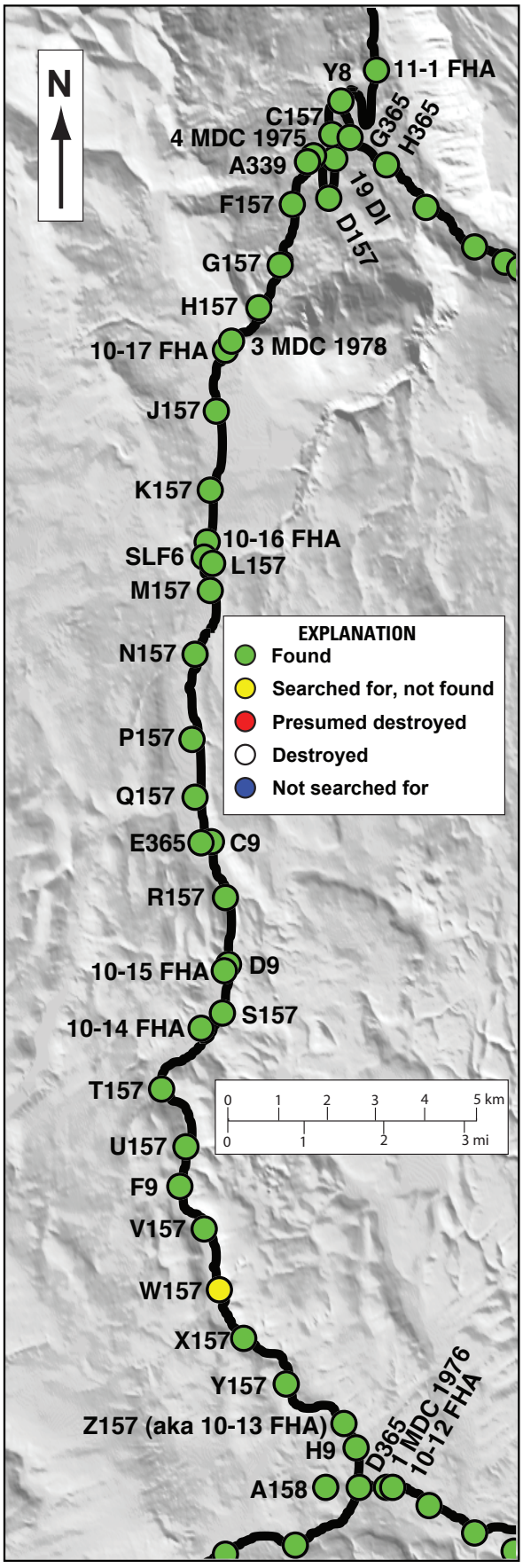

Figure B4. Location and status of benchmarks between Norris Junction and Mammoth Hot Springs Junction. Status is indicated by color code shown in the explanation. See appendix B text and figure B1 caption for additional information.

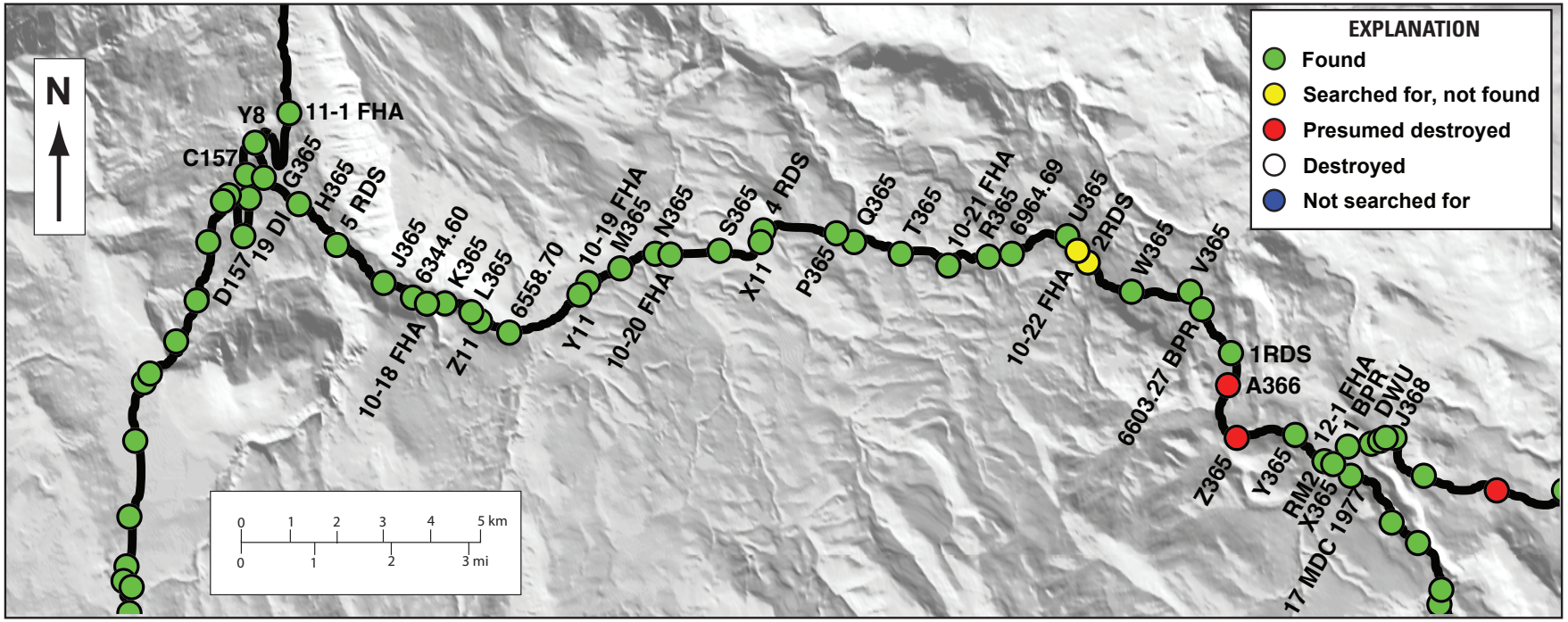

Figure B5. Location and status of benchmarks between the North Entrance of Yellowstone National Park and Tower-Roosevelt Junction by way of Mammoth Hot Springs Junction. Status is indicated by color code shown in the explanation. See appendix B text and figure B1 caption for additional information.

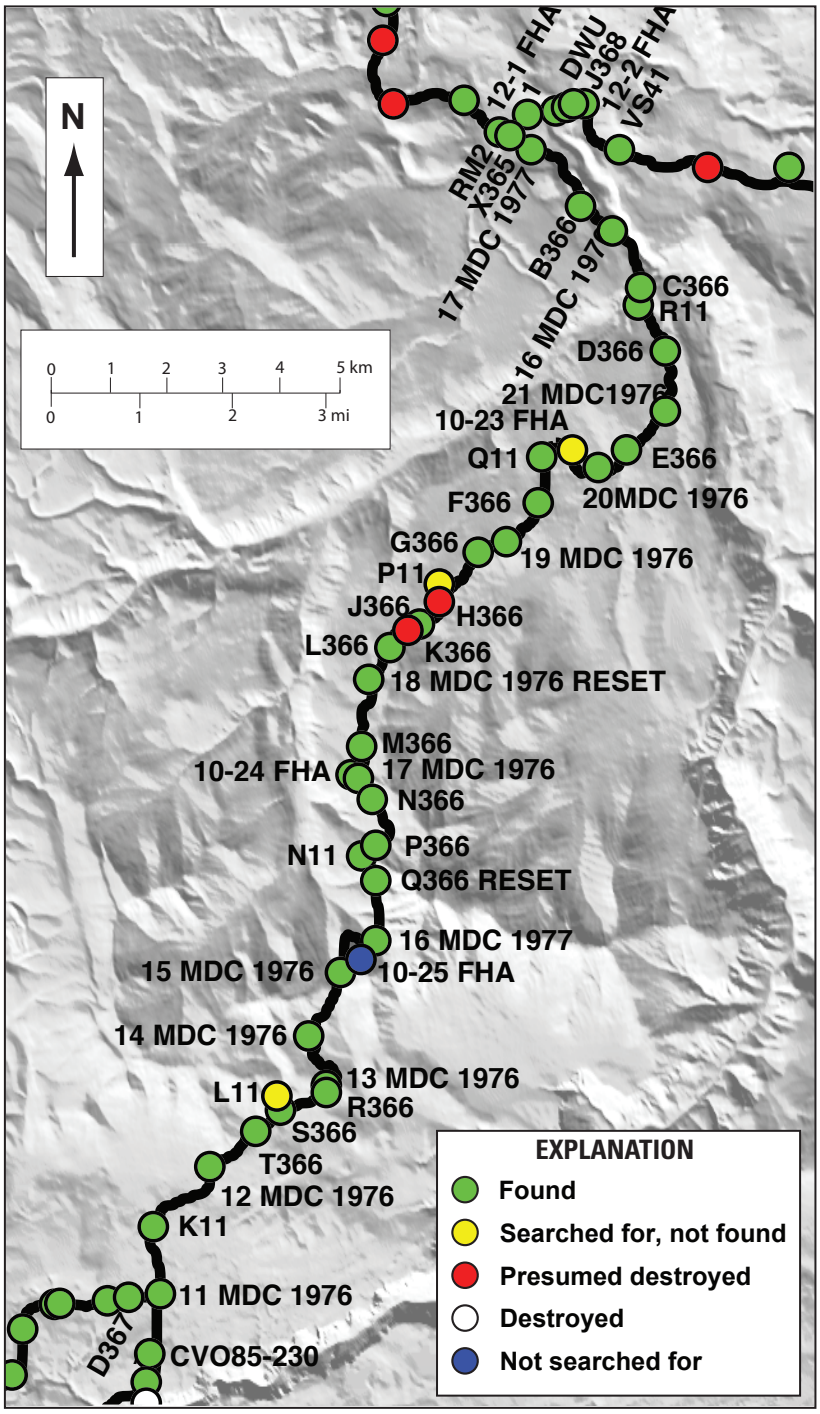

Figure B6. Location and status of benchmarks between Tower-Roosevelt Junction and Canyon Junction. Status is indicated by color code shown in the explanation. See appendix B text and figure B1 caption for additional information.

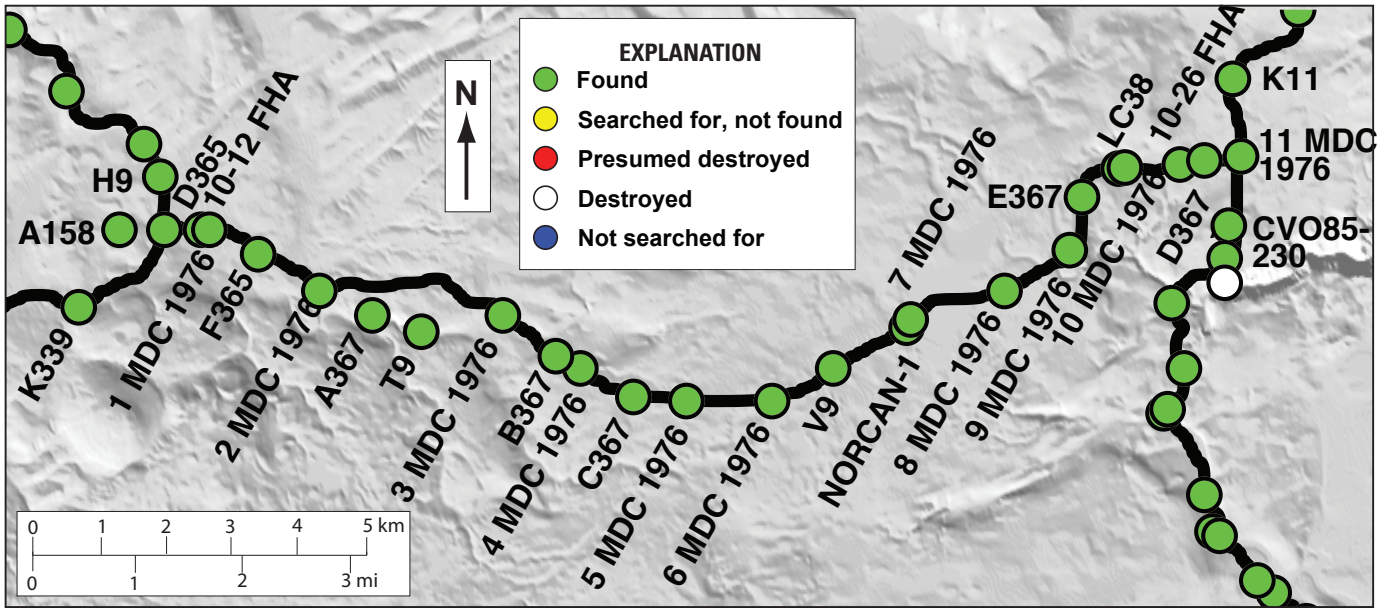

Figure B7. Location and status of benchmarks between Canyon Junction and Norris Junction. Status is indicated by color code shown in the explanation. See appendix B text and figure B1 caption for additional information.

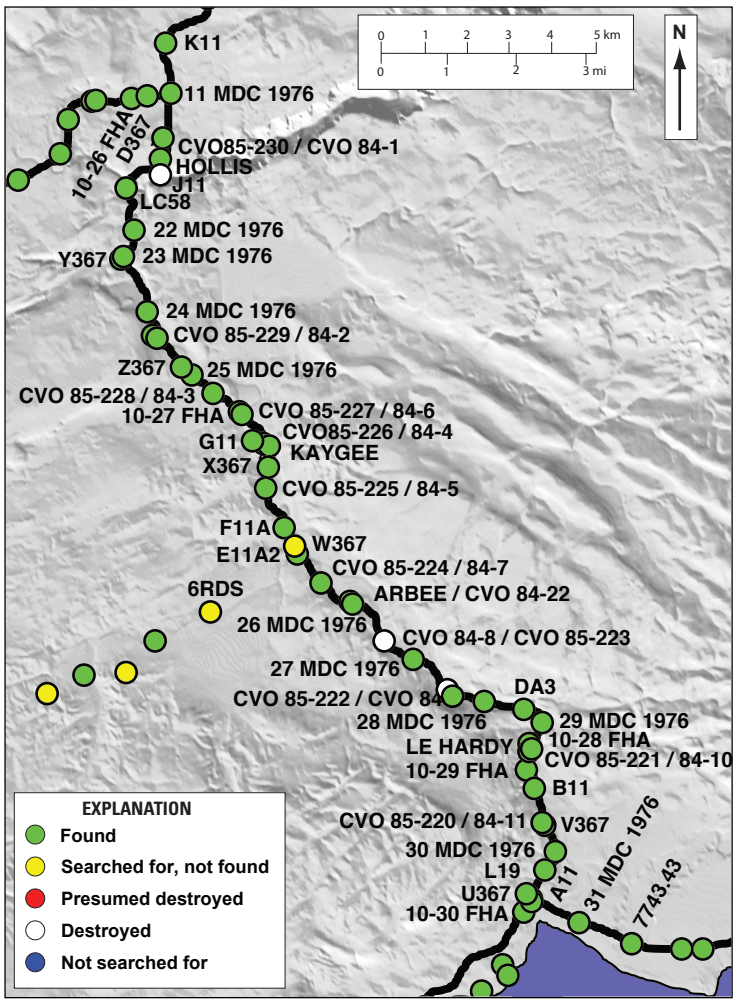

Figure B8. Location and status of benchmarks between Canyon Junction and Fishing Bridge Junction. Status is indicated by color code shown in the explanation. See appendix B text and figure B1 caption for additional information.

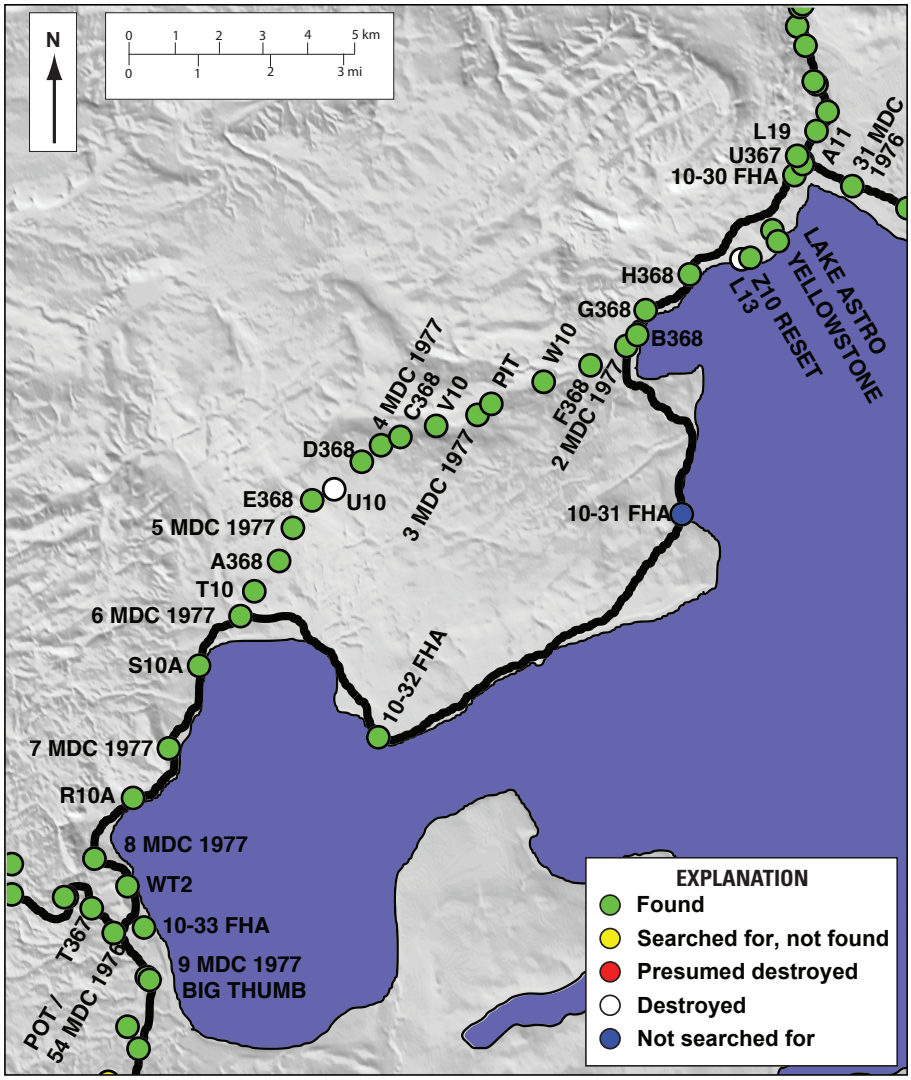

Figure B9. Location and status of benchmarks between Fishing Bridge Junction and West Thumb Junction. Status is indicated by color code shown in the explanation. See appendix B text and figure B1 caption for additional information.

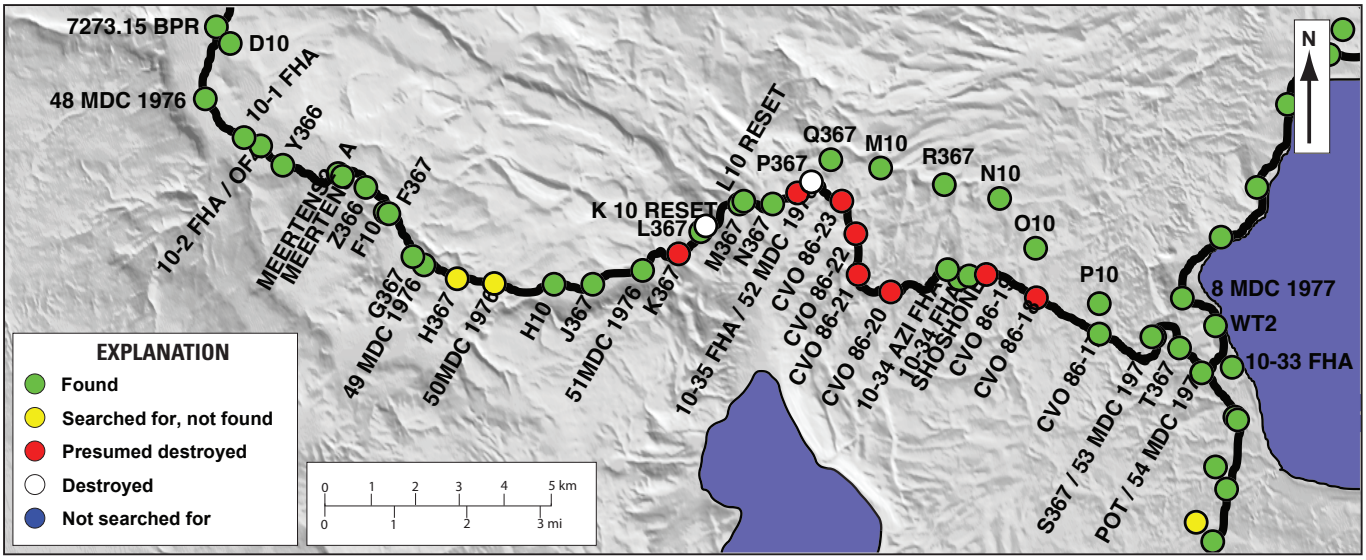

Figure B10. Location and status of benchmarks between West Thumb Junction and Old Faithful Junction. Status is indicated by color code shown in the explanation. See appendix B text and figure B1 caption for additional information.

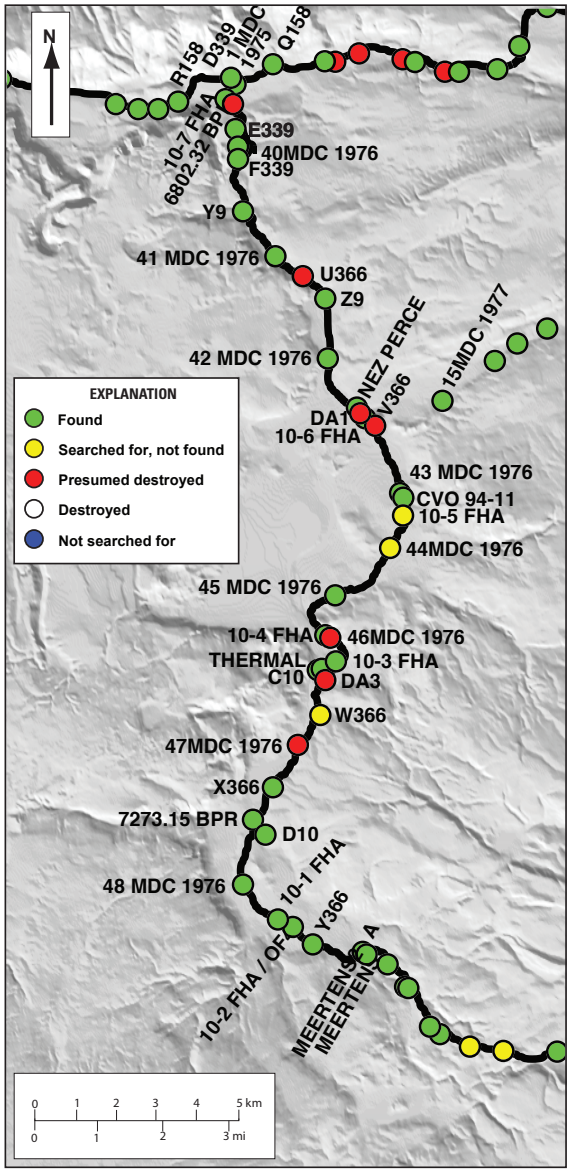

Figure B11. Location and status of benchmarks between Old Faithful Junction and Madison Junction. Status is indicated by color code shown in the explanation. See appendix B text and figure B1 caption for additional information.

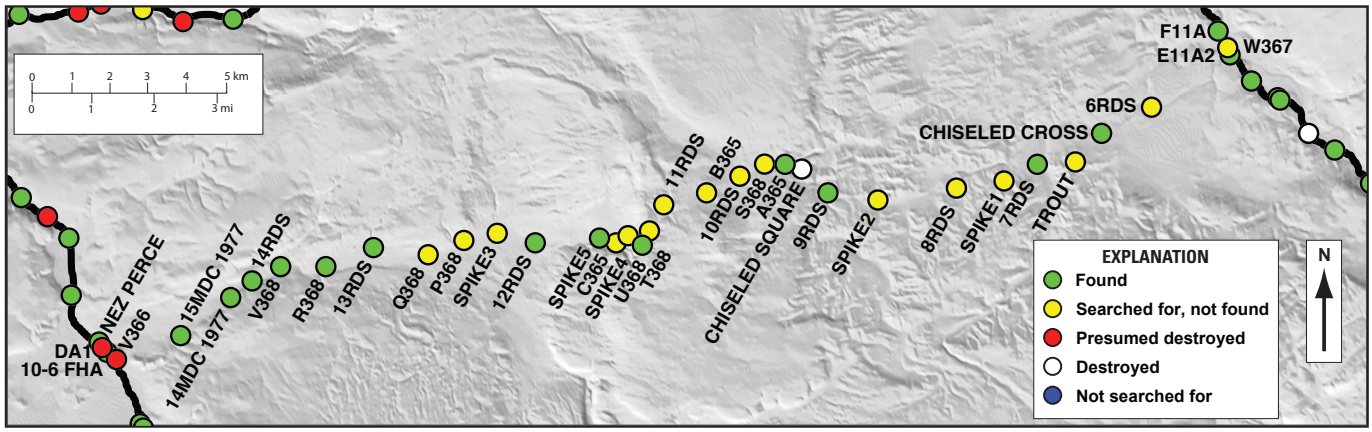

Figure B12. Location and status of benchmarks along the Mary Mountain Trail. Status is indicated by color code shown in the explanation. See appendix B text and figure B1 caption for additional information.

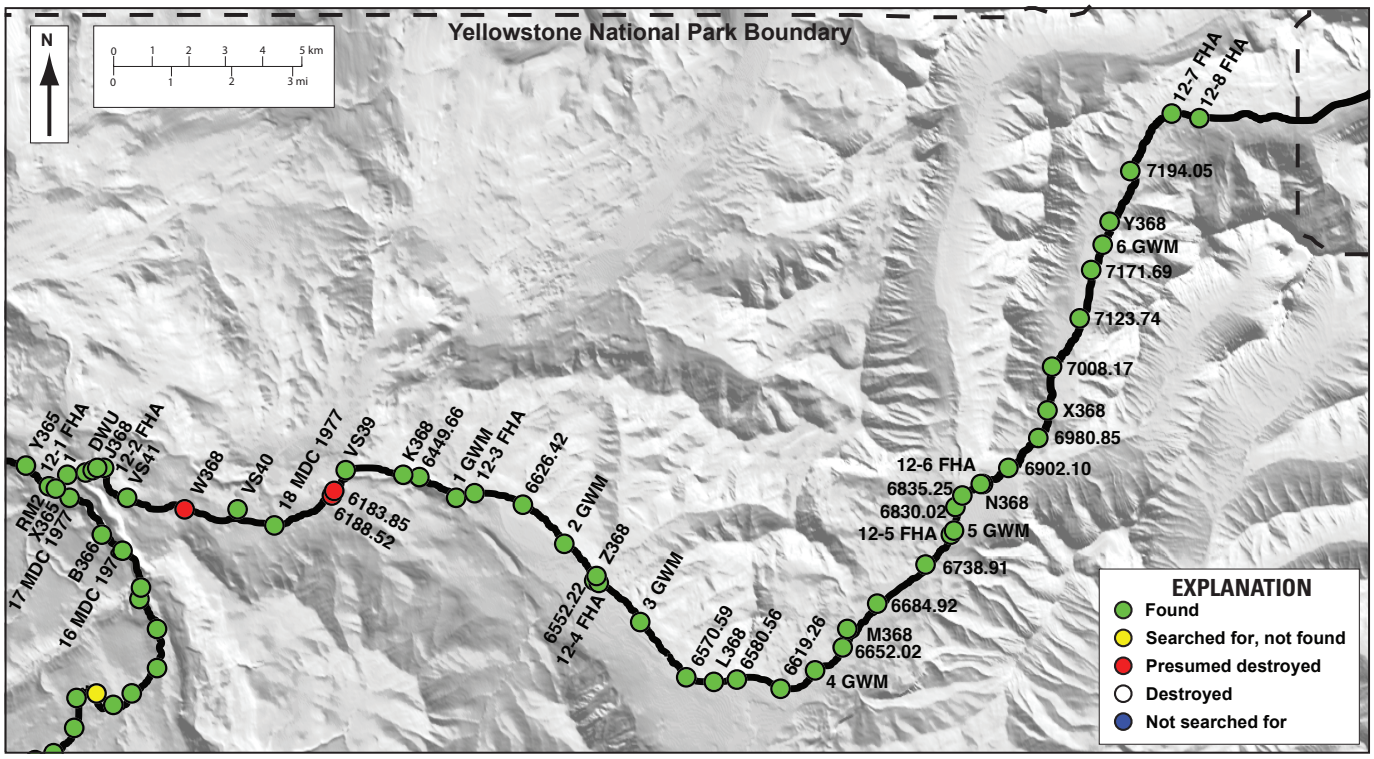

Figure B13. Location and status of benchmarks between the Northeast Entrance of Yellowstone National Park and Tower-Roosevelt Junction. Status is indicated by color code shown in the explanation. See appendix B text and figure B1 caption for additional information.

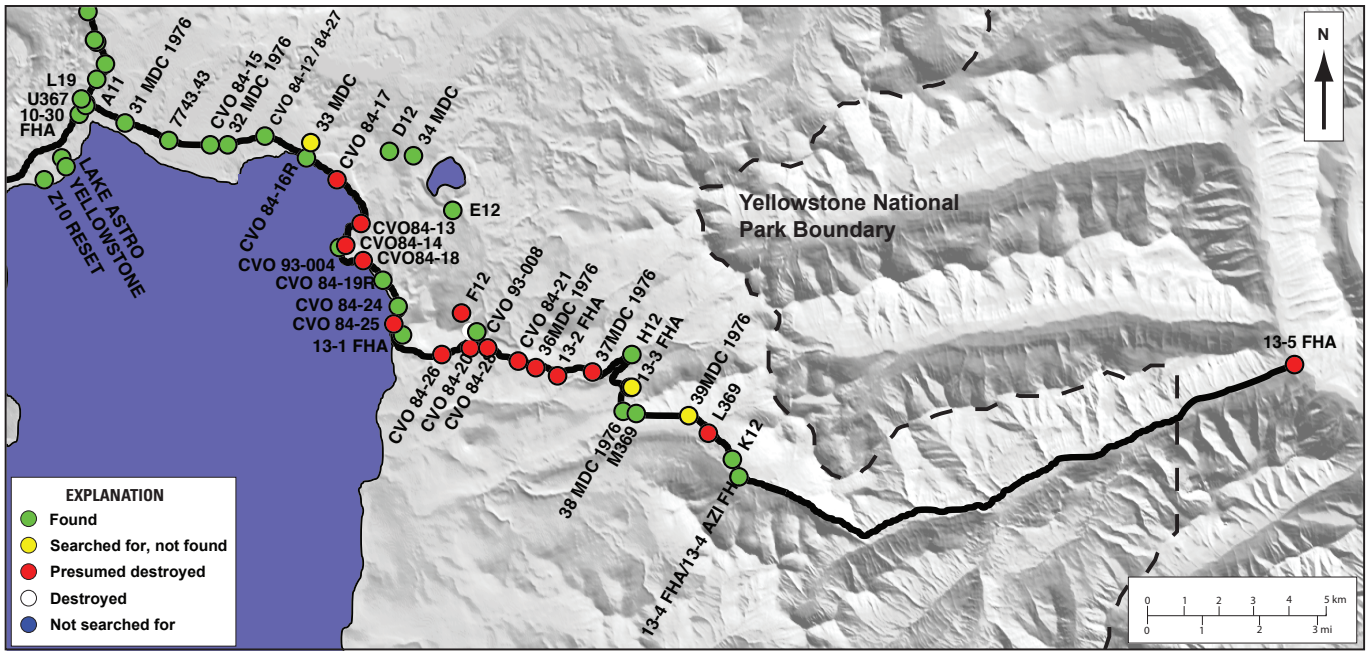

Figure B14. Location and status of benchmarks between the East Entrance of Yellowstone National Park and Fishing Bridge Junction. Status is indicated by color code shown in the explanation. See appendix B text and figure B1 caption for additional information.

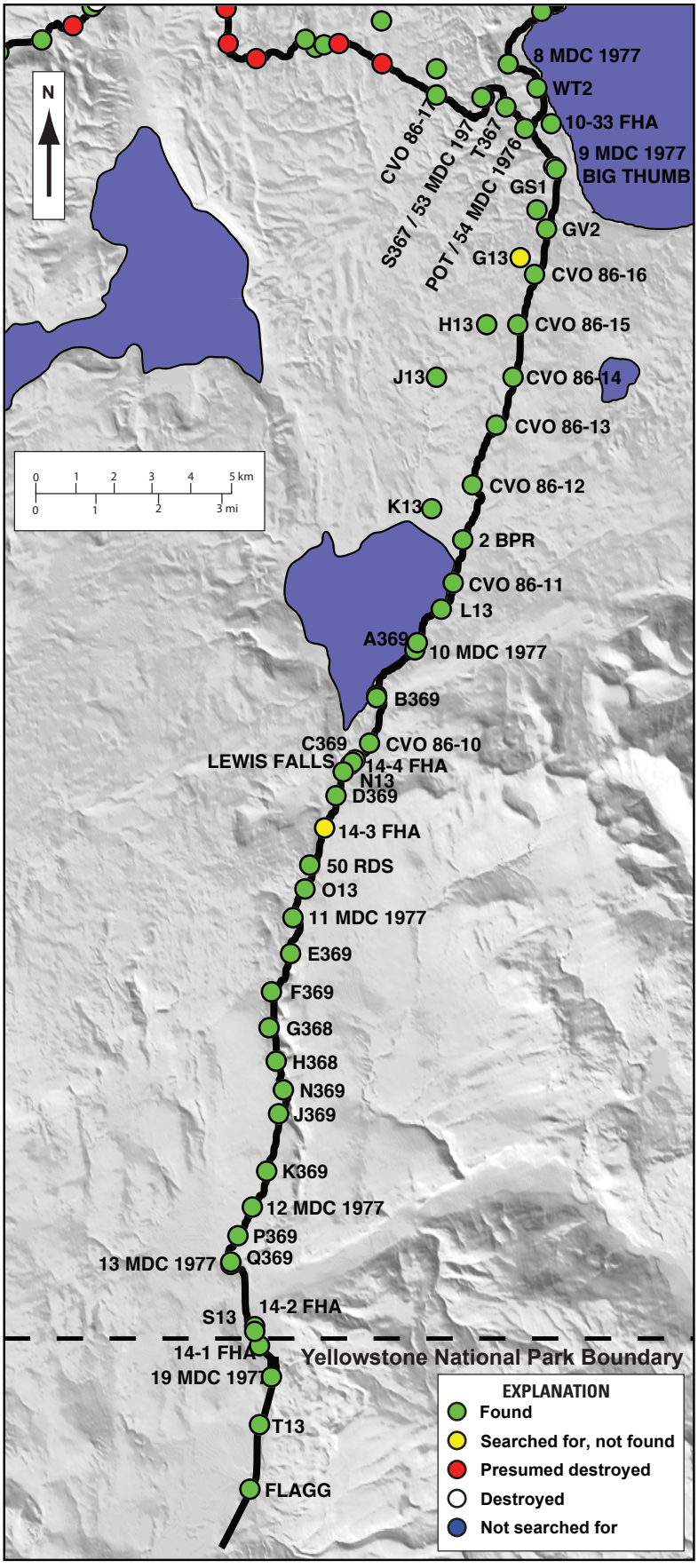

Figure B15. Location and status of benchmarks between the South Entrance of Yellowstone National Park and West Thumb Junction. Status is indicated by color code shown in the explanation. See appendix B text and figure B1 caption for additional information.

Produced in the Menlo Park Publishing Service Center, California
Manuscript approved for publication December 28, 2011
Text edited by James W. Hendley II
Layout and design by Judy Weathers

USGS

Dzurisin and others—History of Surface Displacements at the Yellowstone Caldera from Leveling Surveys and InSAR Observations—Professional Paper 1788